

**The significance of IgM in autoimmune and infectious
diseases**

Inaugural dissertation

to

be awarded the degree of Dr. sc. med.

presented at

the Faculty of Medicine

of the University of Basel

by

Ilaria Callegari

From Camogli, Italy

Basel, 2024

Original document stored on the publication server of the University of Basel

edoc.unibas.ch

Approved by the Faculty of Medicine

On application of

Prof. Dr. Tobias Derfuss, *first supervisor*

Prof. Dr. Michael Sinnreich, *second supervisor*

Dr. Nicholas Sanderson, *further advisor*

Prof. Dr. Francesca Odoardi, *external expert*

Basel, 29.08.2022

Prof. Dr. Primo Schär
Dean

TABLE OF CONTENTS

ACKNOWLEDGMENTS	4
LIST OF ABBREVIATIONS	5
INTRODUCTION	6-12
ANTIBODIES – FOCUS ON IGM	6
AUTOANTIBODIES IN NEUROLOGICAL DISEASES	8
Multiple Sclerosis	8
MACACS AND MONOCLONAL ANTIBODY PRODUCTION	10
OBJECTIVES	13
PUBBLICATIONS	
Potent neutralization by monoclonal human IgM against SARS-CoV-2 is impaired by class switch	14-30
CSF derived monoclonal antibodies identify a novel target antigen in a Multiple Sclerosis patient	31-53
Natalizumab in cerebrospinal fluid and breastmilk of patients with multiple sclerosis	54-62
DISCUSSION	63-65
REFERENCES	66-72

ACKNOWLEDGMENTS

I would like to thank Prof Tobias Derfuss, for accepting me in his lab initially as a guest, despite my poor research background knowledge in the field of neuroimmunology and for seeing in me the potential to complete successfully an ambitious PhD course. Thanks to Tobias, I have learned to have a rigorous approach to research and to integrate apparently small and misleading results into the bigger picture.

Thanks to Nicholas Sanderson, who, while supervising me in the lab, has always been extremely patient in answering my elementary questions, discussing and planning the experimental activities, supporting me during my failures and spreading a contagious research curiosity and an optimistic view on experimental results.

I am grateful to the members of the PhD committee, Prof Michael Sinnreich and Prof Francesca Odoardi, for agreeing in supervising, for their fruitful suggestions and for their external unbiased opinions about the project.

I would like to thank the flow cytometry, microscopy, and bioinformatics cores of the Department of Biomedicine of the University of Basel, and the Biophysics Facility of the Biozentrum of the University of Basel for the constant technical support.

Thanks to all the members of the Derfuss' Lab, including Hye-In, Sebastian, Mika and Noemi who gave a substantial contribution to the research results presented in this thesis and who shared with me hilarious and cheerful times and comforted me during cloudy moments.

A special thanks goes to my family and friends, who constantly sustained me during my career path, guided me in all the decisions and constantly helped me in building the personal and professional identity.

LIST OF ABBREVIATIONS

ACHR	acetylcholine receptor
AQP4	aquaporin 4
BBB	blood brain barrier
FAB	fragment antigen-binding
Fc	fragment crystallizable
CIS	clinically isolated syndrome
CNS	central nervous system
CSF	cerebrospinal fluid
EAE	experimental autoimmune encephalomyelitis
EBV	Epstein Barr Virus
GMFI	geometric mean of the fluorescence intensity
LG1	leucin-rich glioma-inactivated 1
MABs	monoclonal antibodies
MACACS	membrane antigen capture activated cell sorting
MOG	myelin oligodendrocyte glycoprotein
MOGAD	mog-associated disorders
MG	myasthenia gravis
MRI	magnetic resonance imaging
MS	multiple sclerosis
MUSK	muscle-specific tyrosine kinase
NMDAR	N-methyl-D-aspartate receptor
NMOSD	neuromyelitis optica spectrum disorder
OCB	oligoclonal bands
PBMS	peripheral blood mononuclear cells
PNET	peripheral neuroectodermal tumor
PPMS	primary progressive multiple sclerosis
RRMS	relapsing remitting multiple sclerosis
SPMS	secondary progressive multiple sclerosis

INTRODUCTION

ANTIBODIES – FOCUS ON IGM

The humoral immune response is characterised by the production by B cells of antibodies that protect against infection. The type of antibody secreted evolves as long as the immune response develops. Antibodies are composed of two heavy and two light chains. Functionally, all antibodies possess two domains - one that confers the antigen specificity, known as the antigen binding fragment (Fab), and another that drives antibody function, known as the crystallisable fragment (Fc), formed by the assembly of two C-terminal regions of the heavy chain connected by a disulfide bridge between two conserved cysteine residues (Williams & Barclay, 1988). The Fc domain determines the isotope of the antibody. Five isotopes (IgM, IgD, IgG, IgA and IgE) and six subclasses (IgG1-4 and IgA1 and IgA2) exist in humans, each with its own set of effector functions (Schroeder *et al*, 2019). Each antibody has two Fab domains and one Fc domain, generating a molecule that can either exist as a monomer or form multimers (pentamers or hexamers in the case of IgM, dimers in the case of IgA). During the early stages of B cells differentiation, V(D)J recombination takes place to assemble variable (V), diversity (D) and joining (J) segments of the V exon of the immunoglobulin genes, giving rise to diverse repertoires of B lymphocytes, each expressing receptors for a specific antigen (Tonegawa, 1983). After having encountered the cognate antigen, B cells are activated and begin to proliferate in the germinal centres. During this proliferation stage, immunoglobulin genes undergo two types of DNA modification: class-switch recombination and somatic hypermutation. Class-switch recombination consists in the replacement of the heavy constant region gene from the constant mu region to one of the other constant heavy genes, resulting in the switch of the immunoglobulin isotype from IgM/IgD to IgG, IgE or IgA, retaining the antigen-binding properties but assuming new functional capacities due to the newly acquired Fc domain. Somatic hypermutation consists in the massive accumulation of point mutations in the variable genes of the heavy and light chains, giving rise to high-affinity antibodies. Both the Fab and the Fc domains acts together to drive antibody effector function and pathogen clearance (Lu *et al*, 2018). The class of each antibody determines the location to which the antibody is delivered (IgA and IgM for example provide protection in mucosal tissues), the avidity of the antibody, and effector functions like complement activation, neutralisation of virus and toxins, and Fc receptor binding on other immune cells, thus mediating antibody dependent cellular cytotoxicity and antibody dependent phagocytosis. The Fc region can also affect the affinity or kinetics of binding of the antibody by the variable region and thus influence antigen recognition or binding (Torres & Casadevall, 2008).

IgM is the first antibody isotope to be secreted in response to infection and is the only antibody present in all vertebrates (Fellah *et al*, 1992). However, IgM antibodies have historically been considered less interesting than IgG for the development of the humoral response, perhaps due to a reported lower

affinity and to the two distinct waves of high IgM and IgG serum that follow a primary infection or immunization (Eisen, 2014). Early IgM production comes largely from unmutated plasmablasts before class-switching. Although class-switched plasmablasts can contribute to the early antibody response, the production of somatically hypermutated high-affinity IgG from long-lived, germinal center – derived plasma cells dominate the later stages of controlled infection and is associated with immediate protection from subsequent challenge (Victora & Nussenzweig, 2012). Past studies trying to characterize pathogen-specific BCR repertoires used limiting dilution seeding (Banchereau, 2015) or B cell immortalization (Kwakkenbos *et al*, 2010; Traggiai *et al*, 2004) for functional interrogation of secreted antibodies, but analysed only the IgG repertoire, ignoring the presence of both IgM-expressing memory cells as well as the presence of serologically protective IgM response (Banatvala & Chrystie, 1977). Only recently, IgM antibodies have come into focus, after studies in murine models showing that, other than thought previously, antigen-specific IgM long living plasma cells persist in the spleen in response to vaccination or infection and secrete high titres of antigen-specific IgM throughout the lifetime (Bohannon *et al*, 2016). Functionally, IgM antibodies can confer the host protection against viral and bacterial infections (Harada *et al*, 2003; Skountzou *et al*, 2014; Throsby *et al*, 2008; Racine *et al*, 2011) and monoclonal IgM antibodies isolated from human patients have been shown to protect mice against a lethal challenge of H5N1 and H1N1 influenza viruses (Throsby *et al*, 2008). One of the unique features of IgM is the ability to form pentamers and hexamers, enabling high-avidity interactions with antigen (Brewer *et al*, 1994). Interestingly, *in vitro* class switch of monoclonal antibodies from IgM to IgG1 or IgG3 can result in loss of binding capacity, with a similar binding profile shown also by IgM derived Fab fragments, suggesting that the full binding capacity is supported by the IgM Fc domain (Lindner *et al*, 2019). Artificial production of monomeric IgM by mutating the C terminus C575S residue results instead in a similar binding profile as the wild-type IgM, suggesting that the effects of switching the constant region are isotype intrinsic and not due to a change in avidity (Lindner *et al*, 2019). IgM mediated neutralization capacity has been investigated in comparison with their IgG counterparts. Thouvenel *et al* (Thouvenel *et al*, 2021) observed that IgM antibodies against Plasmodium parasites lost their potency if converted to monomeric IgG. Shen *et al* (Shen *et al*, 2019) isolated two influenza-neutralizing antibodies from influenza virus-infected mice 7G6-IgM and 3G10-IgM. When made into a chimeric antibody with human IgG1 constant regions, the potency of the more potent antibody 7G6-IgM fell by around 100-fold, while the less potent 3G10-IgM did not change significantly. The IgM version also offered better *in vivo* protection against challenge with various influenza strains than did the IgG version. An obvious question is what the mechanistic basis for this IgM class-dependent potency might be. Thouvenel *et al* (Thouvenel *et al*, 2021) ascribe the effect of IgM to IgG class switch partly to the reduction in avidity caused by the reduction in valency, and partly to other factors, for example, enhanced steric blockade or epitope accessibility. Either conformational influence of the Fc region on the paratope (Janda *et al*, 2012), or the effect of Fc region flexibility on

the ability of the antigen-binding domains to access the epitope (Tobita *et al*, 2004) might influence antigen binding.

AUTOANTIBODIES IN NEUROLOGICAL DISEASES AND MULTIPLE SCLEROSIS

Autoimmune diseases are caused by the recognition of self molecules by lymphocytes or antibodies, resulting in cellular lysis and/or an inflammatory response in the affected organ. Aberrant responses to self have been linked to over 80 inflammatory disorders, collectively defined as ‘autoimmune diseases’ (Theofilopoulos *et al*, 2017) and more than 25 new types of autoantibodies have been described recently in patient with neurological diseases (Prüss, 2021). The discovery of novel antibodies is fundamental for understanding the disease cause and for diagnostic and therapeutic decision.

Clinical symptoms observed in antibody-associated neurological diseases include memory impairment, behavioural abnormalities, seizures, psychosis, movement disorders, vegetative dysfunction. Two main types of autoantibodies can be detected in serum and cerebrospinal fluid (CSF) of patients with autoantibody associated neurological syndromes. Onconeural antibodies, targeting intracellular antigens, almost always indicate the presence of an underlying cancer (e.g. anti-Hu antibodies); thus, although these antibodies are not pathogenic, they are excellent biomarkers of paraneoplastic syndromes (Graus *et al*, 2016) and can guide the search for the underlying tumor. Auto-antibodies targeting instead neuronal cell surface antigens have direct pathogenic effects and probably cause the neurological disorder. They are associated with distinct neurological syndromes and can occur in patients with or without cancer. Examples of disease-specific autoantibodies against neuronal cell surface-derived antigens and associated with clinically and diagnostically defined syndromes include the N-methyl-D-aspartate receptor (NMDAR) and leucine-rich glioma-inactivated 1 (LGI1) in autoimmune encephalitis; the aquaporin-4 (AQP4) water channel or myelin oligodendocyte glycoprotein (MOG) in patients with neuromyelitis optica spectrum disorders (NMOSDs) and MOG antibody-associated disorders (MOGADs), respectively; and the acetylcholine receptor (AChR) and muscle-specific tyrosine kinase (MuSK) in patients with myasthenia gravis (MG) (Dalmau *et al*, 2007; Irani *et al*, 2010; Huda *et al*, 2019; Spadaro *et al*, 2018; Gilhus, 2016). Complement activation, cross-linking and target receptor internalization, direct stimulation or blockage of the target receptor, interference with protein-protein interactions and antibody-dependent cytotoxicity are all possible mechanisms by which antibodies may exert their pathogenic effect.

Multiple Sclerosis

Multiple Sclerosis (MS) is a chronic demyelinating disease of the central nervous system (CNS). It is typically diagnosed between the third and fourth decade of life, occurs more frequently in women than men and is considered the most common neurological cause of disability in young adults, with a prevalence greater than 1 in 1000 (Wallin *et al*, 2019). The clinical course of MS includes a relapsing-

remitting form (RRMS), that regards approximately 90% of patients who experience self-limiting episodes of neurological dysfunction, and primary progressive form (PPMS) regarding the 10% of patients, in which the neurological disability chronically worsens without any evidence of discrete self-remitting events. Eventually, 50% of patients with RRMS will develop progressive disability independent from relapses in what is called secondary progressive MS (SPMS) (Lublin & Reingold, 1996; Miller & Leary, 2007; Lorscheider *et al*, 2016). The trigger(s) of MS remains unknown, but an interplay between genetic, epigenetic, and environmental factors is believed to have a pathogenic role in the disease (Olsson *et al*, 2016).

The notion that MS is an autoimmune disorder is supported by several, albeit indirect, lines of evidence: CNS plaques contain conspicuous inflammatory infiltrates composed mainly of lymphocytes and macrophages (Kutzelnigg & Lassmann, 2014); intrathecally produced oligoclonal antibodies are present in the CSF (Stangel *et al*, 2013); genetic risk variants revealed by genome-wide association studies are mostly immune system related genes (Sawcer *et al*, 2014); immunotherapies with different mechanisms have shown positive treatment effects (Haghikia *et al*, 2013); and finally, most aspects of multiple sclerosis can be closely mimicked in autoimmune animal models, collectively named experimental autoimmune encephalomyelitis (EAE) (Gold *et al*, 2006).

In the recent years, following the striking efficacy of CD20-depleting therapies in reducing the disease activity (Hauser *et al*, 2008a), the interest for a B cells involvement in the pathogenesis of MS has grown rapidly. Several lines of evidence support an antibody-mediated pathogenesis of the disease, including the presence of antibodies (Mehta *et al*, 1981), B cells (Archelos *et al*, 2000) and activated complement (Storch *et al*, 1998) in active multiple sclerosis lesions and the fact that treatments effective in autoantibody-mediated diseases such as intravenous immunoglobulin (Lisak, 1998) and plasma exchange (Weinshenker *et al*, 1999) may have benefits in some multiple sclerosis patients.

One of the clinical hallmarks of the MS is the presence of intrathecal immunoglobulin production, identifiable at the CSF examination as oligoclonal bands (OCBs) (Johnson *et al*, 1977); OCBs are not only a diagnostic and prognostic tool (Stangel *et al*, 2013) but also one of the strongest evidences for an involvement of humoral immune response. CSF B cell count is generally increased in the CSF of patients with MS, particularly in those with contrast-enhanced lesions on MRI (Eggers *et al*, 2017) and B cells can be detected in the CNS lesions in early to late stages of the disease, most abundantly in active lesions of patients with RRMS (Machado-Santos *et al*, 2018). Moreover, ectopic lymphoid follicle-like structures containing CD20+ B cells, CD138+ plasma cells and follicular dendritic cells have been identified in the leptomeninges of patients with SPMS (Serafini *et al*, 2004; Magliozzi *et al*, 2007; Howell *et al*, 2011). Although apparently restricted to late disease phases, lymphoid-like structures in the brains of patients with MS provide a microenvironment for B cell expansion and maturation, and hence local immunoglobulin production. Interestingly, the phenomenon of B cell accumulation and formation of ectopic lymphoid tissue with distinct T cell areas and B cell follicles occurs also in other antibody-mediated diseases, such as myasthenia gravis and autoimmune thyroiditis

(Roxanis *et al*, 2002; Aloisi & Pujol-Borrell, 2006; Magalhães *et al*, 2002), suggesting that B cell infiltration and lymphoid organization in the MS brain could be causally related to the disease.

The rapid onset of CD20 depletion effect (Hauser *et al*, 2008b) combined with the fact that the therapy doesn't deplete antibody producing cells such as plasmablasts and plasma cells, indicates that the effect of these therapies does not only rely on the global reduction of humoral immunity, and that the pathogenic role of B cells in MS is likely not restricted to antibody production (Hauser, 2015; Hohlfeld & Meinl, 2017). B cells are likely to influence MS pathology through additional effector functions including antigen presentation and roles in proinflammatory and regulatory immune responses (Von Büdingen *et al*, 2015; Krumbholz *et al*, 2012). B cells represent a unique population of APCs, highly specialized in presenting only those antigens that bind to their clonal BCR or Ig molecule. Moreover, B cells entering the CSF are important for recruiting other inflammatory cells and promoting their survival (Lehmann-Horn *et al*, 2015). Finally, B cells from patients with MS have been reported to be inherently polarized toward secretion of high levels of pro-inflammatory molecules including IL-6 and granulocyte macrophage-colony stimulating factor (GM-CSF), and lower levels of regulatory cytokine IL-10 (Li *et al*, 2015; Barr *et al*, 2012). Despite the rapid response of B cell depletion therapy on focal inflammation argues against a primary effect on antibodies, the possible elimination of a yet-to-be-identified autoantibody in MS cannot be completely excluded.

MACACS AND MONOCLONAL ANTIBODIES

The study of class antibody class specific properties requires the use of monoclonal antibodies of different classes specific for a defined pathogen. Research and industrial attention have greatly developed during the past decade, with more than 45 therapeutic antibodies licensed for treatment of neoplastic or autoimmune diseases. However, both have focused overwhelmingly on IgG, with the result that the specific properties of other classes are still very poorly characterized, Methods that have been proposed and widely used for monoclonal antibody production include phage display libraries produced from humans with a humoral response of interest (Plaisant *et al*, 1997; Mao *et al*, 1999). Although this technique has produced numerous useful antibodies, its applicability is limited by differences in binding properties between antibodies expressed in bacterial and eukaryotic cells. In addition, phage display may result in heavy- and light- chain combinations that do not occur in the same B cell in vivo. Human B cells can also be immortalized by Epstein-Barr virus (EBV) transformation (Traggiai *et al*, 2004; Åman *et al*, 1984; Bonsignori *et al*, 2011), with or without the use of toll-like receptor ligands. However, these techniques can be inefficient and transformed clones can be lost because of instability.

One of the technical difficulties relies in the fact that only a small fraction of the total B cells is specific for a certain antigen. A commonly used method for antigen-specific B cell isolation is the selection by fluorochrome-conjugated soluble antigens (Casali *et al*, 1986; Di Niro *et al*, 2010; Scheid *et al*, 2009), followed by immunoglobulin gene cloning, but this has the disadvantage that many antigens lose their

native conformation when produced in a soluble form, and given the importance of antigen conformation for both anti-viral and autoimmune antibodies, the power of this approach may be overestimated. Moreover, affinity of a B cell for a specific antigen may be influenced by factors like glycosylation, interaction with other cell expressed membrane components, assembly into multi-subunit complexes, which all depend on the membrane expression by a suitable cell. Others recently have described effective protocols for antigen-specific B cell isolation include negative selection to exclude polyspecific B cells that bind to irrelevant antigens (Robbiani *et al*, 2020; Thouvenel *et al*, 2021). One known property of B cells is that when the affinity for a membrane protein extracellular domain antigen is high enough, they extract the protein from the membrane and rapidly become highly activated (Batista *et al*, 2001), in a process that requires first a clustering of BCRs at the site of contact, and a two-phase response in which B cells first spread over the antigen-bearing membrane, and then contract thereby collecting bound antigen into a central aggregate (Fleire *et al*, 2006). If the antigen is fluorescent, this allows highly specific sorting of the antigen-specific B cells. Advantages of this system include the possibility to use various membrane expressed antigens in their native conformation, the possibility to use activation markers such as CD69 to further distinguish cells that internalised the antigen from cells that acquired the fluorescent antigen for other reasons, and the possibility to use adherent cells for antigen expression, so that unspecific B cells will only contact the antigen-expressing cells but will not adhere to them and can be easily washed away. We previously applied this property to develop a technique (membrane antigen capture activated cell sorting - MACACS) suitable for isolation of high affinity antigen-specific B cells from the peripheral blood of recently infected donors, or donors affected by antibody-mediated autoimmune diseases (Zimmermann *et al*, 2019). We describe here the application of this property for the selection of rare SARS-CoV-2 spike-protein IgM B cells from the larger proportion of circulating polyreactive B cells, enabling us to produce patient-derived monoclonal antibodies in their native class and thereby assess their intrinsic properties.

Another technical aspect that follows the appropriate selection of antigen-specific B cells, is the antibody engineering and production. Conventionally paired immunoglobulin heavy- and light-chain sequences are cloned in separate vectors. Transient transfection of these vectors in mammalian HEK293 cells enables the production of recombinant monoclonal antibodies (Smith *et al*, 2009). Although these enables the expression of a large number of monoclonal antibodies in a short time, the transient co-transfection of separate vectors doubles the DNA preparation work and requires large amount of transfection reagent for the production of milligrams of antibody, which is a costly, labor- and time-intensive scale-up process. The expression of recombinant antibodies as IgG1 is based on early work cloning the variable regions into an IgG1 backbone using single-cell PCR (Tiller *et al*, 2008), assuming that the binding and functional properties of the antibodies obtained will be equivalent to those of the original class and preventing the study of constant regions and Fc dependent mechanisms. This approach has been also recently employed to study the properties of IgM antibodies

against SARS-CoV-2 (Wang *et al*, 2021; Feldman *et al*, 2021), ignoring the possibility of a dramatic effect of this artificial Fc exchange on antibody functional properties. In the present work, we addressed these limitations by PCR amplification of both the variable and the constant region of both antibody chains from the cDNA of the single antigen-specific B cell; the immunoglobulin chains thus obtained were cloned into a vector hosting a dual antibody expression cassette with a selection marker (Braren *et al*, 2007; Dodev *et al*, 2014), enabling us to obtain stably transfected cell line producing the antibody of interest in the exact form as produced by the isolated B cell. We have applied this method to the production of monoclonal antibodies from both recently infected donors and donors affected by MS.









OBJECTIVES

In this work, we first aimed to optimise the methods for recombinant antibodies production starting from the isolation of circulating antigen-specific B cells. We aimed to produce recombinant antibodies in their native class in order to dissect their class-specific properties. We took advantage from the unique setting offered by the COVID-19 pandemic, which gave us the opportunity to collect blood from donors recently infected by a novel virus and to use them to select SARS-CoV-2 spike-protein specific B cells, applying MACACS, a technique developed in our laboratory that enables enrichment of rare antigen-specific B cells from peripheral blood. We applied this technique to produce recombinant antibodies against a known target and assess their functions when expressed in their native class, including in vitro neutralisation potential, complement activation, affinity measurement and epitope mapping. In vitro class switch of recombinant antibodies enabled the direct comparison of the functional attributes of IgG and IgM.

In the second part of this work, we aimed to identify the target antigen of CSF IgM in MS patients. We first screened two independent cohorts of CSF samples for CSF antibodies binding to the cell surface of a panel of neural or glial derived cell lines. After the identification of IgM binding to a peripheral neuroectodermal tumour (PNET) that reliably differentiates MS from controls, we applied the optimised pipeline for cloning of SARS-CoV-2 spike-specific monoclonal antibodies to the cloning of CSF derived PNET-binding IgM from multiple sclerosis patients, with the aim of using the recombinantly produced IgM for antigen identification by immunoprecipitation and mass spectrometry.

In the last part, we used the incidental detection of natalizumab in the CSF of treated patients while looking for antibodies binding to PNET cells to develop a flow-cytometry based assay and use it to determine natalizumab concentration in CSF, serum, and breastmilk of multiple sclerosis patients.

Potent neutralization by monoclonal human IgM against SARS-CoV-2 is impaired by class switch

Ilaria Callegari^{1,2} , Mika Schneider¹, Giuliano Berloff¹ , Tobias Mühlethaler³, Sebastian Holdermann^{1,2} , Edoardo Galli^{1,2} , Tim Roloff^{4,5}, Renate Boss⁶, Laura Infanti⁷, Nina Khanna⁸, Adrian Egli^{4,5} , Andreas Buser⁷ , Cert Zimmer^{9,10,†} , Tobias Derfuss^{1,2,†} & Nicholas S R Sanderson^{1,2,*,†} 

Abstract

To investigate the class-dependent properties of anti-viral IgM antibodies, we use membrane antigen capture activated cell sorting to isolate spike-protein-specific B cells from donors recently infected with SARS-CoV-2, allowing production of recombinant antibodies. We isolate 20, spike-protein-specific antibodies of classes IgM, IgG, and IgA, none of which shows any antigen-independent binding to human cells. Two antibodies of class IgM mediate virus neutralization at picomolar concentrations, but this potency is lost following artificial switch to IgG. Although, as expected, the IgG versions of the antibodies appear to have lower avidity than their IgM parents, this is not sufficient to explain the loss of potency.

Keywords antibodies; B cells; class switch; MACACS; membrane antigen

Subject Categories Immunology; Microbiology, Virology & Host Pathogen Interaction

DOI 10.15252/embr.202153956 | Received 7 September 2021 | Revised 13 April 2022 | Accepted 27 April 2022

EMBO Reports (2022) e53956

Introduction

Around 80% of the soluble antibody in blood is of the IgG class, with the remainder consisting mostly of IgM and IgA (Loh *et al.*, 2013). Research attention and industrial development have both focused overwhelmingly on IgG, with the result that the class-specific properties of IgM are still very poorly characterized. One

property that might make IgM particularly suitable as an early effector mechanism is the avidity advantage offered by its multimeric (pentameric or hexameric) structure. It has been proposed that this can enable an IgM whose antigen-binding domain has a relatively modest affinity for antigen (as is typical in the early immune response, before affinity maturation has produced high affinity antibodies) to achieve avid binding to antigens with multiple identical epitopes that can simultaneously be bound by the antibody's 10 or 12 antigen-binding sites (Keyt *et al.*, 2020). On the other hand, this mechanism presumably also enhances IgM binding to low affinity self antigens, which can explain their well-known predilection for self-reactivity (Nakamura *et al.*, 1988). The pentameric structure of IgM is also a strong stimulus for complement activation (Sharp *et al.*, 2019), which can contribute to suppression of infection (Kurtovic & Beeson, 2021), but has the potential to exacerbate immunopathology (Polycarpou *et al.*, 2020).

Understanding the class-dependent properties of antibodies requires monoclonal antibodies of various classes against a defined pathogen, but the isolation and characterization of pathogen-specific monoclonal IgM has lagged well behind the study of IgG, because of the technical difficulties in isolating antigen-specific B cells and in producing IgM antibodies recombinantly. In the SARS-CoV-2 pandemic, large numbers of people were infected with a novel pathogen, enabling the collection of blood samples containing pathogen-specific B cells of all classes, during the acute immune response. Having previously developed a suite of techniques suited for isolating IgM B cells specific for viral glycoproteins (Zimmermann *et al.*, 2019), we had the opportunity to isolate and study naturally occurring antibodies in their original classes and assess the importance of class (i.e., Fc region) on antibody functional properties.

1 Department of Biomedicine, University of Basel and University Hospital Basel, Basel, Switzerland
 2 MS Center, Neurologic Clinic and Policlinic, Research Center for Clinical Neuroimmunology and Neuroscience Basel (RC2NB), University Hospital Basel, University of Basel, Basel, Switzerland
 3 Biophysics Facility, Biozentrum, University of Basel, Basel, Switzerland
 4 Applied Microbiology Research, Department of Biomedicine, University of Basel, Basel, Switzerland
 5 Clinical Bacteriology and Mycology, University Hospital Basel, Basel, Switzerland
 6 Federal Food Safety and Veterinary Office, Bern, Switzerland
 7 Regional Blood Transfusion Service, Swiss Red Cross, Basel, Switzerland
 8 Infectious Diseases and Hospital Epidemiology, University Hospital Basel, Basel, Switzerland
 9 Institute of Virology and Immunology, Bern & Mittelhäusern, Switzerland
 10 Department of Infectious Diseases and Pathobiology, Vetsuisse Faculty, University of Bern, Bern, Switzerland
 *Corresponding author. Tel: +41 61 265 2608; E-mail: nicholas.sanderson@unibas.ch
 †These authors contributed equally to this work

Results and Discussion

Serum IgM is polyreactive

We collected serum and peripheral blood mononuclear cells (PBMC) from 34 donors after recovery from PCR-confirmed SARS-CoV-2 infection, 14 vaccinated donors, and 86 donors with no known history of SARS-CoV-2 infection or vaccination from April 2020 to June 2021. Demographic information about donors is presented in Appendix Table S1. We measured binding of serum IgM, IgG, and IgA to TE 671 rhabdomyosarcoma cells stably transfected with SARS-CoV-2 spike protein fused at the carboxyl terminus to mCherry (TE spike-mCherry) or untransfected control cells (TE 0). We used flow cytometry of antibody binding on antigen-expressing cells in addition to ELISA, to enable the assessment of nonspecific binding to normal cell surface proteins, and to improve detection of antibodies whose binding is dependent on membrane-inherent properties such as lateral mobility of antigens. SARS-CoV-2 spike-specific antibodies of the IgG and IgA classes increased in infected and vaccinated donors (Fig 1A).

IgM in serum from all unexposed or vaccinated donors bound in similar measure to spike-expressing and control cells, with a clear spike-specific signal in only 6 convalescent donors when tested by flow-cytometry. Since the presence of spike-specific IgM in donors at this time point after symptom onset is well established (Pickering *et al.*, 2020; Zohar *et al.*, 2020), the lack of a stronger IgM signal on the spike-expressing cells requires some other explanation, for example, nonspecific IgM binding to the non-antigenic cells, in line with the known polyreactivity of IgM in general (Nakamura *et al.*, 1988). To test this explanation, we examined self-reactivity of IgM and IgG antibodies from donors before and after vaccination against SARS-CoV-2. As expected, sera from donors after vaccination showed increased IgG binding to spike-expressing cells, but no change in IgG reactivity to untransfected TE 0 cells. IgM, on the other hand, showed increased reactivity to both spike-expressing and untransfected cells (Fig 1B and C). An alternative explanation is that high affinity antibodies of other classes competitively displace the IgM. To test this hypothesis, we used an IgM capture ELISA, in

which serum IgM is first immobilized on a plate, and then, spike-specific IgM detected with a labeled antigen (Fig 1D). Using this approach, all exposed donors clearly showed spike-binding IgM in serum. While the ELISA approach correctly identifies a higher fraction of exposed donors, the flow cytometric comparison between IgM binding to spike-expressing and non-expressing cells makes clear that some of the exposure-induced IgM binding activity is not virus-specific. Our data do not enable us to assess the quantitative tradeoffs between sensitivity and specificity, since this would require a more comprehensive cohort of control sera including donors exposed to other immunogenic pathogens. Infection with Epstein–Barr Virus, for example, has been shown to induce spurious IgM RBD ELISA reactivity (Pickering *et al.*, 2020).

SARS-CoV-2 spike-specific IgM B cells can be isolated by MACACS

The paucity of reports of high affinity, pathogen-specific IgM antibodies in the literature might reflect several factors. It is possible that such antibodies are not made and that the achievement of high affinity through somatic hypermutation and selection is always accompanied by class switch. Alternatively, the non-detection of these antibodies may have a technical cause, for example masking by abundant polyreactive IgM (Nakamura *et al.*, 1988), or the relative difficulty of producing IgM recombinantly (Chromikova *et al.*, 2015).

To address the potential masking of rarer virus-specific IgM B cells by the larger population of polyreactive IgM B cells, we adopted the strategy of membrane antigen capture activated cell sorting (MACACS) described by Zimmermann *et al.* (2019). This technique identifies B cells whose affinity for a membrane protein extracellular domain antigen is high enough that they can extract the protein from the membrane and become activated in the process (Batista *et al.*, 2001). Using capture of mCherry-tagged spike protein as a measure of antigen capture, and CD69 labeling as a marker of activation (Malinova *et al.*, 2021), we assessed the phenotype of spike-capturing B cells in peripheral blood of 3 convalescent donors (Fig 2). Based on the expression of CD19, CD20, CD21, CD27, CD38, CD138, IgM, IgG, and IgA (Appendix Table S4), we assigned

Figure 1. Spike-protein specific antibodies of classes M, G, and A in human serum.

- A Spike-binding antibodies in serum. Binding by antibodies of classes M, G, and A is detected with secondary antibodies conjugated to different fluorochromes, and the results are shown on the left, middle, and right plots, respectively. Binding (geometric mean fluorescence intensity—GMFI—of corresponding secondary antibody) to TE cells expressing SARS-CoV-2 spike protein is plotted on the vertical axis, and binding to untransfected cells on the horizontal axis. Each point represents a value from one donor. Samples from donors with no known exposure to SARS-CoV-2 antigens ($n = 86$) are plotted with blue circles, recently infected donors ($n = 34$) with red circles, and vaccinated donors ($n = 14$) with green diamonds. Red circles with black triangles correspond to donors from whose B cells monoclonal antibodies were isolated ($n = 5$, Appendix Table S2). *P* values are derived from a two-way analysis of variance followed by Tukey's test to compare the specific binding, that is (binding to spike-expressing cells)/(binding to untransfected cells) between conditions (convalescent or vaccinated against unexposed) within each antibody class. The experiment was independently repeated three times, and results shown come from the third replicate.
- B Change in antibody binding following vaccination against SARS-CoV-2. Binding of antibodies from sera assessed in the experiment shown in (A) is shown for two samples of serum from each of 7 donors. Data are plotted as in (A) with binding to spike-expressing cells on the vertical axis, and to untransfected cells on the horizontal, using blue symbols for samples from before vaccination, and red symbols for samples from 15 to 29 days after the first vaccination (but before any second vaccination). Black lines connect points corresponding to pre/post pairs of samples from each donor. Left plot shows results for IgM and right plot for IgG.
- C Comparison of post-vaccination increase in binding to untransfected cells between IgG and IgM. The increase in binding to untransfected TE 0 cells between pre- and post-vaccination samples is shown on the left with blue symbols for IgG and on the right with black symbols for IgM. The horizontal line at $y = 0$ is the expected result when no increased binding is observed. *P* value is derived from a two-tailed, Wilcoxon matched pairs signed rank test.
- D Comparison of spike-specific IgM, as measured by flow cytometry or ELISA. The left two "FC" are the results of flow cytometry, and the left vertical axis shows the ratio of serum IgM binding to spike-expressing cells, vs binding to non-expressing control cells, as plotted in A. The right two columns show spike-RBD-specific IgM as measured by an IgM-capture ELISA, and the right vertical axis shows the optical densities (OD). *P* values are calculated by two-way analysis of variance, followed by Sidak's multiple comparisons test. The entire experiment was repeated three times, and the data shown are derived from the third replicate.

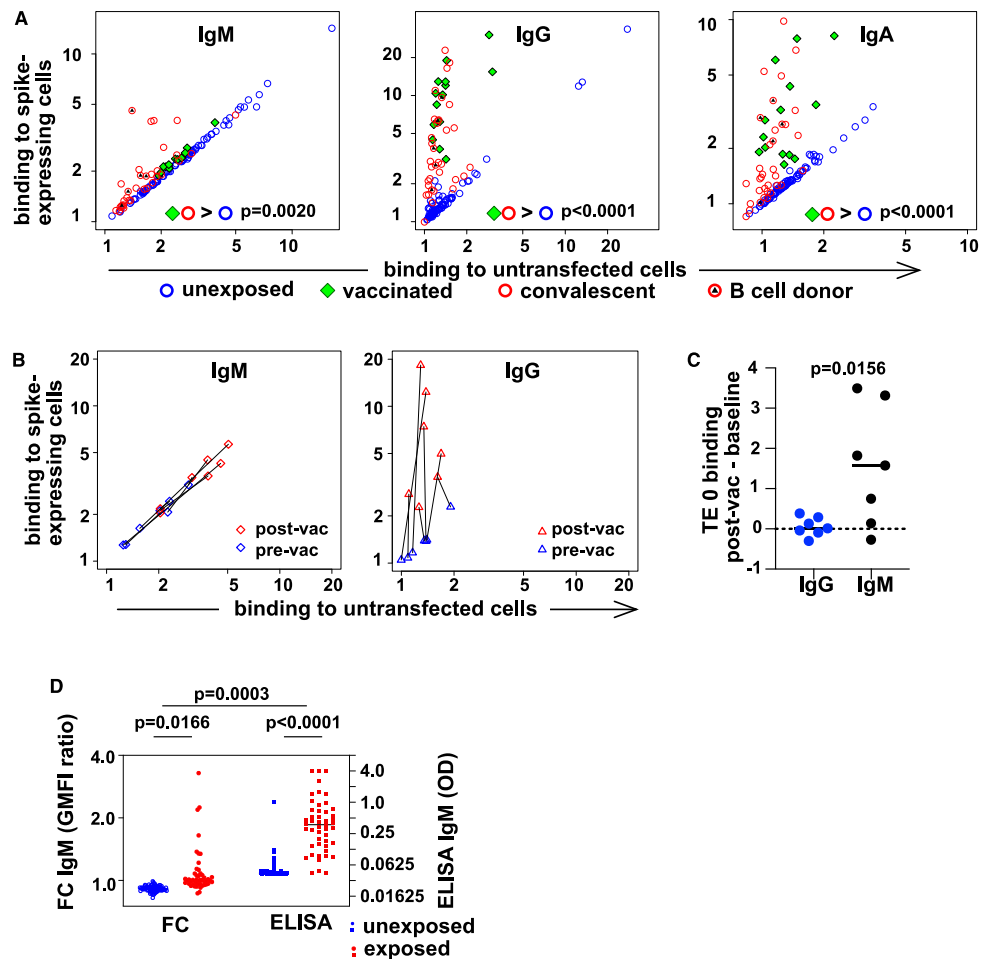


Figure 1.

the B cells to clusters, including memory, naive, and plasma-like (Fig 2A and B). B cells activated by capturing spike protein (Fig 2C) were predominantly memory cells of the IgM and IgG classes (Fig 2D).

To investigate the properties of the antibodies produced by these B cells, we generated monoclonal antibodies from B cells sorted with the same MACAC gate shown in Fig 2C (Fig 2E). 3266 SARS-CoV-2 spike capturing B cells from 5 randomly selected convalescent donors (infected between March and May of 2020) among those with detectable SARS-CoV-2-spike-specific antibodies in serum (Fig 1A and Appendix Table S2) were distributed into single wells of 384-well plates and cultured for 9 days in the presence of IL-21

and CD40 ligand. Resulting single cell supernatants were screened by flow cytometry (Fig 2F) and 326 (79 IgM, 141 IgG and 106 IgA) wells exhibited binding spike-specific binding activity (i.e., ratio of binding to spike-expressing cells divided by binding to control cells) above the threshold of 1.2. Unlike the polyclonal IgM in sera, these monoclonal antibody supernatants were all specific (Fig 2F). It should be noted that while the monoclonal antibodies described here are likely derived mostly from memory cells, while this may not be the case for the soluble IgM in serum.

Feldman *et al* (2021) also reported that spike-specific antibodies cloned from naïve donors exhibited no polyreactivity. One possible reason why we did not observe unspecific binding by the anti-spike

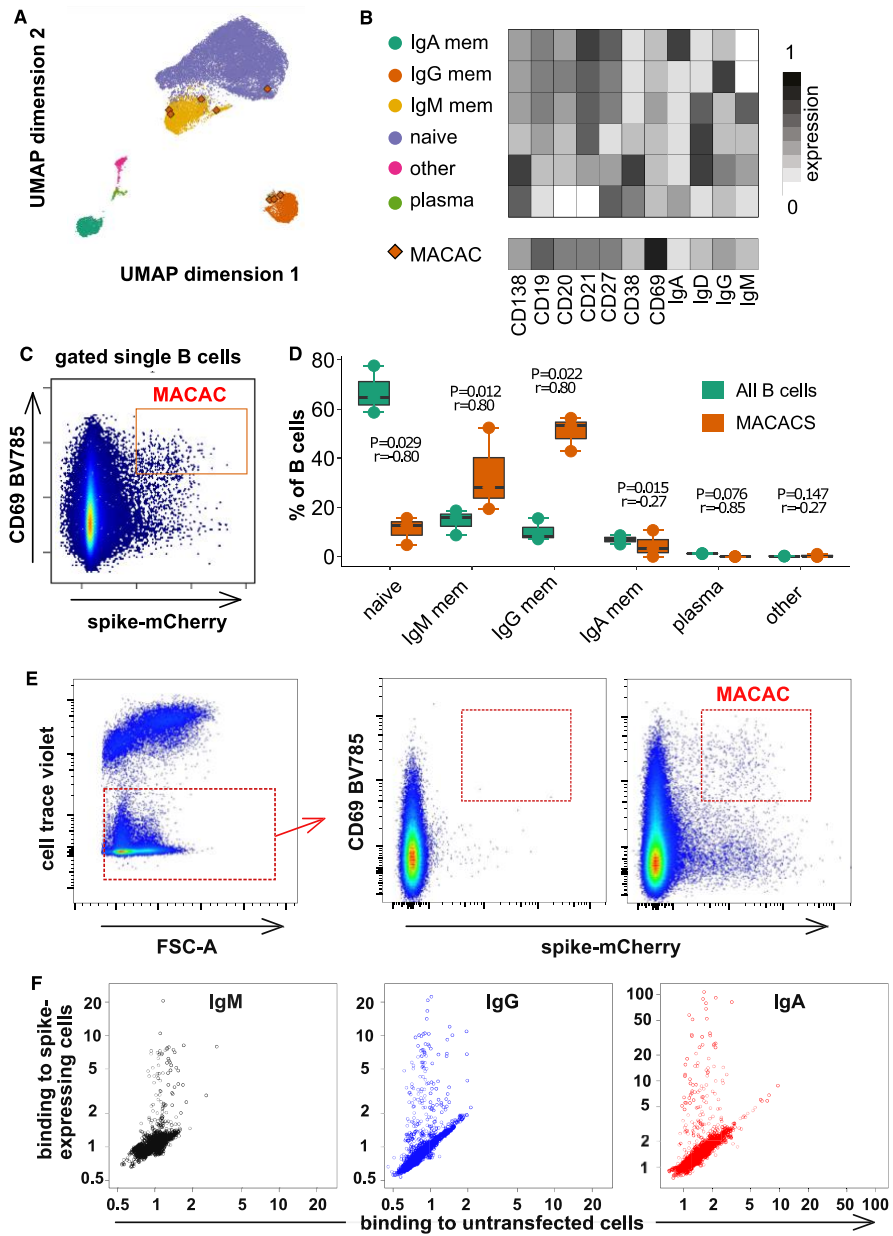


Figure 2.

Figure 2. Spike-capturing B cells from peripheral blood of convalescent donors.

- A Phenotypes of blood B cells. B cells from 15 ml of peripheral blood from each of three convalescent donors were isolated by negative selection with magnetic beads, exposed to adherent cells expressing spike-mCherry for 3 h, then retrieved and labeled with fluorescent antibodies shown in Appendix Table S4 and measured by flow cytometry. (A) UMAP algorithm (5,000 randomly selected cells/sample) was used to depict the major B cell subsets clustered according to marker expression. FlowSOM-based B cell subpopulations are overlaid as a color dimension, and the colors of the clusters are shown on the left of heatmap (B). Cells falling in the MACAC gate (see below) are marked with red rhombi.
- B Heatmap showing mean population expression levels of markers used for UMAP visualization and FlowSOM-clustering. Colors shown in the legend on the left are also used in the UMAP representation in (A).
- C Gating strategy to define CD69-high, mCherry-high, spike-capturing B cells (i.e., membrane antigen capture activated cells, MACAC, red box). Dot plot shows CD69 and mCherry fluorescence for B cells from one of three donors gated by forward and side scatter, and negative for the dye used to mark the antigen donor cells.
- D Relative fractions of different B cell subpopulations, from three donors, as shown in A–B, in all B cells compared to within MACAC B cells. *P* values are based on two-tailed *t*-tests between the groups. Correlation coefficients (*r*) were calculated from the *z*-statistic of the Wilcoxon–Mann–Whitney test. A black horizontal line represents the median. Boxplots represent the interquartile range (IQR). Whiskers extend to the farthest data point within a maximum of 1.5 × IQR. Every point represents one donor.
- E Gating strategy in MACAC sorting. Single cells are selected based on scatter, antigen-expressing TE spike-mCherry cells excluded on Cell Trace Violet label, and the spike-capturing (mCherry-high), activated (CD69-high) B cells (population labeled “MACAC” in red on the right-most plot) are sorted. The middle plot shows B cells that did not adhere to the TE-spike-mCherry antigen-expressing cells (putatively antigen-irrelevant), and the right plot those that did (putatively antigen-recognizing). Plots show data from one of five convalescent donors (those whose serum results are labeled with black triangles in Fig 1A). Cells in the MACAC gate were singly distributed into wells of 384-well plates and cultured for 9 days with IL-21 and CD40L, and then, the single well culture supernatants were screened for anti-spike antibody binding and virus neutralization as described below.
- F Results of single well supernatant screening for antibody binding to SARS-CoV-2 spike protein. Results from 3266 wells from 5 donors are shown for IgM (left), IgG (middle), and IgA (right). Screening and plotting methods are the same as in (Fig 1A).

IgM antibodies lies in the method used for isolating the B cells. Membrane antigen capture requires a higher affinity than is needed simply to bind the antigen (Natkanski *et al.*, 2013). Recently described effective protocols for antigen-specific B cell isolation include negative selection to exclude polyspecific B cells that bind to irrelevant antigens (Robbiani *et al.*, 2020; Thouvenel *et al.*, 2021). MACACS achieves this by positive selection for high affinity.

Monoclonal IgM mediate potent neutralization

Single cell culture supernatants containing antibodies with binding activity against the SARS-CoV-2 spike protein were assessed by measuring their capacity to neutralize VSV*ΔG-S_{Δ21}, a chimeric vesicular stomatitis virus (VSV) expressing the SARS-CoV-2 spike protein. Neutralization of such propagation-competent chimeric viruses has been demonstrated to be highly correlated with neutralization of SARS-CoV-2 itself, and a good readout for spike-binding (Case *et al.*, 2020; Dieterle *et al.*, 2020). Of the 326 supernatants we tested (Fig EV1), 31 showed detectable neutralization of the virus at a dilution of 20 or higher (11 IgM, 14 IgG, and 6 IgA). B cells from wells containing neutralizing antibodies of any of the three classes, and four non-neutralizing antibodies as controls (2 IgG, 2 IgA) were lysed, reverse-transcribed, and their transcriptomes surveyed by RNA sequencing. Immunoglobulin heavy and light genes were extracted bioinformatically then amplified from the original cDNA and recombinantly expressed in the same class as observed in the B cells for testing, yielding 6 IgA, 11 IgG, and 3 IgM. Sequences of heavy and light chains of the antibodies shown in Appendix Table S3 are available in GenBank Accession numbers OM584288-OM584289, and OM687904-OM687941 and in Dataset EV1. We observed virus-neutralizing antibodies of all three classes (Fig 3A–C).

Neutralization of the wild-type SARS-CoV-2 by the six most potent antibodies (3 IgM, 2 IgA, and 1 IgG) was assessed by determining the neutralization dose 50% (ND50), that is, the concentration of antibody at which the probability of a single cell infection event occurring is 50% (Wulff *et al.*, 2012). ND50 values are shown in Fig 3D and range from 36 ng/ml to 679 ng/ml.

IgM-mediated virus neutralization is not explained by complement activation

IgM are the most effective immunoglobulin class in activating complement. It is reported that complement component C1q synergizes with IgG2 antibodies to neutralize West Nile Virus in a mouse system (Mehlhop *et al.*, 2009). We hypothesized that the potency of the IgM antibodies observed in virus neutralization *in vitro* might be enhanced by the complement system. We therefore examined antigen-dependent activation of complement by anti-spike antibodies of 3 classes (Fig 3E). As expected, IgM antibodies were significantly more effective in activating complement than IgG1, and IgA antibodies induced no complement activation, despite comparable antibody binding (Fig EV2A). We next tested neutralization by IgM 2J17 in the presence of complement-sufficient human serum, or serum with the complement system degraded by heat inactivation (Fig 3F). We observed a small enhancement of neutralization in the presence complement-sufficient serum, but this difference was not statistically significant.

Neutralization is dependent on class

We then considered the possibility that the potency of the IgM antibodies might be a result of the higher avidity conferred by the polymeric structure. To test this, we examined the relative binding of antibodies expressed as IgM or IgG1 in a competitive setting. We prepared 3 IgM antibodies 2J17, 2E14, and 3N8 with the same light chains and variable regions of the heavy chains, but with the constant regions switched to IgG1. The artificially class-switched antibodies thus produced maintained the binding specificity of their IgM equivalents when tested individually (Fig EV2A and B). However, when the IgM and IgG were mixed and allowed to bind their target competitively, the IgM versions of each antibody out-competed their IgG partners (Fig 4A), that is, binding of IgG in presence of IgM was significantly lower than in its absence ($P = 0.0101$). Conversely, no effect of competition from the IgG was seen on the IgM. When we tested neutralization by these artificially class-switched antibodies, all

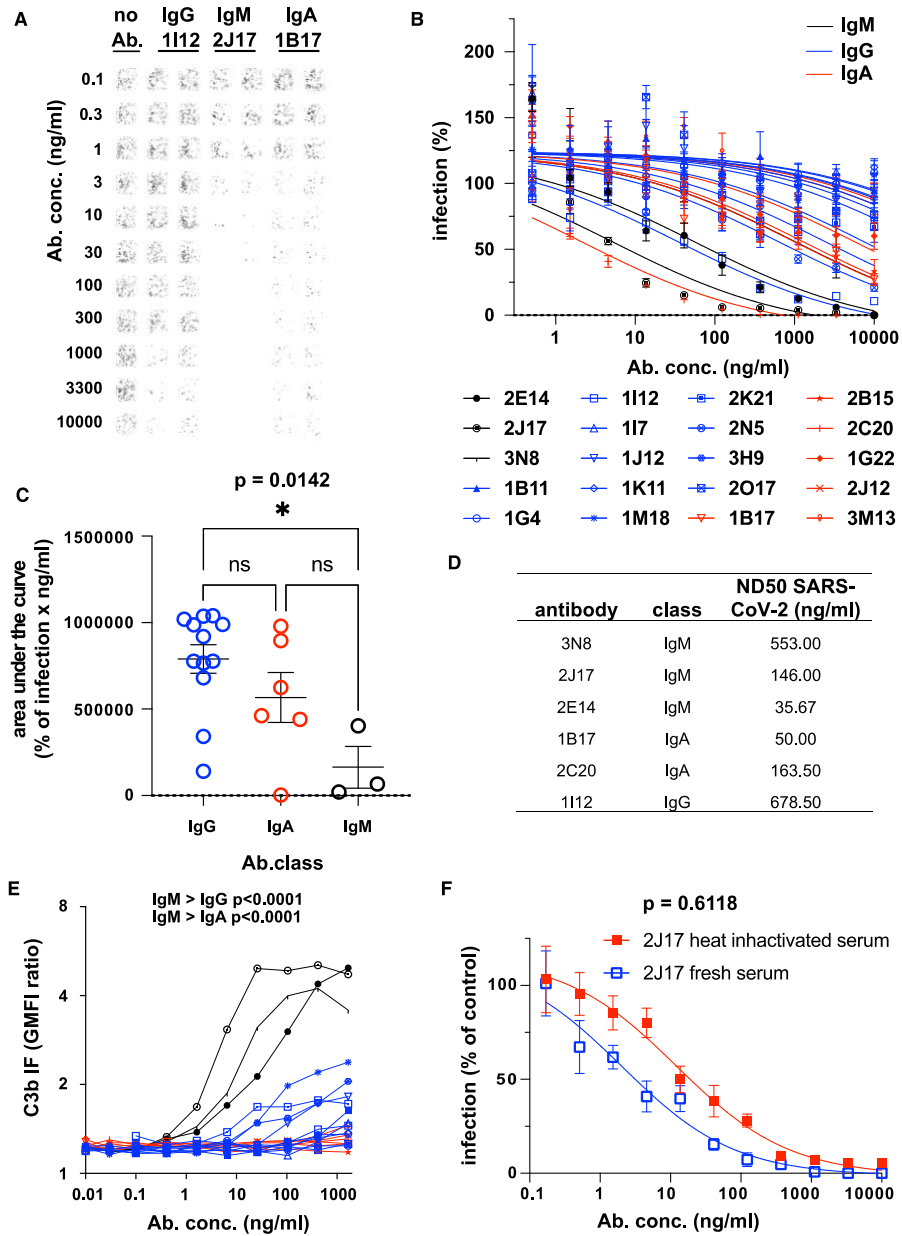


Figure 3.

Figure 3. Native IgM antibodies specific for SARS-CoV-2 spike protein mediate virus neutralization.

- A** Example of neutralization of chimeric VSV*ΔG-S_{Δ21} by donor-derived IgG, IgM and IgA antibodies. 100 pfu VSV*ΔG-S_{Δ21} was mixed with antibody at specified concentrations for 1 h and then added to Vero cells. After 24 h, the cells were imaged and infected wells identified by GFP expression, here pseudocolored with GFP-bright shown in black against a white background. Virus neutralization is manifested as reduction in GFP. Images shown here come from wells infected with virus alone (left column), virus pre-incubated with the moderately neutralizing IgG 1112 (second and third columns), the potent neutralizing IgM 2J17 (fourth and fifth columns), or with the moderately potent IgA 1B17 (sixth and seventh columns). Each antibody was tested in the range of concentrations shown to the left of the images, from 10,000 down to 0.1 ng/ml.
- B** Neutralization curves from each of the cloned antibodies using plaque reduction assay of VSV*ΔG-S_{Δ21}. The horizontal axis shows the serial dilution of the antibodies. The vertical axis shows, for each well exposed to antibody, the ratio of infected cell plaque count to the corresponding value from control wells without antibody. Each point is the mean of 9 values pooled from three independent experiments each with triplicate wells. Error bars indicate standard error. Antibodies tested are listed below the figure and include 3 IgM (black lines and symbols), 11 IgG (blue lines and symbols), and 6 IgA (red lines and symbols).
- C** Quantification of results from (B). Area under the curve is plotted for every antibody and compared between different antibody classes by one-way ANOVA followed by Tukey's test (mean from three biological replicates and SEM). Area under the curve was chosen as a measure of neutralization capacity, rather than ND50 (as used in subsequent figures), because some antibodies included in this figure exhibited no neutralization at the concentrations tested, precluding the calculation of an ND50.
- D** SARS-CoV-2 Neutralization Test. Antibodies that showed neutralization of the chimeric VSV*ΔG-S_{Δ21} were tested for neutralization of wild-type SARS-CoV-2 virus. Concentrations of antibodies needed to neutralize 100 pfu are expressed as ND50 (mean from two independent experiments, each with quadruplicate wells, or 3 independent experiments for 2E14 and 2J17). The ND50 of 2E14 was lower than 2J17 in three independent experiments although this difference was not significant by paired two-tailed t-test ($P = 0.3876$).
- E** Flow cytometric determination of antibody-dependent complement deposition on cells. Cells expressing SARS-CoV-2 spike protein and untransfected control cells were incubated with various concentrations of antibody in the presence of fresh human serum (from a SARS-CoV-2 unexposed donor). Activation of the complement cascade was measured by flow cytometric assessment of complement component C3b deposition on the surface of the cells. Results for the 3 IgM, (black), 11 IgG, (blue), and 6 IgA antibodies (red) are shown. P values were calculated by two-way analysis of variance, followed by Tukey's test.
- F** Influence of complement on virus neutralization. A plaque reduction neutralization assay like that shown in Fig 3A–C was conducted with IgM 2J17 in the presence of either fresh, complement-sufficient human serum, or heat-inactivated serum. The concentration of 2J17 is shown on the horizontal axis. The vertical axis shows, for each well exposed to antibody, the ratio of infected cell plaque count to the corresponding value from control wells with serum (either fresh or inactivated) but without antibody. The points plotted with filled red symbols corresponds to the condition with heat-inactivated serum, and the open blue symbols results with fresh serum. Each symbol corresponds to the mean of nine wells pooled from three independent experiments, each with triplicate wells. Error bars correspond to standard error. P value was calculated using a paired, two-tailed t-test.

three previously virus-neutralizing IgM antibodies lost neutralizing ability when expressed as IgG1 (Fig 4B and C).

If the greater neutralization potency of IgM is due to the avidity advantage of their multimeric structure, then the same advantage ought to be gained by switching a weakly neutralizing IgG or IgA to IgM. We tested virus neutralization by IgG 1112, and 2 IgA 2C20 and 1B17, all artificially switched to IgM (Fig 4D). Results were heterogeneous, with 2 antibodies slightly increasing in potency, and one losing potency, although none of these changes was statistically significant.

Early studies of recombinantly produced human monoclonal antibodies (Tiller *et al*, 2008) often involved switching of IgM antibodies to IgG for recombinant production and testing, and this approach has been employed by the few workers to study the properties of IgM antibodies against SARS-CoV-2 (Feldman *et al*, 2021; Wang *et al*, 2021). Our results make clear that this exchange is likely to have a dramatic effect on their functional properties. Wang *et al* (2021) successfully isolated a large number of RBD-binding monoclonal antibodies of IgM, IgG, and IgA classes; the IgG and IgA included several highly potent neutralizing antibodies, but the IgM,

Figure 4. Class dependency of neutralization by spike-specific IgM.

- A** The effect of competition on concentration versus binding curves of three spike-specific, class-switched antibodies. Antibodies were expressed either as IgM, as originally isolated (black symbols and lines), or artificially switched to IgG1 (blue lines and symbols). For each antibody, identified by name at the top of each plot, the binding of the antibody alone ("alone", open symbols), or the competitive binding of the antibody in a mixture of IgM and IgG1 ("compet.", filled symbols) is shown. In the competition scenario, each of the two classes of the antibody were added together at the concentration shown on the horizontal axis. The vertical axis shows the ratio of geometric mean fluorescence of human IgM, or IgG on spike-expressing cells divided by the corresponding signal on spike-non-expressing control cells. Each point shows the mean of 3 values from three independent experiments. Error bars show standard error. P value was calculated by comparing the area under the curve of each antibody class in the "alone" condition with the binding of the "competition" condition by paired, two-tailed t-test.
- B** Virus neutralization by antibodies expressed as IgM or IgG1. A plaque reduction neutralization assay as described in Fig 3A and B was used to measure neutralization by the three, donor-derived IgM (black lines and open symbols) and their artificially class-switched IgG1 equivalents (blue lines and filled symbols). Horizontal axis shows the antibody concentration and the vertical axis shows the level of infection expressed as percentage GFP expression compared to control wells with no antibody added. Each point shows the mean of nine replicate values pooled from three independent experiments, each with triplicate wells. Error bars show standard error.
- C** Comparison of virus neutralization by antibodies expressed as IgM or IgG1 shown in B. Area under the curve was calculated from each of the three independently performed experiments. P was calculated by paired, two-tailed t-test.
- D** Affinities of donor-derived spike-binding IgG1 ($n = 8$) and donor-derived IgM ($n = 3$) expressed as IgG1, measured by surface plasmon resonance. P value was calculated by unpaired two-tailed t-test. The K_d derived from each antibody measurement are shown in Appendix Table S5. Sensograms of each tested antibody are shown in Fig EV2.
- E** Virus neutralization by antibodies artificially class switched from IgA or IgG1 to IgM. A plaque reduction neutralization assay as described in Fig 3A and B was used to measure neutralization by the two donor-derived IgA (pink and light blue lines) and one donor-derived IgG (Bordeaux lines). The antibodies expressed in their original classes (IgA or IgG) are plotted with filled symbols of the same colors as the lines, and their artificially class-switched IgM equivalents are plotted with open symbols. Horizontal axis shows the antibody concentration and the vertical axis shows the level of infection expressed as percentage GFP expression compared to control wells with no antibody added. Each point shows the mean of nine replicate values pooled from three independent experiments, each with triplicate wells. ND50 was calculated from each of the three independently performed experiments. P was calculated by paired, two-tailed t-test for each antibody pair.

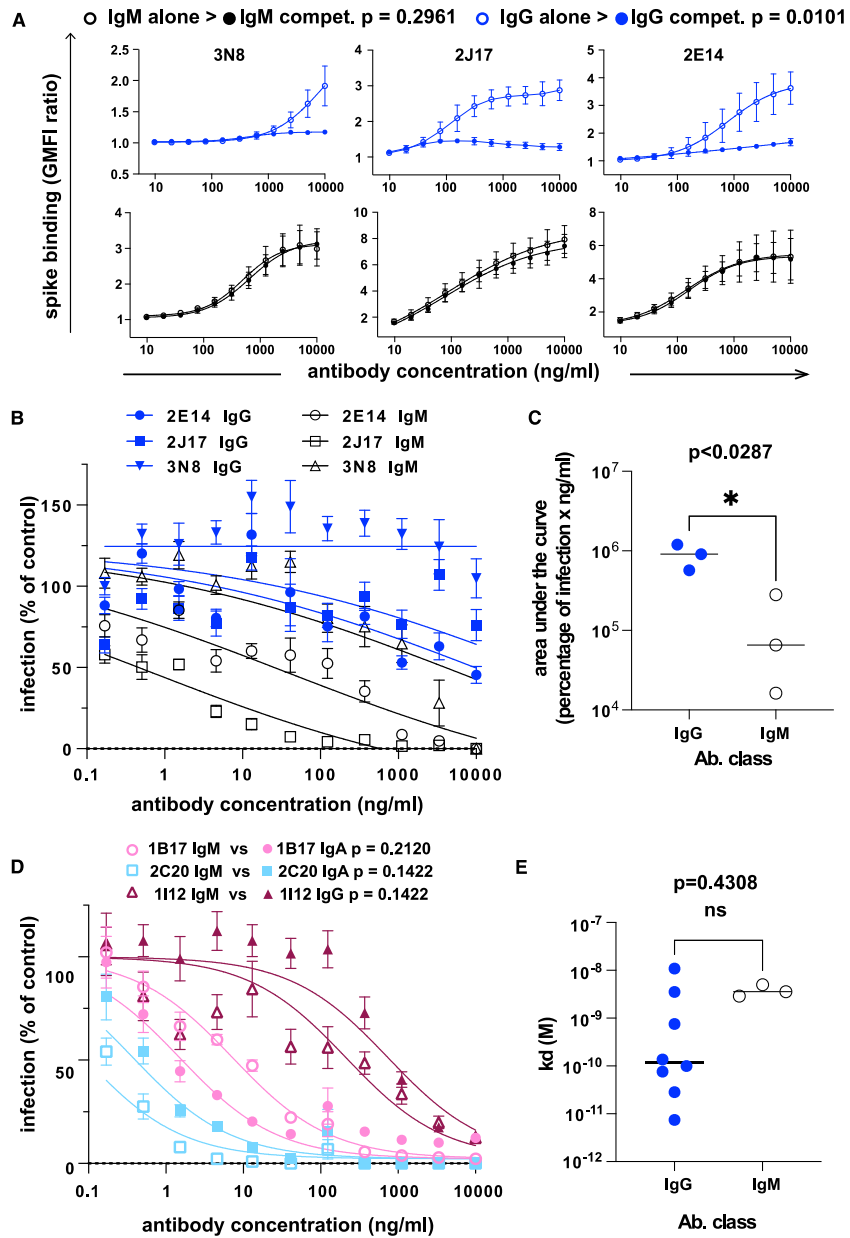


Figure 4.

which were expressed as IgG1 after artificial class switch were fewer and less potent. This is the opposite of what we observed when expressing the antibodies in their native classes. Thouvenel *et al* (2021) also observed that IgM antibodies against Plasmodium parasites lost their potency if converted to monomeric IgG. An obvious question is what the mechanistic basis for this IgM class-dependent potency might be. Thouvenel *et al* (2021) ascribe the effect of IgM to IgG class switch partly to the reduction in avidity caused by the reduction in valency, and partly to other factors, for example, enhanced steric blockade or epitope accessibility. Either conformational influence of the Fc region on the paratope (Janda *et al*, 2012), or the effect of Fc region flexibility on the ability of the antigen-binding domains to access the epitope (Tobita *et al*, 2004) might influence antigen binding.

We are not aware of any other studies of natively expressed, natural IgM monoclonal antibodies in human SARS-CoV-2, but the

phenomenon may be relevant in other contexts. Shen *et al* (2019) isolated two influenza-neutralizing antibodies from influenza virus-infected mice 7G6-IgM and 3G10-IgM. When made into a chimeric antibody with human IgG1 constant regions, the potency of the more potent antibody 7G6-IgM fell by around 100-fold, while the less potent 3G10-IgM did not change significantly. The IgM version also offered better *in vivo* protection against challenge with various influenza strains than did the IgG version.

Affinity of IgM variable regions is at lower end of the range shown by IgG

To directly measure binding affinities of antibodies of different classes, we used surface plasmon resonance (SPR) to measure the affinities of the 3 IgM (2E14, 2J17, 3N8) and 8 antibodies originally isolated as IgG. To eliminate the confound of valency, all 11

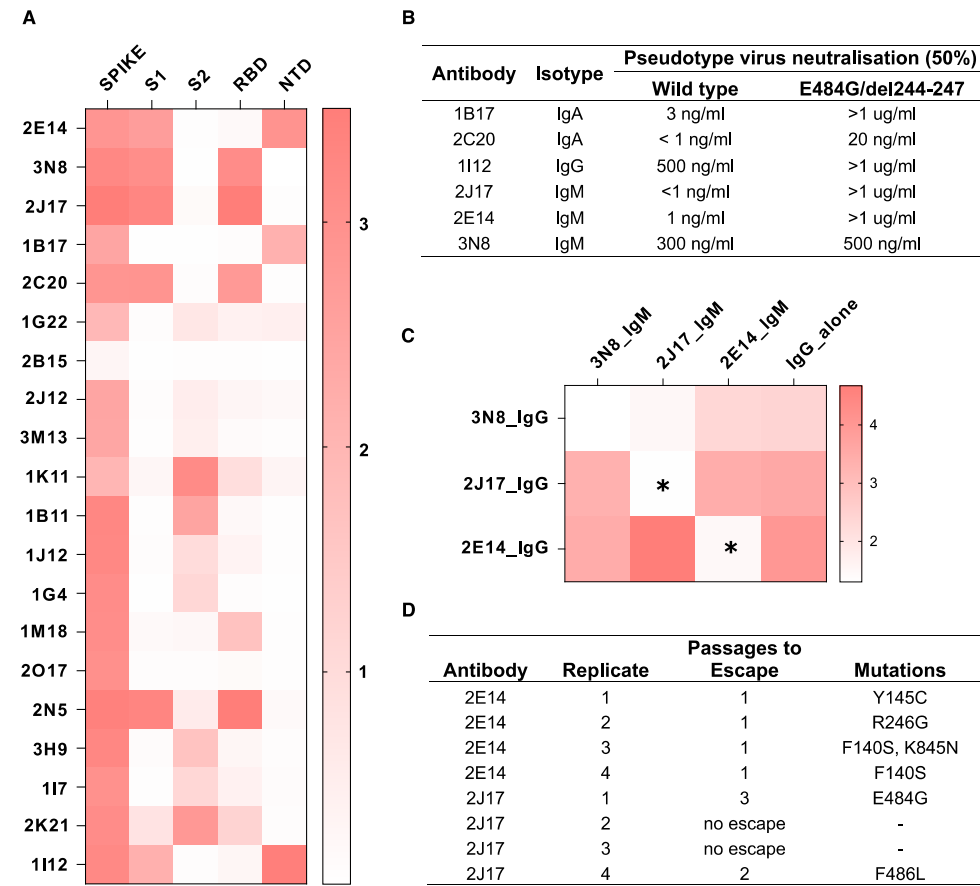


Figure 5.

Figure 5. Epitopes recognized by spike-binding antibodies.

- A** Heatmap of antibody binding to spike protein subdomains (complete spike extracellular domain "spike", S1, S2, RBD and NTD) in ELISA. Color gradient shown on right represents optical density at 450 nm (OD). Values are mean OD from two independent experiments. Analogous ELISA results for 3 IgM and their IgG1-class-switched derivatives are shown in Fig EV2B.
- B** Susceptibility of different neutralizing antibodies to spike protein mutations. A neutralization assay was performed with 3 IgM, 1 IgG and 2 IgA using VSV Δ G(Fluc) pseudotyped with wild-type (wt) spike protein or with spike variant harboring the deletion of amino acids 244–247, located in the NTD, and the substitution E484G, located in the RBD, from a SARS-CoV-2 isolate from an immunosuppressed COVID-19 patient (del244-247/E484G). ND50 values were determined from quadruplicate wells, from an experiment performed once. Neutralization curves are shown in Fig EV4.
- C** Flow-cytometric epitope binning of monoclonal IgM, utilizing competitive displacement of IgG by IgM with identical variable region (as shown in Fig 4A). Cells expressing SARS-CoV-2 spike protein and untransfected control cells were incubated with each of 3 neutralizing IgM antibodies artificially switched to IgG1, either alone, or mixed with one of the 3 antibodies expressed as IgM. The binding of each IgG1 alone is shown in the last column of the heatmap, and in competition with each other IgM in columns 1–3. Color shade represents the specific IgG binding (ratio of GMFI on TE spike-mCherry cells to TE 0 cells). Values are mean GMFI ratios from three independent experiments. When IgM binds the same epitope as the IgG (automatically the case when the source antibody is the same), the IgM will displace the IgG, resulting in a reduction in the IgG signal. Asterisks mark those combinations of antibodies with a statistically significant decrease in binding of the IgG1 in the presence of IgM, compared to the IgG alone across 3 independent experiments, ($P < 0.05$, two-way analysis of variance, followed by Tukey's test).
- D** Summary of escape mutations induced by potent neutralizing IgM 2E14 and 2J17. Vero cells in 24-well plates were infected with VSV Δ G-S Δ 221, in the presence of serial dilutions from 10 μ g per ml of neutralizing antibody (or without antibody as control), and 2 days later, virus from the well containing the highest concentration of antibody that still showed some virus proliferation was used to infect fresh wells of Vero cells, again in the presence of antibody in a serial dilution. The process was repeated for three passages, and at the last passage, the cells were lysed, RNA extracted, reverse transcribed and sequenced, and consensus spike gene reads extracted and aligned against the reference SARS-CoV-2 genome MN908947.3. The table shows de novo amino acid mutations that arose in each of four replicates with each of the two neutralizing antibodies, as well as the number of passages needed for the escape mutant to emerge. In two of the replicates with 2J17, no escape was observed. Consensus sequences of spike genes from each replicates and from control wells with no antibody added are shown in Dataset EV2.

antibodies, regardless of original class, were expressed as IgG1. We initially used whole spike protein as target antigen, but some antibodies failed to bind this antigen in the SPR apparatus, and for these, we used the subdomain of the protein bound by that antibody (see results below on epitope specificity). Antibodies originally isolated as IgG had a wide range of K_d from 28 pM to 11 nM. When expressed as monomeric IgG1, affinities of the antibodies originally isolated as IgM were at the lower end of this range, with the highest affinity for 2E14 at $K_d = 2.89$ nM (Fig 4E, Appendix Table S5 and Fig EV3). The one neutralizing IgG that we isolated, 11I2, had an affinity below that of the IgM-derived antibodies, suggesting that it is not because of inadequate monomeric affinity that the IgM antibodies fail to neutralize when switched to IgG.

The monomeric (i.e., bivalent) affinity of the recombinant antibodies is relevant to the question regarding the antibodies described here is whether they are representative of those that are secreted *in vivo*. To obtain T cell help, necessary for a high affinity antibody response, a B cell must not only bind an antigen, but internalize it for processing and presentation. The dependence of this mechanism on antigen affinity was well established by Batista and Neuberger (1998), Batista and Neuberger (1998). Although an IgM antibody can achieve enhanced avidity by virtue of higher valency, this effect is thought not to be relevant to B cell activation, because the monomeric affinity of the BCR is thought to be the parameter that determines BCR signaling and antigen uptake (Natkanski *et al*, 2013). We propose that an important advantage of the MACACS technique is the specific identification of those B cells whose monomeric BCR affinity for the target antigen is high enough to enable BCR signaling, antigen uptake, and presentation, and thereby the acquisition of T cell help and differentiation into plasma cells. The fact that the neutralizing IgM we examined would have been functionally impaired if secreted as IgG raises the question of how a B cell avoids premature class switch. The results shown here suggest that a B cell ought not to switch from IgM to IgG until it has achieved a certain affinity through maturation, but do not explain how this decision is made. One attractive idea is that the soluble, high avidity IgM might out-compete IgG of a similar monomeric affinity, thereby forcing the

evolution of B cells with higher affinity BCR, as suggested by Zhang *et al* (2013). The opposite perspective is that beneficial antibodies can be produced in the IgM class even by B cells whose monomeric BCR affinity is modest. By this logic, to make the decision whether to become activated in response to an encountered multivalent antigen, a B cell ought to probe the antigen with multiple BCR, and integrate the signals. This may be one function of the spreading and contraction response of B cells (Fleire *et al*, 2006) on which the MACACS technique is based. Such multi-BCR antigen scanning would offer an alternative mechanism for class-appropriate affinity testing, if the signal required for plasma cell differentiation and antibody secretion were to have a higher threshold for class-switched B cells than for IgM B cells.

The results described here do not enable us to determine the mechanistic basis for the class-dependent potency of 2J17 and 2E14. Competitive displacement of IgG by IgM with the same variable region is consistent with the widely postulated higher avidity of IgM, but since the measured affinities of the IgG1 derivatives of the neutralizing IgM have affinities similar to the neutralizing IgG 11I2, the reduction of avidity caused by class switch cannot be the only factor. Similarly, the effects of Fc region on the paratope, and epitope accessibility are hypothesized to affect binding, and therefore by the same logic are insufficient to explain the loss of neutralization. Yet another possibility is a post-entry mechanism involving signaling of the attached antibody to the infected cell (Green *et al*, 1992).

Neutralizing IgM target RBD and NTD

Precise binding specificity to the spike protein was investigated by ELISA using recombinant subdomains as antigen. Binding of each of the 3 IgM, 6 IgA, and 11 IgG to the whole spike extracellular domain, the S1 and S2 subdomains, the N-terminal domain (NTD) and the receptor-binding domain (RBD) are shown as a heatmap in Fig 5A. One IgA (2B15), despite showing replicable binding to spike-expressing cells, showed no binding to any of these antigens in ELISA, an observation also made by Wang *et al* (2021) (Wan

et al., 2020). All antibodies identified as neutralizing recognized either the RBD or the NTD. We examined the impact of mutations in these domains by measuring neutralization of a virus pseudotyped with the spike protein of a clinical SARS-CoV-2 isolate with mutations in NTD (del244-247), and the RBD (E484G) (Figs 5B and EV4) (Weigang *et al.*, 2021). Neutralizing potency of the RBD-binding IgM 2J17 and the NTD-binding IgM 2E14 both fell to below the detection limit of ND50 > 1 µg/ml when confronted with the mutated spike protein. The effect of the mutations on the RBD-binding IgA 2C20 was much more modest, retaining an ND50 of 20 ng/ml. We compared the epitope specificities of the IgMs with one another by a flow cytometric method exploiting the effect shown in Fig 4A, that IgM can competitively displace their IgG equivalents with the same variable domain (Fig 5C). Spike-expressing cells labeled with mixtures of IgM and IgG showed reduced binding of IgG in the presence of IgM of the same specificity. IgM 2E14 had no effect on binding of either 2J17 or 3N8 confirming that 2E14 binds an independent epitope. The potency of 2E14 and 2J17 enabled investigation of their fine epitope specificity by escape mutation studies. We passaged the chimeric virus VSV*ΔG-S_{Δ21} in the presence of each of the neutralizing antibodies until escape was observed and then sequenced the spike genes (Fig 5D, Dataset EV2). IgM 2E14 induced mutations in the NTD at residues F140, Y145, and R246. 2J17 suppressed escape in some replicates completely, but where escape occurred, the mutations were located in the RBD at residues E484 and F486.

In terms of their epitope specificity, 2J17 and 2E14 seem to function like numerous reported neutralizing IgG, by binding the region around E484 in the RBD, and the supersite in the NTD, respectively. Mutations of E484 are well known to mediate escape from neutralizing antibodies and are present in the beta and gamma variants of the virus (Harvey *et al.*, 2021). The mutation E484K is selected by the neutralizing antibody C121, which uses the same VH gene 1-2 used by 2J17 (Robbiani *et al.*, 2020; Weisblum *et al.*, 2020). The combination of mutations at F140 and R246 is characteristic of escape from antibodies binding the NTD antigenic supersite described by McCalum *et al.* (2021). The structures of the antibodies are not obviously typical of reported anti-spike antibodies; neither of them uses a VH gene identified as over-represented in RBD-binding antibodies by Robbiani *et al.* (2020), although the KV1-33 used by 2J17 was also over-represented in this sample. The CoV-AbDab database (Raybould *et al.*, 2021) of SARS-CoV-2-related antibodies includes two examples of antibodies with the same combination of VH and VL genes used by 2J17 and 2E14, namely C004 described by Robbiani *et al.* (2020), and COVA2-26 described by Brouwer *et al.* (2020), respectively. The antibodies in the CoV-AbDab database with the highest degree of CDRH3 similarity to 2J17 and 2E14 have only 53% and 25% identity, respectively, offering no evidence that these two antibodies are part of an identified public clonotype.

Our study makes clear that the influence of isotype must be considered when investigating the properties of naturally produced antibodies. The powerful influence of class on neutralization we observed here was unexpected, but other important functions of antibodies are known to be class- and subclass-dependent. The influence of antibody class on complement activation, for example, is well established (Lu *et al.*, 2018). Antibodies of different classes also affect the immune system via class-specific Fc receptors in different ways (Boudreau & Alter, 2019; Zohar *et al.*, 2020). Using

membrane antigen capture to identify high affinity antigen-specific B cells reveals properties of IgM in acute infection that may previously have been obscured by abundant polyreactive B cells and antibodies. The next challenge will be to develop assays that visualize the complex, class- and specificity-dependent interactions of antibodies with the rest of the immune system, that are nonetheless simple enough to be used at revealingly high throughput.

Materials and Methods

Blood samples

Serum and blood samples were donated by consenting convalescent, vaccinated, or unexposed donors. A subset of the donors, including all those from whom B cells were taken for monoclonal antibody isolation, were recruited as part of a trial of convalescent plasma donation as a therapy for COVID-19. Vaccinated donors all received the Moderna COVID-19 mRNA-1273 vaccine, and donors designated “fully vaccinated” received two doses. The project was reviewed and authorized by the Ethikkommission Nordwest und Zentralschweiz, Project Number 2021-00961. Blood for cell isolation was collected in S-Monovette tubes (S-Monovette® K3 EDTA, 7.5ml, REF 01.1605.100) with EDTA. Blood for serum was collected in S-Monovette tubes (S-Monovette® Serum, 7.5 ml, REF 01.1601.100) and allowed to coagulate for 1 h at room temperature. Serum was separated from coagulated blood by centrifugation at 2,000 g at 20°C, and stored at -20°C until use. Peripheral blood mononuclear cells (PBMC) were separated from EDTA-treated blood by density gradient centrifugation over Lymphoprep (Axon Lab, D015644) according to the manufacturer's instructions, mixed with 90% fetal calf serum (FCS) and 10% dimethyl sulfoxide, frozen in an isopropanol-containing freezing box at -80°C and then stored in or over liquid nitrogen until use.

Biosafety

Experiments with pseudotyped, vesicular stomatitis-derived virions were conducted in the University of Basel at Biosafety level 2. Experiments involving live SARS-CoV-2 were conducted at the Institute for Virology and Immunology in Middelhäusern, Switzerland, at BSL3, under permits from the Bundesamt für Gesundheit (Swiss Federal Health Department).

SARS-CoV-2 spike protein and cell lines

A sequence-optimized DNA fragment encoding the SARS-CoV-2 spike protein (uniprot accession number P0DTC2) was cloned into the pcDNA6 plasmid between HindIII and EcoRI sites. This fragment was amplified by PCR and fused in frame with mCherry by cloning into pcDNA3 mCherry LIC cloning vector (a gift from Scott Gradia, Addgene plasmid # 30125). This plasmid was used to prepare the cell line TE spike-cherry by transfection with jetPrime (Polyplus, PPLU114-15), and selection with 0.5 µg/ml puromycin. pCMV3 encoding human CD40 ligand was purchased from Sino Biological (HG10239-UT). Transfected TE 671 cells were grown under hygromycin selection, sorted for CD40L expression using PE-conjugated mouse anti-human CD154 (BD Pharmingen, 557299), irradiated at 72 Gy for mitotic inactivation, and kept frozen in liquid nitrogen

until use. Vero cells were a gift from Daniel Pinschewer. TE 671 cells were purchased from ATCC (LGC, Wesel, Germany, CRL-8805) and were cultured following the manufacturer indications. Suspension serum-free FreeStyleTM293-F cells (Life Technologies) cultured in FreeStyleTM293 Expression Medium (Life Technologies) were grown in 125 ml sterile Erlenmeyer flasks with vented caps at densities between 300,000 and 500,000 viable cells/ml, rotating at 135 rpm on an orbital shaker platform. Cells were tested for mycoplasma contamination yearly.

SARS-CoV-2 IgM-capture ELISA

Serum IgM reactivity against SARS-CoV-2 was assessed using WANTAI SARS-CoV-2 IgM ELISA (WS-1196) according to the manufacturer's instructions. Briefly, microwell strips pre-coated with antibody directed against human IgM were incubated with 1:10 diluted human serum, washed five times, then incubated with HRP-conjugated SARS-CoV-2 spike protein RBD antigen, and developed after five washes using the chromogen solution. The reaction was stopped with sulfuric acid, and plates were read at 450 nm immediately after stopping.

Monoclonal antibody ELISA

384-well plates were coated with goat anti-human IgG (Southern Biotec, 2014-01), anti-human IgM (Southern Biotec, 2023-01), or anti-human IgA (Southern Biotec, 2053-01) antibodies overnight at 4°C, then washed once with PBS and blocked with PBS-1% BSA at room temperature for 90 min. Plates were then washed three times with PBS 0.05% Tween, incubated with 15 µl of serially diluted samples for 2 h at room temperature, washed three times with PBS 0.05% Tween, and incubated with anti-IgG-HRP (Southern Biotec 2014-05), anti-IgM-HRP (Southern Biotec 2023-05), anti-IgA-HRP (Southern Biotec 2053-05), or goat anti-Ig-HRP (Southern Biotec, 2010-05) in PBS-0.1% BSA for 1 h at room temperature. Plates were then washed three times with 80 µl/well of PBS-0.05% Tween and developed with TMB ELISA substrate (SureBlue Reserve TMB Microwell Peroxidase Substrate, REF 53-00-00) until a blue color was visible; the reaction was stopped with sulfuric acid and plates were read at 450 nm immediately after stopping.

Assessment of spike subunit specificity by ELISA

Spike subunit ELISA was based on the method described by Rodda *et al.* (2021). 96-well plates (Corning) were coated with 2 µg/ml of recombinant SARS-CoV-2 S1+S2 (Sino Biological 40589-V08H4), SARS-CoV-2 S1 (Sino Biological 40591-V08H), SARS-CoV-2 S2 (Sino Biological 40590-V08H1), SARS-CoV-2 RBD (Sino Biological 40592-V08H), or SARS-CoV-2 NTD (Sino Biological 40591-V49H) diluted in PBS and incubated at 4°C overnight. Plates were washed with PBS-T (PBS containing 0.05% Tween-20) and blocked in 2% BSA for 1 h at 37°C. Monoclonal antibodies diluted at 10 µg/ml in 0.1% BSA were added and incubated at 37°C for 1 h. After washing three times in PBS-T, secondary antibodies diluted in 0.1% BSA were added to the wells. Secondary antibodies used were: anti-human IgG-HRP (Southern Biotec 2014-05), anti-IgM-HRP (Southern Biotec 2023-05), anti-IgA-HRP (Southern Biotec 2053-05). Plates were incubated with secondary antibodies for 1 h at 37°C. Plates were then washed three

times with PBS-T and developed with TMB ELISA substrate (SureBlue Reserve TMB Microwell Peroxidase Substrate, REF 53-00-00) until a blue color was visible; the reaction was stopped with sulfuric acid and plates were read at 450 nm immediately after stopping.

Spike-specific B cell isolation by MACACS

MACACS was conducted as described by Zimmermann *et al.* (2019), adapted to isolated B cells specific for the spike protein of the SARS-CoV-2 virus. PBMC were thawed and rested for 1 h in RPMI-10 at 37°C, and then, B cells were isolated from with the Pan B cell isolation, human kit (Miltenyi, 130-101-638). B cells were then added to an adherent layer of TE spike-cherry that had been prelabelled with 5 µM of Cell Trace Violet (Invitrogen, C34557). After 20 min, non-adherent B cells were washed away gently, and the cells adhering to the cell layer were incubated at 37°C for a further 160 min. B cells were then vigorously washed off with DPBS, collected by centrifugation, labeled with Brilliant Violet 785-conjugated anti-CD69 antibody (Biolegend 310932) and sorted in a flow cytometric cell sorter (BD SORP Aria III), using the gating strategy shown in Fig 1D. Sorted mCherry-high, CD69-high B cells were cultured in 384-well plate wells at an average density of 0.9 cells/well, in RPMI with 40% FCS, 0.05 ng/µl IL-21 (Gibco, PHC0215), together with 50,000 irradiated TE CD40L cells/well. After 9 days of culture, 15 µl of supernatant was withdrawn from each well and screened for spike-binding antibodies as described above. B cells from positive wells were lysed in 20 µl of 15 mM Tris-HCl, pH 8.0 containing 0.5 U/µl of recombinant murine RNase inhibitor (NEB, M0314L). RNA was extracted from this lysate by Zymo Quick-RNA microprep kit (R1050 & R1051), and reverse transcribed with the SMART-Seq v4 Ultra Low Input RNA Kit for Sequencing (Takara, 634888). One hundred nanograms of the thus generated cDNA was used to prepare sequencing libraries with the DNA prep kit (Illumina). The libraries were sequenced paired-end 150 bp on a NextSeq 500 sequencer (Illumina) yielding an average of one million reads per lysate. Reads mapping to immunoglobulin gene sequences were extracted from the resulting single-cell transcriptomes with a custom script in R (Dataset EV3 and 4), using packages Shortread (Morgan *et al.*, 2009) and Biostrings, reassembled with EZassembler (Masoudi-Nejad *et al.*, 2006), and assigned to V(D)J genes using IgBLAST (<https://www.ncbi.nlm.nih.gov/igblast/>).

Flow cytometric characterization of the mCherry-capturing and CD69-high MACAC population was based on the MACACS procedure with three modifications. Non-adherent B cells were not removed after 20 min; in addition to the anti-CD69 antibody, cells were labeled with the cocktail of fluorescently labeled antibodies specified in Appendix Table S4 and instead of sorting, fluorescent signals were analyzed on an LSRFortessa cytometer (BD Biosciences). Single B cells were gated and transformed as previously described (Galli *et al.*, 2019; Diebold *et al.*, 2022). Briefly, data were transformed using the arcsinh function of the R environment. Cofactors were automated determined using the FlowVS package. Percentile normalization was then applied ranging from 0.01th and 0.999th percentile. Clustering and meta-clustering were performed using the FlowSOM package, using following parameters: IgA, IgG, CD38, CD27, CD20, IgM, CD21, CD138, IgD. A UMAP was built using the same parameters (n_neighbors = 50, min_epochs = 200, min

dist = 0.1). MACACS cells were defined as B cells expressing CD69 > 0.7 and mCherry > 0.5. All plots were drawn using ggplot2.

Cloning and production of recombinant antibodies

Based on the deduced heavy and light chain sequences, two pairs of primers were designed to target the 5' untranslated regions of the V gene, and the 3' untranslated region of the constant regions (Appendix Table S6). The heavy and light chains were amplified from the same single-cell lysate-derived cDNA used for sequencing by one round of PCR using Phusion polymerase (NEB, M0530S) with 25 cycles, following the manufacturer's instructions. Light and heavy chain amplicons were cloned into the MCS1 and MCS2 sites of the pVITRO hygro dual expression plasmid (Invivogen, pvitro1-mcs), and the resulting plasmids transfected into Freestyle HEK cells (Invitrogen, R79007). On the day of transfection, each 125-ml flask containing 14 ml of cells at 1×10^6 viable cells/ml was transfected with pVITRO hygro dual expression plasmid expressing the heavy and the light chain of each of the recombinant antibodies, using 293-ectin Transfection Reagent (Gibco, 12347019) according to the manufacturer's instructions. 24 h post-transfection, hygromycin B (50 µg/ml) was added to transfected cells, which were then maintained in culture under selection for 2 weeks at densities between 3×10^5 and 5×10^5 viable cells/ml. Cultured supernatants were harvested after 16 days, centrifuged at 2,000 g for 20 min, passed over 0.45 µm filters (Sartorius). Cell supernatants were buffer-exchanged into PBS using Amicon Ultra 15 50-K columns (Sigma, UFC905024) following the manufacturer's instructions, and the resulting antibody-containing supernatants were stored at 4°C or at -20°C until use. Recombinant antibodies were quantified by ELISA.

In vitro class switch

To switch the immunoglobulin expression plasmids from mu to gamma, we fused the variable region of the heavy chain to the gamma 1 constant region by a two-step fusion PCR with the primers shown in Appendix Table S7. In the first step, we amplified the variable region of the heavy chain from the pVITRO expression plasmid with a forward primer in the plasmid backbone (pVITRO_MCS2_for_out) and a reverse primer whose first 24 bases are complementary to the 5' end of the gamma 1 constant region, and whose last 19 bases are complementary to the 3' end of the J gene (J gene specific, e.g., IGJH4_Gcon_fus_rev). At the same time, we amplified the gamma 1 constant region from a pVITRO expression plasmid encoding an IgG1 antibody, using the primer pair (gamma1_constant_for and pVITRO_MCS2_rev_out). In the second step, we fused these two products, using 10 ng of each purified first step product as template, a forward primer matching the pVITRO backbone just 5' to the MCS2 cloning site (pVITRO_MCS2_for_in), and a reverse primer complementary to the pVITRO backbone, just 3' to the MCS2 cloning site (pVITRO_MCS2_rev_in). The fused product was cleaned with Macherey Nagel gel and PCR cleanup kit (740609) according to the manufacturer's instructions, cut with EcoRV and NheI and cloned into the original IgM encoding plasmid after excision of the heavy chain coding region with the same two restriction enzymes. The resulting plasmid was transfected into Freestyle cells as described above. Class switch from IgG or IgA to IgM was achieved by an exactly analogous procedure, using

the primers J3_02_rev_fus_to_mu or J6_02_rev_fus_to_mu, depending on the J gene of the source heavy chain.

Antibody purification

Antibody-containing cell culture supernatants were buffer exchanged into PBS using Amicon Ultra 15 50K columns (Sigma), to a final volume of 10 ml. For IgM purification, ammonium sulfate (Sigma-Aldrich A4418) was added to IgM-containing supernatants to reach final concentration of 0.7 M. Solid ammonium sulfate was supplemented to the sample in small amounts while continuously stirring to avoid precipitation of IgM and the sample was passed through a 0.45 µm filter.

Column operations were performed at constant flow rate of 1 ml/min. HiTrap IgM Purification HP column (Sigma-Aldrich GE17-5110-01) was equilibrated with 10 ml binding buffer (20 mM sodium phosphate pH 7.5, 0.7 M ammonium sulfate). Supernatant was applied to the column twice and the column was washed with 15 ml binding buffer. Elution of bound IgM was performed with 20 mM sodium phosphate pH 7.5 using a one-step gradient and 0.5 ml elution fractions were collected. 20 µl from each elution fraction were analyzed on Superdex® 200 Increase 10/300 GL SEC column (Sigma-Aldrich GE28-9909-44) connected to a LC-4000 Series HPLC System (JASCO). Sample-containing fractions were pooled and concentrated, and IgM were purified with a final run of Superdex 200 Increase.

For IgA purification, column operations were performed at constant flowrate of 1 ml/min. HiTrap KappaSelect (Sigma-Aldrich GE17-5458-11) and HiTrap LambdaFabSelect (Sigma-Aldrich GE17-5482-11) columns were equilibrated with 10 ml phosphate-buffered saline (PBS, 10 mM phosphate buffer pH 7.4, 2.7 mM KCl, 140 mM NaCl). The IgA-containing supernatants were applied to the column (KappaSelect for 3M13, 1G22, 2J12, 1B17, 2B15 and LambdaFabSelect for 2C20) twice and the column was washed with 15 ml PBS. Elution of bound IgA was performed with 0.1 M glycine buffer, pH 2.7 (from KappaSelect) or 0.1 M acetate buffer, pH 3.5 (from LambdaFabSelect) using a one-step gradient and 0.5 ml elution fractions were collected. Eluted fractions were immediately adjusted to physiologic pH with the addition of 50 µl 1 M Tris-HCl pH 8.0.

IgG were purified using Protein G HP SpinTrap (Cytiva 28903134) following the manufacturer's instructions.

Neutralization assays

Three different assays were used to assess virus neutralization by antibodies. Supernatants from expanded single B cells were tested using GFP-expressing vesicular stomatitis virus pseudotyped with SARS-CoV-2 spike protein (chimeric GFP-expressing vesicular stomatitis virus). Monoclonal antibodies were tested with this same assay, and a subset was also against wild-type SARS-CoV-2 by a classical plaque assay; and the impact of a clinically relevant mutation in the spike protein on neutralization was assessed using a luciferase-expressing VSV (VSV*ΔG(FLuc) pseudotypes) pseudotyped with either mutant or wild-type spike protein, using a luciferase endpoint instead of GFP plaque measurement. Each neutralization assay was performed either two or three times, as indicated in the corresponding figure legend, on three separate days,

using the same antibody preparation; each experiment included triplicate or quadruplicate wells for every antibody dilution step.

Plaque reduction assay using chimeric GFP-expressing vesicular stomatitis virus

A modified SARS-CoV-2 spike cDNA was synthesized by GenScript (Leiden, The Netherlands). The cDNA was based on the sequence of the Wuhan-Hu-1 isolate (NC_045512.2) but the encoded spike protein had the cytoplasmic domain truncated by 21 amino acids. The S1/S2 cleavage site contained the mutation R685G. In addition, the spike protein harbored several mutations which are likely a consequence of the adaptation to VeroE6 cells: H655Y, D253N, W64R, G261R, A372T (Dieterle *et al.*, 2020). The cDNA was cloned into the pVSV* Δ G(MERS-S) plasmid vector to replace the MERS-CoV spike gene and the chimeric virus VSV* Δ G-S Δ 21 was generated as described previously (Pfaender *et al.*, 2020).

For the plaque reduction assay, Vero cells were seeded at 3000 cells per well into 384-well plates ("assay plates") in Dulbecco's modified Eagle's medium (DMEM) with 10% fetal calf serum, 100 U/ml penicillin, and 100 μ g/ml streptomycin added (DMEM-10) and grown overnight. The next day, antibodies were mixed at various concentrations in 384-well plate wells ("mixing plates"), each with 100 plaque forming units of VSV* Δ G-S Δ 21 in 40 μ l DMEM, incubated for 1 h at 37°C, then added to Vero cells in the assay plates. After one 90 min, 40 μ l of DMEM with 1% methylcellulose was added to each well, and the assay plates incubated for a further 24 h at 37°C. Plates were then imaged in the GFP channel with an automated fluorescent microscope (Nikon Ti2), and data saved as .nd2 files. Numbers of GFP-expressing (i.e., infected) plaques were extracted using an automated macro in ImageJ. For comparison of neutralization between conditions, ND50 (calculated in Prism using four parameter non-linear regression) was used where possible; when this was not possible because one or more of the conditions showed no detectable neutralization, the area under the infection/concentration curve was used instead.

SARS-CoV-2 Neutralization by classical plaque assay

Serial dilutions of control sera and samples were prepared in quadruplicates in 96-well cell culture plates using DMEM cell culture medium (50 μ l/well). To each well, 50 μ l of DMEM containing 100 tissue culture infectious dose 50% (TCID₅₀) of SARS-CoV-2 (SARS-CoV-2/München-1.1/2020/929) were added and incubated for 60 min at 37°C. Subsequently, 100 μ l of Vero E6 cell suspension (100,000 cells/ml in DMEM with 10% FBS) were added to each well and incubated for 72 h at 37°C. The cells were fixed for 1 h at room temperature with 4% buffered formalin solution containing 1% crystal violet (Merck, Darmstadt, Germany). Finally, the microtiter plates were rinsed with deionized water and immune serum-mediated protection from cytopathic effect was visually assessed. Neutralization doses 50% (ND50) values were calculated according to the Spearman and Kärber method.

Neutralization of VSV* Δ G(Fluc) pseudotypes

The spike protein cDNA of SARS-CoV-2 containing the D614G mutation and a truncation of the cytoplasmic domain by 18 amino acids but otherwise based on based on the Wuhan-Hu-1 reference

sequence (NC_045512.2) was cloned into the pCAGGS plasmid taking advantage of the KpnI and XhoI endonuclease restriction sites. A spike variant containing the E484G substitution and a deletion of amino acids 244–247 were generated by overlapping PCR technology. Transcomplementation of the VSV* Δ G(Fluc) vector (Rentsch & Zimmer, 2011) was performed as described recently (Zettl *et al.*, 2020). Antibody-mediated neutralization of the pseudotyped VSV* Δ G(Fluc) was performed by taking advantage of the firefly luciferase reporter as described previously (Zettl *et al.*, 2020).

Flow cytometry

For flow cytometry screening of spike-binding antibodies in serum, 100,000 TE 0 cells and the same number of TE spike-cherry cells per well were incubated with serial 2-fold dilutions of serum, starting from 1:20 in PBS. Incubation was done in 96-well plates, for 30 min, on ice. Cells were then washed twice with cold PBS and labeled with 100 μ l of PBS containing Dylight-405-conjugated anti-human IgM (JIR 109-475-129), FITC-conjugated anti-human IgG (JIR 109-096-098), and Alexa Fluor 647-conjugated anti-human IgA (JIR 109-605-011) for 30 min on ice, washed twice with cold PBS and measured on a Beckman Coulter CytoFLEX flow cytometer equipped with a 96-well plate reader.

A similar technique was used for testing the supernatants of spike-protein specific expanded B cells; in this case, 10 μ l TE0/Tespike-cherry cells were incubated on ice with 15 μ l of supernatant from each expanded B cell, in a 384-well plate (Thermo Scientific). After 30 min' incubation on ice, cells were transferred to a 96-well plate, washed twice in PBS, and labeled as described above.

Surface plasmon resonance

SPR measurements were conducted on a Biacore T100 (T200 Sensitivity Enhanced, GE Healthcare Life Sciences). His-tagged spike protein or spike protein sub-domains (full-length extracellular domain, RBD, or S2; Sino Biological, catalog numbers 40589-V08H4, 40592-V08H, 40590-V08H1) were captured on a CM5 sensor chip (Cytiva) using the His Capture Kit, Type 2 (Cytiva) resulting in capture levels of 170 RU for Spike, 100 RU for S2, and 60 RU for RBD. All runs were conducted with HBS-P+ buffer (10 mM HEPES, 150 mM NaCl, 0.05% (v/v) Surfactant P20, pH 7.4; Cytiva). The different antibodies were injected in increasing concentrations (1.6, 8, 40, 200, 1,000 nM) for single cycle kinetics with a contact time of 120 s and dissociation time of 600 s at a flowrate of 30 μ l/min. Dissociation constants (KD) were calculated with the BiacoreT200 Evaluation software 3.0 using the two-state-reaction model.

VSV* Δ G-S Δ 21 escape mutants

The selection of VSV* Δ G-S Δ 21 mutants which escaped antibody-mediated inhibition was performed according to a recently described procedure (Walter *et al.*, 2022). Briefly, approximately 100 focus-forming units of VSV* Δ G-SD21 were incubated with serially diluted IgM prior to infection of Vero E6 cells in 24-well plates. Two days later, cell culture supernatants from the wells containing the highest antibody concentration which did not completely inhibit virus plaque expansion was collected and subjected to a second round of selection on Vero E6 cells grown in 96-well microtiter

plates in the presence serially diluted IgM. Virus recovered after a third round of selection was used to infect Vero E6 cells grown in 6-well plates. Cells were lysed in GeneZol (GeneAid, New Taipei City, Taiwan) and total RNA isolated according to the manufacturer's instructions. Abundance of spike gene cDNA was quantified by an in-house quantitative PCR for SARS-CoV-2 (Leuzinger *et al*, 2021) and diluted to Ct = 20.

The diluted RNA was amplified and sequenced as described in Stange *et al* (2021) (Stange *et al*, 2021) with the following modifications: 35 cycles and v4.1 primers (https://github.com/artic-network/artic-ncov2019/tree/master/primer_schemes/nCoV-2019/V4.1) were used in the amplification.

Initial data analysis was done with the COVGAP pipeline (Stange *et al*, 2021).

Statistics

Statistical treatments are explained in figure legends. We considered relevant sources of biological variation to include inter-individual differences between human donors, and genetic differences between individual virions. Possible sources of non-biological (i.e., technical) variability include experimental variables that vary from day to day, as well as from well to well, and so on. Therefore, rather than attempting to distinguish between “biological” and “technical” replicates, we have designed all experiments to cover both of these types of variability, and have explained the temporal and spatial structure in each figure legend. Experimental designs include single assays (e.g., virus neutralization by supernatants from single B cells); two or three temporal repeats (i.e., performed on different occasions) of single measurements (IgM and epitope ELISAS, flow cytometric measurements of antibody binding); and three temporal repeats of triplicate or quadruplicate technical replicates (neutralization assays). Statistics were calculated using GraphPad Prism. Plots were generated in R or in Prism, and compound figures were assembled using Inkscape.

Data availability

Sequences of heavy and light chains of the antibodies shown in Appendix Table S3 are available in GenBank Accession numbers OM584288-OM584289, and OM687904-OM687941.

Expanded View for this article is available online.

Acknowledgements

These studies were supported by the Swiss National Science Foundation (grant numbers 189043 and 189151). Technical support was provided by the flow cytometry, microscopy, and bioinformatics cores of the Department of Biomedicine of the University of Basel, and the Biophysics Facility of the Biozentrum of the University of Basel. We are grateful to Gennaro De Libero and John Lindner for technical and theoretical advice. Open access funding provided by Universität Basel.

Author contributions

Ilaria Callegari: Conceptualization; Data curation; Formal analysis; Investigation; Visualization; Methodology; Writing—original draft; Writing—review & editing. **Mika Schneider:** Investigation. **Giuliano Berloff:** Formal analysis; Investigation; Methodology. **Tobias Mühlenthaler:** Formal analysis;

Investigation; Methodology. **Sebastian Holdermann:** Investigation; Methodology. **Edoardo Galli:** Software; Formal analysis; Visualization; Writing—review & editing. **Tim Roloff:** Data curation; Software; Investigation; Methodology; Writing—original draft; Writing—review & editing. **Renate Boss:** Investigation. **Laura Infanti:** Conceptualization; Data curation; Project administration. **Nina Khanna:** Resources; Data curation; Supervision. **Adrian Egli:** Conceptualization; Resources; Supervision; Project administration. **Andreas Buser:** Conceptualization; Resources; Supervision. **Gert Zimmer:** Conceptualization; Resources; Data curation; Formal analysis; Funding acquisition; Investigation; Methodology; Writing—original draft; Writing—review & editing. **Tobias Derfuss:** Conceptualization; Resources; Supervision; Funding acquisition; Methodology; Writing—original draft; Project administration; Writing—review & editing. **Nicholas S R Sanderson:** Conceptualization; Data curation; Software; Formal analysis; Validation; Investigation; Visualization; Methodology; Writing—original draft; Project administration; Writing—review & editing.

Disclosure and competing interests statement

The authors declare that they have no conflict of interest.

References

- Batista FD, Iber D, Neuberger MS (2001) B cells acquire antigen from target cells after synapse formation. *Nature* 411: 489–494
- Batista FD, Neuberger MS (1998) Affinity dependence of the B cell response to antigen: a threshold, a ceiling, and the importance of off-rate. *Immunity* 8: 751–759
- Boudreau CM, Alter G (2019) Extra-neutralizing FcR-mediated antibody functions for a universal influenza vaccine. *Front Immunol* 10. <https://doi.org/10.3389/fimmu.2019.00440>
- Brouwer PJM, Caniels TC, van der Straten K, Snitselaar JL, Aldon Y, Bangaru S, Torres JL, Okba NMA, Claireaux M, Kerster C *et al* (2020) Potent neutralizing antibodies from COVID-19 patients define multiple targets of vulnerability. *Science* 369: 643–650
- Case JB, Rothlauf PW, Chen RE, Liu Z, Zhao H, Kim AS, Bloyet L-M, Zeng Q, Tahan S, Droit L *et al* (2020) Neutralizing antibody and soluble ACE2 inhibition of a replication-competent VSV-SARS-CoV-2 and a clinical isolate of SARS-CoV-2. *Cell Host Microbe* 28: 475–485.e5
- Chromikova V, Mader A, Steinfellner W, Kunert R (2015) Evaluating the bottlenecks of recombinant IgM production in mammalian cells. *Cytotechnology* 67: 343–356
- Diebold M, Galli E, Kopf A, Sanderson N, Callegari I, Ingelfinger F, Núñez NG, Benkert P, Kappos L, Kuhle J *et al* (2022) Immunological predictors of dimethyl fumarate-induced lymphopenia. *Ann Neurol* 91: 676–681
- Dieterle ME, Haslwanter D, Bortz RH, Wirchnianski AS, Lasso G, Vergnolle O, Abbasi SA, Fels JM, Lauderilch E, Florez C *et al* (2020) A replication-competent vesicular stomatitis virus for studies of SARS-CoV-2 spike-mediated cell entry and its inhibition. *Cell Host Microbe* 28: 486–496.e6
- Feldman J, Bals J, Altomare CG, Denis KS, Lam EC, Hauser BM, Ronsard L, Sangesland M, Moreno TB, Okonkwo V *et al* (2021) I human B cells engage the receptor binding domain of SARS-CoV-2, variants of concern, and related sarbecoviruses. *Sci Immunol* 6: eabl5842
- Fleire SJ, Goldman JP, Carrasco YR, Weber M, Bray D, Batista FD (2006) B cell ligand discrimination through a spreading and contraction response. *Science* 312: 738–741
- Galli E, Hartmann FJ, Schreiner B, Ingelfinger F, Arvaniti E, Diebold M, Mrdjen D, van der Meer F, Krieg C, Nimer FA *et al* (2019) GM-CSF and CXCR4 define a T helper cell signature in multiple sclerosis. *Nat Med* 25: 1290–1300

- Green EM, Armstrong SJ, Dimmock NJ (1992) Mechanisms of neutralization of a nairovirus (Dugbe virus) by polyclonal IgG and IgM. *J Gen Virol* 73: 1995–2001
- Harvey WT, Carabelli AM, Jackson B, Gupta RK, Thomson EC, Harrison EM, Ludden C, Reeve R, Rambaut A, Peacock SJ et al (2021) SARS-CoV-2 variants, spike mutations and immune escape. *Nat Rev Microbiol* 19: 409–424
- Janda A, Eryilmaz E, Nakouzi A, Cowburn D, Casadevall A (2012) Variable region identical immunoglobulins differing in isotype express different paratopes. *J Biol Chem* 287: 35409–35417
- Keyt BA, Baliga R, Sinclair AM, Carroll SF, Peterson MS (2020) Structure, function, and therapeutic use of IgM antibodies. *Antibodies* 9: 53
- Kurtovic L, Beeson JG (2021) Complement factors in COVID-19 therapeutics and vaccines. *Trends Immunol* 42: 94–103
- Leuzinger K, Gosert R, Søgaard KK, Naegele K, Bielicki J, Roloff T, Bingisser R, Nickel CH, Khanna N, Sutter ST et al (2021) Epidemiology and precision of SARS-CoV-2 detection following lockdown and relaxation measures. *J Med Virol* 93: 2374–2384
- Loh RKS, Vale S, McLean-Tooke A (2013) Quantitative serum immunoglobulin tests. *Aust Fam Physician* 42: 195–198
- Lu LL, Suscovich TJ, Fortune SM, Alter G (2018) Beyond binding: antibody effector functions in infectious diseases. *Nat Rev Immunol* 18: 46–61
- Malinova D, Wasim L, Newman R, Martínez-Riño A, Engels N, Tolar P (2021) Endophilin A2 regulates B-cell endocytosis and is required for germinal center and humoral responses. *EMBO Rep* 22: e51328
- Masoudi-Nejad A, Tonomura K, Kawashima S, Moriya Y, Suzuki M, Itoh M, Kanehisa M, Endo T, Goto S (2006) EGAssembler: online bioinformatics service for large-scale processing, clustering and assembling ESTs and genomic DNA fragments. *Nucleic Acids Res* 34: W459–W462
- McCallum M, De Marco A, Lempp FA, Tortorici MA, Pinto D, Walls AC, Beltramello M, Chen A, Liu Z, Zatta F et al (2021) N-terminal domain antigenic mapping reveals a site of vulnerability for SARS-CoV-2. *Cell* 184: 2332–2347.e16
- Mehlhop E, Nelson S, Jost CA, Gorlatov S, Johnson S, Fremont DH, Diamond MS, Pierson TC (2009) Complement protein C1q reduces the stoichiometric threshold for antibody-mediated neutralization of west Nile virus. *Cell Host Microbe* 6: 381–391
- Morgan M, Anders S, Lawrence M, Aboyou P, Pagès H, Gentleman R (2009) ShortRead: a bioconductor package for input, quality assessment and exploration of high-throughput sequence data. *Bioinformatics* 25: 2607–2608
- Nakamura M, Burastero SE, Ueki Y, Larrick JW, Notkins AL, Casali P (1988) Probing the normal and autoimmune B cell repertoire with Epstein-Barr virus. Frequency of B cells producing monoreactive high affinity autoantibodies in patients with Hashimoto's disease and systemic lupus erythematosus. *J Immunol* 141: 4165–4172
- Natkanski E, Lee W-Y, Mistry B, Casal A, Molloy JE, Tolar P (2013) B cells use mechanical energy to discriminate antigen affinities. *Science* 340: 1587–1590
- Pfaender S, Mar KB, Michailidis E, Kratzel A, Boys IN, Vlkovski P, Fan W, Kelly JN, Hirt D, Ebert N et al (2020) LY6E impairs coronavirus fusion and confers immune control of viral disease. *Nat Microbiol* 5: 1330–1339
- Pickering S, Betancor G, Galão RP, Merrick B, Signell AW, Wilson HD, Kia IK MT, Seow J, Graham C, Acors S et al (2020) Comparative assessment of multiple COVID-19 serological technologies supports continued evaluation of point-of-care lateral flow assays in hospital and community healthcare settings. *PLoS Pathog* 16: e1008817
- Polycarpou A, Howard M, Farrar CA, Greenlaw R, Fanelli G, Wallis R, Klavinskis LS, Sacks S (2020) Rationale for targeting complement in COVID-19. *EMBO Mol Med* 12: e12642
- Raybould MJ, Kovaltuk A, Marks C, Deane CM (2021) CoV-AbDab: the coronavirus antibody database. *Bioinformatics* 37: 734–735
- Rentsch MB, Zimmer G (2011) A vesicular stomatitis virus replicon-based bioassay for the rapid and sensitive determination of multi-species type I interferon. *PLoS One* 6: e25858
- Robbiani DF, Gaebler C, Muecksch F, Lorenzi JCC, Wang Z, Cho A, Agudelo M, Barnes CO, Gazumyan A, Finkin S et al (2020) Convergent antibody responses to SARS-CoV-2 in convalescent individuals. *Nature* 584: 437–442
- Rodda LB, Netland J, Shehata L, Pruner KB, Morawski PA, Thouvenel CD, Takehara KK, Eggenberger J, Hemann EA, Waterman HR et al (2021) Functional SARS-CoV-2-specific immune memory persists after mild COVID-19. *Cell* 184: 169–183.e17
- Sharp TH, Boyle AL, Diebold CA, Kros A, Koster AJ, Gros P (2019) Insights into IgM-mediated complement activation based on in situ structures of IgM-C1-C4b. *Proc Natl Acad Sci USA* 116: 11900–11905
- Shen C, Zhang M, Chen Y, Zhang L, Wang G, Chen J, Chen S, Li Z, Wei F, Chen J et al (2019) An IgM antibody targeting the receptor binding site of influenza B blocks viral infection with great breadth and potency. *Theranostics* 9: 210–231
- Stange M, Marii A, Roloff T, Seth-Smith HMB, Schweitzer M, Brunner M, Leuzinger K, Sgaard KK, Gensch A, Tschudin-Sutter S et al (2021) SARS-CoV-2 outbreak in a tri-national urban area is dominated by a B.1 lineage variant linked to a mass gathering event. *PLoS Pathog* 17: e1009374
- Thouvenel CD, Fontana MF, Netland J, Krishnamurthy AT, Takehara KK, Chen Y, Singh S, Miura K, Keitany GJ, Lynch EM et al (2021) Multimeric antibodies from antigen-specific human IgM+ memory B cells restrict Plasmodium parasites. *J Exp Med* 218: e20200942
- Tiller T, Meffre E, Yurasov S, Tsujii M, Nussenzweig MC, Wardemann H (2008) Efficient generation of monoclonal antibodies from single human B cells by single cell RT-PCR and expression vector cloning. *J Immunol Methods* 329: 112–124
- Tobita T, Oda M, Azuma T (2004) Segmental flexibility and avidity of IgM in the interaction of polyvalent antigens. *Mol Immunol* 40: 803–811
- Walter JD, Scherer M, Hutter CAJ, Garaeva AA, Zimmermann I, Wyss M, Rheinberger J, Ruedin Y, Earp JC, Egloff P et al (2022) Biparatopic sybodies neutralize SARS-CoV-2 variants of concern and mitigate drug resistance. *EMBO Rep* 23: e54199
- Wan J, Xing S, Ding L, Wang Y, Gu C, Wu Y, Rong B, Li C, Wang S, Chen K et al (2020) Human-IgG-neutralizing monoclonal antibodies block the SARS-CoV-2 infection. *Cell Rep* 32: 107918
- Wang Z, Lorenzi JCC, Muecksch F, Finkin S, Viant C, Gaebler C, Cipolla M, Hoffmann H-H, Oliveira TY, Oren DA et al (2021) Enhanced SARS-CoV-2 neutralization by dimeric IgA. *Sci Transl Med* 13: eabf1555
- Weigang S, Fuchs J, Zimmer G, Schnepf D, Kern L, Beer J, Luxenburger H, Ankerhold J, Falcone V, Kemming J et al (2021) Within-host evolution of SARS-CoV-2 in an immunosuppressed COVID-19 patient as a source of immune escape variants. *Nat Commun* 12: 6405
- Weisblum Y, Schmidt F, Zhang F, DaSilva J, Poston D, Lorenzi JCC, Muecksch F, Rutkowska M, Hoffmann HH, Michailidis E et al (2020) Escape from neutralizing antibodies 1 by SARS-CoV-2 spike protein variants. *Elife* 9: e61312

- Wulff NH, Tzatzaris M, Young PJ (2012) Monte Carlo simulation of the Spearman-Kaerber TCID50. *J Clin Bioinforma* 2: 5
- Zettl F, Meister TL, Vollmer T, Fischer B, Steinmann J, Krawczyk A, Vkovski P, Todt D, Steinmann E, Pfaender S et al (2020) Rapid quantification of SARS-CoV-2-neutralizing antibodies using propagation-defective vesicular stomatitis virus pseudotypes. *Vaccines* 8: 1–13
- Zhang Y, Meyer-Hermann M, George LA, Figge MT, Khan M, Goodall M, Young SP, Reynolds A, Falciani F, Waisman A et al (2013) Germinal center B cells govern their own fate via antibody feedback. *J Exp Med* 210: 457–464
- Zimmermann M, Rose N, Lindner JM, Kim H, Gonçalves AR, Callegari I, Syedbasha M, Kaufmann L, Egli A, Lindberg RLP et al (2019) Antigen extraction and B cell activation enable identification of rare membrane antigen specific human B cells. *Front Immunol* 10: 829
- Zohar T, Loos C, Fischinger S, Atyeo C, Wang C, Slein MD, Burke J, Yu J, Feldman J, Hauser BM et al (2020) Compromised humoral functional evolution tracks with SARS-CoV-2 mortality. *Cell* 183: 1508–1519.e12



License: This is an open access article under the terms of the Creative Commons Attribution License, which permits use, distribution and reproduction in any medium, provided the original work is properly cited.

CSF derived monoclonal antibodies identify a novel target antigen in a Multiple Sclerosis patient

Ilaria Callegari^{1,2}, Johanna Oechtering², Hye In Kim¹, Mika Schneider¹, Sebastian Holdermann¹, Jens Kuhle², Mikael Khalil³, Ludwig Kappos², Andreas Junker⁴, Nicholas Sanderson^{1,2}, Tobias Derfuss^{1,2}

1: University of Basel, Clinical Neuroimmunology Lab, Department of Biomedicine, Basel, Switzerland, 2: University Hospital Basel, MS Center, Neurologic Clinic and Policlinic, Research Center for Clinical Neuroimmunology and Neuroscience Basel (RC2NB), Basel, Switzerland
3: Medical University of Graz, Department of Neurology, Graz, Austria
4: University Hospital Essen, Department of Neuropathology, Essen, Germany

Abstract

Introduction

Persistent intrathecal immunoglobulin production, mainly of the IgG subtype, detected as oligoclonal bands, is a diagnostic hallmark of Multiple sclerosis (MS), which can be found in 98% of MS patients. Up to 25% of patients show additional persisting intrathecal IgM synthesis, which, unlike their blood counterpart, show a high degree of somatic hypermutation, suggesting an antigen driven production. Despite intensive investigations, the antigenic stimulus that initiates or perpetuates B cell activation and intrathecal immunoglobulin production in MS patients is still a matter of debate.

Aims

The aim of our study was to identify the target antigen of intrathecally produced cerebrospinal fluid (CSF) IgM antibodies.

Methods

Two independent cohorts of MS patients and control CSF samples were screened in a blinded fashion by flow-cytometry for antibody binding on a panel of nervous system related cell lines. B cells from prospectively collected CSF were sorted, single cells expanded and immunoglobulin genes from wells resembling the cell specific binding pattern of the original CSF sample were sequenced. Heavy and light chain sequences were then used to produce CSF derived monoclonal IgM, which were used for immunoprecipitation and mass spectrometry.

Results

We identified CSF IgM binding to a Peripheral Neuro-Ectodermal Tumor (PNET) cell line in 10% of MS donors and less than 1% of controls, independently from CSF IgM content. We sorted and expanded 1678 single B cells from a CSF sample with this IgM reactivity and produced 5 recombinant IgM with the same cell-line specificity. One of these IgM clones (B3) showed the same binding specificity of the original CSF sample. Immunoprecipitation and mass spectrometry in combination with transcriptomic analysis of membrane proteins expressed by cell lines bound or not bound by B3 allowed to identify isoform 1 of SCARA5 as a target. Testing IgM binding to SCARA5 in a cohort of CSF including MS patients, inflammatory patients and non-inflammatory controls confirmed that SCARA5 is one of the targets of CSF IgM in a small percentage of MS patients. Labeling of chronic MS lesions confirmed expression of SCARA5 by neurons, foamy macrophages around lesions and astrocytes.

Conclusions

We identified a novel autoantigen targeted by intrathecally produced and highly hypermutated CSF IgM. Interference with SCARA5 ferritin-independent iron transport function may contribute to the disease pathogenesis.

Introduction

MS is a chronic demyelinating condition of the central nervous system (CNS) of unknown aetiology and the most common neurological cause of disability in young adults, with a prevalence greater than 1 in 1000 (Wallin *et al*, 2019). The notion that MS is an autoimmune disorder is supported by several, albeit indirect, lines of evidence, including inflammatory infiltrates composed by lymphocytes and macrophages in the CNS plaques (Kutzelnigg & Lassmann, 2014); intrathecally produced oligoclonal antibodies (Stangel *et al*, 2013); the presence of genetic risk variants mostly in immune system related genes (Sawcer *et al*, 2014); positive treatment effects by immunotherapies (Haghikia *et al*, 2013).

MS has been associated with inflammatory T helper cell profiles and T cells play key roles in adoptive transfer models of demyelinating disease (Gold *et al*, 2006); therefore, historically, MS research has focused on T cells. However, in the recent years, especially following the striking efficacy of CD20-depleting therapies in reducing the disease activity (Hauser *et al*, 2008), interest for a B cells involvement in the pathogenesis of MS has grown rapidly.

One of the clinical hallmarks of MS is the presence of intrathecal immunoglobulin production, identifiable at the CSF examination as oligoclonal bands (OCBs) (Johnson *et al*, 1977); OCBs are not only a diagnostic and prognostic tool (Stangel *et al*, 2013) but are one of the strongest pieces of evidence of the immune pathogenesis of the disease, and of an involvement of humoral immune response. Indeed, OCBs are not exclusively found in MS, but also in other diseases that have been shown to be antibody mediated, such as limbic encephalitis (Gultekin *et al*, 2000), or in infectious diseases of the central nervous system, where they are specific for the pathogen involved (Meinl *et al*, 2006). Interestingly, a comparison of the immunoglobulin transcriptomes of B cells with the corresponding immunoglobulin proteomes in patients with MS demonstrated that intrathecal B cells are the source of immunoglobulin oligoclonal bands in the CSF (Obermeier *et al*, 2008).

Immunoglobulin M (IgM) OCBs are present in approximately 30–40% of patients (Villar *et al*, 2005a), and their presence has been associated with more active disease (Villar *et al*, 2002; Oechtering *et al*, 2021, 2022) and potentially with therapeutic responses to B cell-directed therapy (Villar *et al*, 2014). Moreover, IgM sequences from the cerebrospinal fluid of patients with multiple sclerosis or neuroborreliosis show a high degree of somatic hypermutation, suggesting an antigen driven IgM response (Beltrán *et al*, 2014), rather than a bystander response.

Despite intensive investigations, the antigenic stimuli that initiates or perpetuates B cell activation and immunoglobulin production in MS patients is still a matter of debate. Using recombinant antibody technology, in this study we aim to clone recombinant monoclonal IgM from CSF samples selected based on IgM reactivity against a neuroectodermal tumour cell line, and to use these patient-derived antibodies to identify molecular targets of CSF IgM in MS patients.

Methods

Patient samples

CSF samples from patients undergoing diagnostic lumbar puncture at the Neuropoliklinik, University Hospital, Basel and from University Hospital of Graz were collected and immediately processed. All the donors gave informed consent according to the procedures reviewed by the institutional ethics committee. Each sample was collected using a 15 ml falcon tube, centrifuged at 400 g at room temperature for 10 minutes; the CSF supernatant was then aliquoted and frozen in -80°C. For the prospective part of the study, the CSF samples were analyzed for PNET-binding IgM by flow cytometry, immediately after collection, while the CSF cell pellet was resuspended in RPMI supplemented with 40% FCS (R40) and kept on ice for further processing or stored within 2h in liquid nitrogen.

Cell lines

Cell lines used included: PNET (neuroectodermal tumor), SW1088 (astrocytoma), A172 (glioblastoma), STTG1 (grade IV astrocytoma) and DAOY (desmoplastic cerebellar medulloblastoma), HEK (embryonic kidney), HeLa (epithelial), TE671 (rhabdomyosarcoma), SVGp12 (astroglial, SV40 transformed). All cell lines were purchased from ATCC (LGC, Wesel, Germany) and were cultured following the manufacturer indications. TE cells transfected with human CD40 Ligand (Edgar Meinel, Ludwig-Maximilians-Universität, Munich, Germany) were used as feeder cells for B cell expansion. For irradiation, cells were washed in PBS, trypsinized, resuspended in ice-cold FCS and kept on ice during irradiation (75 Gy).

CSF single B cells expansion and immunoglobulin sequencing

B cells from PNET-binding IgM positive CSF samples were sorted and expanded using the protocol described by Huang *et al.* (Huang *et al.*, 2013) and subsequent modifications. Briefly, as soon as a CSF sample arrived, CSF cells were resuspended R40, transferred to a sterile flow cytometry tube, spun down at 300g, 4°C for 3 minutes and resuspended in 100 uL of PBS plus 1 uL of the following antibodies: FITC-conjugated anti-CD3 (BioLegend 317306), anti-CD4 (BioLegend 357406), anti-CD14 (BioLegend 301804), anti-CD16 (BioLegend 360716), anti-CD56 (BioLegend 318304); PE-conjugated anti-CD19 (BioLegend 363004). Cells were incubated on ice for 20 minutes, then washed once, resuspended in 100 uL of sterile PBS and sorted using a FACS Aria III (BD Biosciences). The gate was set on the CD19-positive, CD3/CD4/CD14/CD56-negative population. Sorted CD19+ cells were cultured in 384-well plate wells at an average density of 0.9 cells/well, in RPMI with 40% FCS, 0.05 ng/μl IL-21 (Gibco, PHC0215), together with 50,000 irradiated TE CD40L cells/well. After 9 days of culture, 15 μl of supernatant was withdrawn from each well and screened for PNET-binding antibodies as described above. B cells from positive wells were lysed in 20 μl of 15 mM Tris-HCl, pH 8.0 containing 0.5 U/μl of recombinant murine RNase inhibitor (NEB, M0314L). RNA was extracted from this lysate by Zymo Quick-RNA microprep kit (R1050 & R1051), and reverse transcribed with the SMART-Seq v4 Ultra Low Input RNA Kit for Sequencing (Takara, 634888). One hundred nanograms of the thus generated cDNA was used to prepare sequencing libraries with the DNA prep kit (Illumina). The libraries were sequenced paired-end 150 bp on a NextSeq 500 sequencer (Illumina) yielding an average of one million reads per lysate. Reads mapping to immunoglobulin gene sequences were extracted from the resulting single-cell transcriptomes with a custom script in R (Dataset EV3 and 4), using packages Shortread (Morgan *et al.*, 2009) and Biostrings, reassembled with EZassembler (Masoudi-Nejad *et al.*, 2006), and assigned to V(D)J genes using IgBLAST (<https://www.ncbi.nlm.nih.gov/igblast/>).

Extraction and assembly of immunoglobulin gene sequences

Based on the deduced heavy and light chain sequences, DNA constructs encoding the inferred amino acid sequence from leader to several bases into the constant region were synthesized by IDT with restriction sites at the termini to enable in-frame cloning into pVITRO and the resulting plasmids transfected into Freestyle HEK cells (Invitrogen, R79007). On the day of transfection, each 125 ml flask containing 14 ml of cells at 1×10^6 viable cells/mL was transfected with pVITRO hygro dual expression plasmid expressing the heavy and the light chain of each of the recombinant antibodies, using 293fectin Transfection Reagent (Gibco, 12347019) according to the manufacturer's instructions. 24 h post-transfection, hygromycin B (50 μ g/ml) was added to transfected cells, which were then maintained in culture under selection for 2 weeks at densities between 3×10^5 and 5×10^5 viable cells/ml. Cultured supernatants were harvested after 16 days, centrifuged at 2000 g for 20 minutes, passed over 0.45 mm filters (Sartorius). Cell supernatants were buffer-exchanged into PBS using Amicon Ultra 15 50-K columns (Sigma, UFC905024) following the manufacturer's instructions, and the resulting antibody containing supernatants were stored at 4°C or at -20°C until use. Recombinant antibodies were quantified by ELISA.

Flow cytometry

For flow cytometry screening of PNET-binding antibodies in CSF, 100000 PNET cells and the same number of SW1088 cells per well were incubated with a 1 to 4 dilution of the CSF in PBS. Incubation was done in 96-well-plates, for 30 minutes, on ice. Cells were then washed twice with cold PBS and labeled with 100 μ l of PBS containing Dylight-405-conjugated anti-human IgM (JIR 109-475-129), FITC-conjugated anti-human IgG (JIR 109-096-098) and Alexa Fluor 647-conjugated anti-human IgA (JIR 109-605-011) for 30 minutes on ice, washed twice with cold PBS and measured on a Beckman Coulter CytoFLEX flow cytometer equipped with a 96-well plate reader.

A similar technique was used for testing the supernatants from expanded B cells; in this case, 10 μ l PNET cells were incubated on ice with 15 μ l of supernatant from each expanded B cell, in a 384-well plate (Thermo Scientific). After 30 minutes' incubation on ice, cells were transferred to a 96-well plate, washed twice in PBS and labeled as described above.

For testing effect of surface proteins removal on monoclonal antibody binding, cells were trypsinized, washed twice with PBS and resuspended in HBSS 5 mM CaCl plus Pronase (SigmaAldrich) 2 mg/ml, then incubated for 1h at 37°C. Cells were then labeled with each monoclonal antibody or CSF as described above. Deglycosilation was performed using PNGase, neuraminidase, Endo-O-Glycosidas, Endoglycosidase F1, F2, F3 (EDEGLY and NDEGLY, Sigma) alone or in combination, following manufacturer instructions.

ELISA

384-well plates were coated with goat anti-human IgG (Southern Biotec, 2014-01), anti-human IgM (Southern Biotec, 2023-01), or anti-human IgA (Southern Biotec, 2053-01) antibodies overnight at 4°C, washed once with PBS and blocked with PBS- 1% BSA at room temperature for 90 minutes. Plates were then washed three times with PBS 0.05% Tween, incubated with 15 μ l of serially diluted samples for 2 h at room temperature, washed three times with PBS 0.05% Tween and incubated with anti-IgG-HRP (Southern Biotec 2014-05), anti-IgM-HRP (Southern Biotec 2023-05), anti-IgA-HRP (Southern Biotec 2053-05) or goat anti-Ig-HRP (Southern Biotec, 2010-05) in PBS-0.1% BSA for 1h at room temperature. Plates were then washed three times with 80 μ l/well of PBS-0.05% Tween and developed with TMB ELISA substrate (SureBlue Reserve TMB Microwell Peroxidase Substrate, REF 53-00-00) until a blue color was visible; the reaction was stopped with sulfuric acid and plates were read at 450 nm immediately after stopping.

Western blot

Cell lysates were prepared as follows: cultured cells were washed with PBS, trypsinized and washed twice with PBS. The cell pellet was then resuspended in 1ml/5,000,000 of cells of RIPA buffer (Thermo Fisher) with addition of Halt Protease Inhibitor Cocktail (Thermo Fisher). The lysate was incubated on ice for 15 min and sonicated at frequency of 50 kHz for 30 seconds on ice, then centrifuged at 14,000 g, at 4°C for 30 minutes. The supernatant was transferred to a clean tube and the protein concentration was assessed using Pierce BCA Protein Assay kit (Thermo Fisher). For SDS PAGE, samples were prepared using 30 ug of proteins from each lysate, mixed with NuPAGE LDS sample buffer 4x (Thermo Fisher) and heated at 70°C for 10 minutes. Proteins were then separated using 4-12% Bis-Tris gels (Thermo Fisher) in MOPS running buffer, transferred to a nitrocellulose membrane and probed by immunoblot using each of the produced recombinant anti-PNET IgM.

Immunoprecipitation and mass spectrometry

Cultured PNET cells from three T150 flask were washed twice with ice cold PBS and then incubated with B3 for 30 minutes at 37°C, washed twice in PBS and trypsinized. Cells were then retrieved in R10, centrifuged at 300 g for 3 minutes at 4°C, washed twice in PBS, and the pellet lysed in 500 uL of Pierce IP lysis buffer containing Halt Protease Inhibitor Cocktail (Thermo Fisher). The lysate was sonicated at low power for 10 1 second pulses and incubated on ice for 30 minutes, then centrifuged for 30 minutes at 10'000 g at 4°C. The supernatant was then incubated with Dynabeads (Thermo Fisher, 5 mio of beads every 40 mg of cell pellet) previously coated with unconjugated Donkey anti-human IgM (JIR 709-005-073) for 30 minutes at 4°C on a rotor. The suspension was then washed twice with Pierce IP lysis buffer. The product from immunoprecipitation was eluted by incubating the suspension with 106 mM Tris HCl, 5% LDS and boiling the samples for 10 min at 70°C. The elution product was run on an 4-12% Bis-Tris gels (Thermo Fisher) in MOPS running buffer, transferred to a nitrocellulose membrane and probed by immunoblot using Alexa Fluor 680 conjugated streptavidin to detect biotinylated membrane proteins and each our recombinant IgM. Samples were then cooled down to RT and 0.5 µL of 1M iodoacetamide was added to the samples. Cysteine residues were alkylated for 30 min at 25°C in the dark. Digestion and peptide purification was performed using S-trap™ technology (Protifi) according to the manufacturer's instructions. In brief, samples were acidified by addition of 2.5 µL of 12% phosphoric acid (1:10) and then 165 µL of S-trap buffer (90% methanol, 100 mM TEAB pH 7.1) was added to the samples (6:1). Samples were briefly vortexed and loaded onto S-trap™ micro spin-columns (Protifi) and centrifuged for 1 min at 4000 g. Flow-through was discarded and spin-columns were then washed 3 times with 150 µL of S-trap buffer (each time samples were centrifuged for 1 min at 4000 g and flow-through was removed). S-trap columns were then moved to the clean tubes and 20 µL of digestion buffer (50 mM TEAB pH 8.0) and trypsin (at 1:25 enzyme to protein ratio) were added to the samples. Digestion was allowed to proceed for 1h at 47 °C. After, 40 µL of digestion buffer was added to the samples and the peptides were collected by centrifugation at 4000 g for 1 minute. To increase the recovery, S-trap columns were washed with 40 µL of 0.2% formic acid in water (400g, 1 min) and 35 µL of 0.2% formic acid in 50% acetonitrile. Eluted peptides were dried under vacuum and stored at -20 °C until further analysis. Samples were acquired at the Proteomic Core Facility, Biozentrum, Basel.

SCARA5 cloning

RNA was extracted by PNET cells using quickRNA (Zymo) following the manufacturer instructions and reverse transcribed using SuperScript™ III RT (200 units/µl), followed by removal of RNA complementary to the cDNA by incubating the cDNA with E.Coli RNase H at 37°C for 20 minutes. Amplification of SCARA5 sequence was carried out by nested PCR using primers designed on the basis of publicly available DNA sequence. The resulting PCR product was used for cloning into competent cells and the resulting plasmid transfected into HEK293 cells.

Statistics

Statistics were calculated using GraphPad Prism. Plots were generated in R or in Prism, and compound figures were assembled using Inkscape.

Results

CSF PNET binding IgM discriminate MS patients from controls

To test whether the CSF from MS patients contains antibodies of any class binding to cell surface determinant of neural derived cells, we tested two independent cohorts of CSF (n = 360 for cohort 1; n = 200 for cohort 2) in a retrospective fashion by flow cytometry. We identified CSF IgM binding to a peripheral neuroectodermal tumor (PNET) cell line in the 10% of MS patients and less than 1% of control samples (Fig 1A). PNET-binding IgM were able to discriminate MS from not MS patients, independently from intrathecal IgM synthesis (Fig 1B).

We next prospectively screened a total of 212 patients (72 MS, 40 inflammatory non-MS and 100 non-inflammatory) with the aim to sort B cells from CSF positive for PNET-binding IgM and produce from them monoclonal antibodies recapitulating the binding of the original CSF sample. From this cohort, we identified PNET binding IgM in the 11 % of MS patients and 3 % of controls (p = 0.0378, Fisher's exact test). Clinical features of tested MS donors are shown in Table 1.

Binding specificity and somatic hypermutation

From 1 CSF sample (D2358) from a CIS patient, positive for PNET-binding IgM, 1678 CD19 positive B cells were sorted, distributed into single wells of 384 well plates and cultured for 10 days in the presence of IL-21 and CD40 ligand (Fig 2A). Resulting single cell supernatants were screened by flow cytometry. Five wells exhibited binding (i.e. ratio of binding of the single cell supernatant to PNET divided by the binding of secondary antibody) to the target PNET cell line above the threshold of 1.2. Given the low number of cells that it is possible to obtain from each single donor and the interference that antibody labeling could have with the following expansion phase, we were not able to assess the phenotype of sorted and expanded B cells. From the 5 positive hits (Fig 2B), B cells were lysed, reverse-transcribed and their transcriptomes surveyed by RNA sequencing. Immunoglobulin heavy and light genes were extracted bioinformatically and recombinantly expressed in the same class as observed in the B cells from the supernatant testing, yielding 5 IgM, whose binding on PNET cells was confirmed.

The variable region sequence of the heavy and light chain of each recombinant IgM was aligned with the corresponding heavy and light variable germline sequence, thus enabling us to determine the degree of somatic hypermutation: three antibodies (G8, D20, G12) were germline, one was moderately mutated (M16) and one antibody had high degree of somatic hypermutation (B3) in both heavy and light chain (Fig 2C). This is in line with previous observation that intrathecally produced IgM are somatically hypermutated, suggesting an antigen-driven production. The reversion to unmutated heavy and light chain variable regions led to the drastic reduction in the binding capacity of the highly mutated recombinant antibody B3 (Fig 2D). When a combination of mutated HC and reverted LC or vice versa was used to produce B3, the binding was abolished by the presence of reverted HC, significantly reduced in the presence of reverted LC suggesting a role in the binding capacity of both mutated chains. Following Beltran et al. (2014), we examined the ratio of silent to replacement mutations of B3 IgM. The rationale is that antigen-driven mutation will favor amino acid-changing (replacement) mutations in the complementarity-determining regions (CDR) but will favor silent mutations in the framework regions (FR). This can be expressed as the ratio of replacement to silent mutations, whose average value in CSF IgM B cells Beltran et al. (Beltrán *et al*, 2014) reported as close to 2.9 in the FR and 6.6

in the CDR, the latter an unexpectedly high value, suggesting that the immunoglobulin mu genes of B cells in the CSF are subject to antigen-driven selection. The values we found for our most mutated antibody were strikingly similar, at 1.4 and 6.5 for the FR and CDR respectively. We conclude that this antibody is a representative of the class described by Beltrán *et al.* (Beltrán *et al.*, 2014) and that investigation of its specificity promises to give insight into this interesting population of cells.

IgM are the most effective immunoglobulin class in activating complement (Coulie & van Snick, 1985) and complement deposition is found to be present in MS lesions. We therefore tested if CSF derived IgM can induce antigen-dependent complement activation. After incubating the target PNET cell line with each of the monoclonal antibodies plus serum as a source of complement we observed that B3 was able to induce C3b deposition (Fig 3A).

Since IgM are often described as polyreactive (Nakamura *et al.*, 1988), i.e., they bind equally to antigen and non-antigen expressing cells, we tested whether the CSF derived monoclonal IgM are polyreactive, by assessing the binding of our five monoclonal antibodies on a panel of seven cell lines. All the germline antibodies and the moderately mutated IgM bound equally to multiple cell types, as well as to the target PNET (Figure 3B). The most highly mutated antibody B3 bound selectively to the PNET cell line, and therefore we decided to focus our investigations on this antibody, hypothesizing that it is part of a clone(s) that produce the PNET-binding antibodies in the CSF.

Effect of Pronase and Deglycosylation on the binding of CSF and recombinant antibodies

It has been proposed that intrathecal IgM are produced by CD5 positive B cells, responsible for the production of the so-called natural antibodies, which are usually IgM directed against nonprotein antigens (Villar *et al.*, 2005b). To narrow down the molecular nature of the target of B3, we tested the binding of each antibody to the PNET cells by flow cytometry before and after treatment with either Pronase, a mixture of enzymes that cleave the surface cell proteins in a nonspecific way, or different combinations of deglycosylation enzymes, including neuraminidase to remove terminal N- or O-acetylneuraminic acids, PNG-ase to remove N-linked sugars, and a combination of Neuraminidase, Galactosidase, n-acetylglucosaminidase and endoglycosidases to remove the largest part of surface sugars. Deglycosylation did not affect the antibody binding (Figure 3C). Instead, we observed a reduction in the binding of all the produced antibodies after treatment with Pronase, compared with untreated condition (Fig 3D). These results led us to conclude that the molecular target of our CSF derived monoclonal antibodies is a surface protein rather than a glycan.

Immunoprecipitation and membrane transcriptome analysis of bound cell lines identify SCARA5 as target antigen of CSF derived monoclonal IgM B3

Immunoprecipitation method is well established; however, most protocols assume an IgG antibody, and the immunoglobulin binding proteins A and G that are well suited for this purpose do not bind to IgM. To identify the target antigen of B3 by immunoprecipitation, we first artificially class switched it from IgM to IgG, by fusing the variable region of the heavy chain with the constant region of an IgG1. When testing the binding of the B3 IgG1 to PNET cells by flow cytometry, the binding on the target cell line was almost completely abolished (Fig 4A). We therefore modified the standard protocol for immunoprecipitation, by replacing the use protein G or protein A with magnetic beads coated with anti-human IgM. To avoid unspecific binding to intracellular proteins, live PNET cells were first incubated with B3, then washed and lysed; the lysate was next incubated with anti-IgM coated Dynabeads, washed and magnetically retrieved. By this method we were able to immunoprecipitate hemagglutinin (HA) from cells stably transfected with HA using a monoclonal anti-HA IgM. We next applied this method to immunoprecipitate the target of B3 from PNET cells. Mass spectrometry analysis of three independent experiments each including two to three technical replicates allowed to identify SCARA5 as a candidate target. Analysis of the membrane transcriptome from a panel of cell

lines either bound or not by confirmed SCARA5 as a membrane protein whose mRNA is enriched in PNET cells compared to unbound cells. SCARA5 is a type II membrane protein that forms an homotrimer on the cell surface and that exists in four known isoforms. We verified expression of SCARA5 in PNET cells by PCR amplification. We were able to confirm the expression of isoform 1 and 3 by PNET cells, 495 and 400 amino acid long respectively, (is it correct?) and we identified a novel 176 aa long isoform. We confirmed that B3 binds to SCARA5 isoform 1 and 3 and does not bind to isoform 6, by expressing each transiently in HeLa cells and assessing correct expression and binding by B3 by flow cytometry (Fig 4B).

Antigen validation and cohort screening

To test if the newly identified antigen explains the PNET IgM reactivity we observe in the CSF of MS patients, we screened a cohort of 307 CSF samples (87 from RRMS, 116 from CIS, 23 from SPMS, 14 from PPMS, 27 from inflammatory controls, 40 from non-inflammatory controls) for the presence of antibodies of any class binding to PNET cells, SCARA5 isoform 1 or SCARA5 isoform 6. We confirmed the binding of CSF IgM to PNET cells in 11 % of CIS, 10 % of RRMS patients and 3% of control patients. We identified RRMS case with IgM binding to PNET cells and to SCARA5 isoform 1 (Fig 5A). None of the PPMS, SPMS or non-inflammatory controls showed reactivity against PNET cells or cells expressing SCARA5 isoform 1. These results confirm that SCARA5 is a target highly specific for CSF IgM in MS donors but does not fully explain the observed IgM reactivity against PNET.

Brain pathology

Transcripts of molecules involved in cellular iron import like SCARA5 have been shown to be elevated in the periplaque white matter, suggesting an upregulation of cellular defense against iron toxicity in active MS lesions, and upregulation of glial iron shuttling in the periplaque white matter, around active lesions. To verify the protein expression of our newly identified SCARA5 target in MS lesions, we immunolabeled formalin-fixed, paraffin-embedded autoptic brain lesions from MS donors with a mouse polyclonal anti-SCARA5. We observed labeling of neurons, foamy macrophages and astrocytes around chronic MS lesions (Fig 5B). This result confirms that our target is expressed in pathological MS lesions in human brain tissue.

Discussion

Antibodies are produced intrathecally in several CNS disorders, and OCBs are found in the cerebrospinal fluid (CSF) of 98% of patients subsequently diagnosed with multiple sclerosis (Petzold, 2013). The most obvious outstanding question about CSF antibodies in MS concerns their target antigen(s).

In this paper, we aimed to identify the target of intrathecally produced IgM. During the screening of two blind cohorts of CSF samples, we have identified cell-binding IgM in the 10-15% of MS patients and in less than 1% of controls. These antibodies are not associated with a similar binding reactivity in serum, are restricted to the IgM class and recognize a cell surface antigen of a peripheral neuroectodermal tumour cell line. To identify their molecular target, we have applied recombinant antibody technologies to produce five monoclonal IgM from the CSF of one MS patient and used one of them, B3, to immunoprecipitate the target and validate it by confirming the binding of B3 on transiently transfected cells and by screening a cohort of MS derived CSF samples.

CSF B cells have been shown to be the source of CSF OCBs in MS patients through comparison of the CSF B cells transcriptome and the proteome of the CSF (Obermeier *et al*, 2008), thus providing a firm basis for the use of CSF B cells for our investigations about intrathecally produced antibodies. Moreover, CSF B cells from MS samples are clonally expanded, and their derived immunoglobulins

contain abundant somatic hypermutations (Qin *et al*, 1998, Beltran *et al*, 2014), thus suggesting an antigen-driven immune response. In fact, OCBs are not unique to MS and among other CNS diseases with intrathecal Ig synthesis and OCBs, all are inflammatory, and most are infectious, where they are directed against the causative agent of the disease, thus providing a rationale for the hypothesis that MS OCBs are directed against disease-relevant antigen(s) (Gilden 2016).

Despite this evidence, results regarding the identification of immunoglobulins' target antigen(s) in MS have not accumulated fast and the only autoantibodies that have been convincingly associated with MS-like diseases are Myelin Oligodendrocyte Glycoprotein (MOG) and Aquaporin-4 (Majed *et al*, 2016, Jarius *et al*, 2016), which however appear to be mainly produced peripherally and not intrathecally.

Most investigations on CSF OCBs in MS have focused on IgG, however, the presence of IgM OCB has been reported to be associated with a more active inflammatory disease phenotype, both in relapsing and in primary progressive multiple sclerosis (Villar *et al*, 2002, 2003, 2005a, 2014), a higher likelihood of conversion from CIS to clinically definite MS (Huss *et al*, 2018; Pfuhl *et al*, 2019; Ozakbas *et al*, 2017; Perini *et al*, 2006) and with spinal manifestation and independent more pronounced neuroaxonal injury in early MS, suggesting a distinct clinical phenotype and pathophysiology (Oechtering *et al*, 2022). Intriguingly, Beltran and colleagues (Beltrán *et al*, 2014) report that IgM genes from B cells in the CSF of MS patients are somatically hypermutated, counter the general assumption that IgM antibodies are usually naïve, germline-encoded Ig produced by B cells that have not yet encountered antigens, and consistent with intrathecal, antigen-driven B cell activation. In our case, the binding specificity of CSF derived monoclonal antibodies correlated with the somatic hypermutations observed in the variable regions of HC and LC and the highest binding specificity was observed for an antibody (B3) which had the highest absolute number of mutations. The ratio of replacement to silent mutation at FR and CDR for this antibody, together with the evidence of reduced binding after reversion of HC and LC mutations to germline sequences, allowed us to hypothesize that this antibody is part of the clone(s) that produce PNET-binding IgM in the CSF that has undergone antigen-driven affinity maturation.

Antibodies recognizing intracellular proteins are abundant in human serum (Pröbstel *et al*, 2016) and ubiquitous intracellular proteins have been identified as the target of recombinant antibodies produced from OCBs of MS patients (Brändle *et al*, 2016), suggesting emergence of novel epitopes during tissue destruction followed by humoral response to cell death. To avoid the identification of antibodies produced against intracellular epitopes, released during tissue destruction, we have decided to screen the CSF antibody response for cell surface antigens. In fact, a large proportion of directly pathogenic autoantibodies in neurological diseases in which the pathogenic antigen is already known, target cell surface proteins, such as ionotropic glutamate receptors or ion channels and neurotransmitter receptors (Karim & Jacob, 2018) and their described pathomechanisms include direct interference with the surface protein function, complement activation and other immune effector mechanisms. Moreover, screening for antibodies recognizing antigens expressed on the surface of live cells guarantees that the antigens are in the physiological conformation (identified as an important methodological parameter by Hohlfeld *et al*. (Hohlfeld *et al*, 2016), and greatly reduces the background, because B cells are constantly exposed to cell surface proteins, and in general tolerized to them. Transcriptomic screening of membrane proteins from cells bound by B3 compared to the unbound cells, together with immunoprecipitation of B3 target from live PFSK1 cells enabled us to identify SCARA5 as the target of this monoclonal antibody.

SCARA5 is a scavenger receptor, a superfamily of membrane-bound receptors that recognize self and non-self targets. It is a type II transmembrane protein that forms homotrimers on the cell surface and functions as a transferrin independent ferritin receptor for both iron delivery and ferritin removal (Li *et al*, 2009; Yu *et al*, 2020). Dysregulation of iron metabolism and the resultant cytotoxicity is

increasingly being implicated in MS. Physiologically, in an adult brain iron is mainly found in oligodendrocytes and myelin, while in MS patients accumulation occurs, mainly in microglia and other macrophages, suggesting an occurring pathogenic process (Bagnato *et al*, 2011). Iron within the catalytic center of various enzymes is essential for normal brain metabolism (Todorich *et al*, 2009), however free ferrous iron ions, released in case of tissue injury, are a source of toxic reactive oxygen species (ROS) (Kell, 2009), which can lead to lipid oxidation amplification of oligodendrocytes damage (Baldacchino *et al*, 2022). In active MS lesions, iron accumulates mainly extracellularly, presumably because of destruction of iron containing oligodendrocytes and myelin, while inactive demyelinating lesions show lower iron load compared to the surrounding NAWM, suggesting a clearing process (Hametner *et al*, 2013). Elevated transcripts of SCARA5 as well as of other iron import related molecules were described in MS lesions, more pronounced in the periplaque white matter, suggesting a cellular defense response against iron toxicity in active MS lesions (Hametner *et al*, 2013). The exact mechanism by which SCARA5 binding antibodies may contribute to the disease is still the objective of experimental work. However, antibody response against SCARA5 may be the result of overexpression of a tissue specific isoform following myelin damage and iron accumulation in MS lesion; moreover, antibody mediated blockage of SCARA5 could potentially exacerbate iron mediated cytotoxicity and lead to impaired remyelination.

In addition to SCARA5, ferritin binding capacity has also been described for SCARA1 (Yu *et al*, 2020), whose mRNA expression has been found to be upregulated in the rims of chronic active MS lesions and which is expressed by foamy macrophages in the rim and by ramified microglia around chronic active MS lesions and astrocytes (Hendrickx *et al*, 2013), similarly to what we observe for SCARA5. Scavenger receptors were originally identified by their ability to bind modified LDL (Husemann *et al*, 2002; Plüddemann *et al*, 2007) but they are now known to bind multiple ligands. SCARA1 is constitutively expressed by mononuclear phagocytes, such as macrophages, dendritic cells (DCs), and Kupffer cells in peripheral tissues, and by microglia in the CNS (Yamada *et al*, 1998; Platt *et al*, 2002) and has been shown to be involved in the uptake of myelin phagocytosis in vitro by microglia (Gitik *et al*, 2010; Reichert & Rotshenker, 2003; Smith, 2001), suggesting that this process could result in beneficial remyelination, leading to regeneration of axons in the CNS. However, SCARA1 deficient mice showed less severe EAE disease course and diminished demyelination (Levy-Barazany & Frenkel, 2012), by reducing activation and proliferation of CD4⁺ T cells and suggesting different roles of SCARA1 played by tissue specific expression of scavenger receptors. Intriguingly, SCARA5-null mice seem normal at birth and are fertile; however, elderly mice exhibit symptoms of autoimmune disease with lymphoid cell accumulation in the interstitial connective tissue of many organs and about one third of the null mice develop antinuclear antibodies (Ojala *et al*, 2013).

We cannot exclude that the identified SCARA5 IgM reactivity may be the result of an immune response during tissue inflammation and destruction process and may represent an immunological epiphenomenon. Also, we cannot exclude that the observed IgM response targets a complex of which SCARA5 may be one of the components.

Taken together, our results indicate SCARA5 as a target of autoantibodies in a small subset of MS patients. More precise data regarding the time point at which anti-SCARA5 reactivity is induced and the relation with the associated phenotype and prevalence must be assembled in large cohorts of patients with inflammatory demyelinating CNS disorders. Moreover, the pathological relevance of anti-SCARA5 antibodies will have to be assessed in vivo.

References

- Bagnato F, Hametner S, Yao B, Van Gelderen P, Merkle H, Cantor FK, Lassmann H & Duyn JH (2011) Tracking iron in multiple sclerosis: A combined imaging and histopathological study at 7 Tesla. In *Brain* pp 3599–3612. Oxford University Press
- Baldacchino K, Peveler WJ, Lemgruber L, Smith RS, Scharler C, Hayden L, Komarek L, Lindsay SL, Barnett SC, Edgar JM, *et al* (2022) Myelinated axons are the primary target of hemin-mediated oxidative damage in a model of the central nervous system. *Exp Neurol* 354: 114113
- Beltrán E, Obermeier B, Moser M, Coret F, Simó-Castelló M, Boscá I, Pérez-Miralles F, Villar LM, Senel M, Tumani H, *et al* (2014) Intrathecal somatic hypermutation of IgM in multiple sclerosis and neuroinflammation. *Brain* 137: 2703–2714
- Brändle SM, Obermeier B, Senel M, Bruder J, Mentele R, Khademi M, Olsson T, Tumani H, Kristoferitsch W, Lottspeich F, *et al* (2016) Distinct oligoclonal band antibodies in multiple sclerosis recognize ubiquitous self-proteins. *Proc Natl Acad Sci U S A* 113: 7864–7869
- Coulie PG & van Snick J (1985) Enhancement of IgG anti-carrier responses by IgG2 anti-hapten antibodies in mice. *Eur J Immunol* 15: 793–798
- Gilden DH. Infectious Causes of Multiple Sclerosis. *Lancet Neurol* 2006, 4(3), 195-202
- Gitik M, Reichert F & Rotshenker S (2010) Cytoskeleton plays a dual role of activation and inhibition in myelin and zymosan phagocytosis by microglia. *FASEB J* 24: 2211–2221
- Gold R, Lington C & Lassmann H (2006) Understanding pathogenesis and therapy of multiple sclerosis via animal models: 70 Years of merits and culprits in experimental autoimmune encephalomyelitis research. *Brain* 129: 1953–1971 doi:10.1093/brain/awl075
- Gultekin SH *et al.*, Paraneoplastic limbic encephalitis: neurological symptoms, immunological findings and tumour association in 50 patients. *Brain* 2000 Jul;123 (Pt 7):1481-94
- Haghikia A, Hohlfeld R, Gold R & Fugger L (2013) Therapies for multiple sclerosis: Translational achievements and outstanding needs. *Trends Mol Med* 19: 309–319 doi:10.1016/j.molmed.2013.03.004
- Hametner S, Wimmer I, Haider L, Pfeifenbring S, Brück W & Lassmann H (2013) Iron and neurodegeneration in the multiple sclerosis brain. *Ann Neurol* 74: 848–861
- Hauser SL, Waubant E, Arnold DL, Vollmer T, Antel J, Fox RJ, Bar-Or A, Panzara M, Sankar N, Agarwal S, *et al* (2008) B-cell depletion with rituximab in relapsing-remitting multiple sclerosis. *N Engl J Med* 358: 676–688
- Hendrickx DAE, Koning N, Schuurman KG, Van Strien ME, Van Eden CG, Hamann J & Huitinga I (2013) Selective upregulation of scavenger receptors in and around demyelinating areas in multiple sclerosis. *J Neuropathol Exp Neurol* 72: 106–118
- Hohlfeld R, Dornmair K, Meinl E & Wekerle H (2016) The search for the target antigens of multiple sclerosis, part 2: CD8+ T cells, B cells, and antibodies in the focus of reverse-translational research. *Lancet Neurol* 15: 317–331 doi:10.1016/S1474-4422(15)00313-0 [PREPRINT]

- Huang J, Doria-Rose NA, Longo NS, Laub L, Lin CL, Turk E, Kang BH, Migueles SA, Bailer RT, Mascola JR, *et al* (2013) Isolation of human monoclonal antibodies from peripheral blood B cells. *Nat Protoc* 8: 1907–1915
- Husemann J, Loike JD, Anankov R, Febbraio M & Silverstein SC (2002) Scavenger receptors in neurobiology and neuropathology: Their role on microglia and other cells of the nervous system. *Glia* 40: 195–205 doi:10.1002/glia.10148
- Huss A, Abdelhak A, Halbgebauer S, Mayer B, Senel M, Otto M & Tumani H (2018) Intrathecal immunoglobulin M production: A promising high-risk marker in clinically isolated syndrome patients. *Ann Neurol* 83: 1032–1036
- Jarius S *et al.*, MOG-IgG in NMO and Related Disorders: A Multicenter Study of 50 Patients. Part 1: Frequency, Syndrome Specificity, Influence of Disease Activity, Long-Term Course, Association With AQP4-IgG, and Origin. *J neuroinflammation* 2016; 13(1), 279
- Johnson KP, Arrigo SC, Nelson BJ & Ginsberg A (1977) Agarose electrophoresis of cerebrospinal fluid in multiple sclerosis: A simplified method for demonstrating cerebrospinal fluid oligoclonal immunoglobulin bands. *Neurology* 27: 273–277
- Karim AR & Jacob S (2018) Experience with newer central nervous system autoantibodies. *Ann Clin Biochem* 55: 7–17 doi:10.1177/0004563217724818
- Kell DB (2009) Iron behaving badly: Inappropriate iron chelation as a major contributor to the aetiology of vascular and other progressive inflammatory and degenerative diseases. *BMC Med Genomics* 2
- Kutzelnigg A & Lassmann H (2014) Pathology of multiple sclerosis and related inflammatory demyelinating diseases. In *Handbook of Clinical Neurology* pp 15–58. Elsevier B.V.
- Levy-Barazany H & Frenkel D (2012) Expression of Scavenger receptor A on antigen presenting cells is important for CD4+ T-cells proliferation in EAE mouse model. *J Neuroinflammation* 9
- Li JY, Paragas N, Ned RM, Qiu A, Viltard M, Leete T, Drexler IR, Chen X, Sanna-Cherchi S, Mohammed F, *et al* (2009) Scara5 Is a Ferritin Receptor Mediating Non-Transferrin Iron Delivery. *Dev Cell* 16: 35–46
- Majed M *et al.*, Clinical Utility of Testing AQP4-IgG in CSF: Guidance for Physicians. *Neurol Neuroimmunol Neuroinflamm* 2016; 3(3), e231
- Meinl E *et al.*, B lineage cells in the inflammatory central nervous system environment: migration, maintenance, local antibody production, and therapeutic modulation. *Ann neurol* 2006 Jun;56(6):880-92
- Nakamura M, Burastero SE, Ueki Y, Larrick JW, Notkins AL & Casali P (1988) Probing the normal and autoimmune B cell repertoire with Epstein-Barr virus. Frequency of B cells producing monoreactive high affinity autoantibodies in patients with Hashimoto's disease and systemic lupus erythematosus. *J Immunol* 141: 4165–72
- Obermeier B, Mentele R, Malotka J, Kellermann J, Kümpfel T, Wekerle H, Lottspeich F, Hohlfeld R & Dornmair K (2008) Matching of oligoclonal immunoglobulin transcriptomes and proteomes of cerebrospinal fluid in multiple sclerosis. *Nat Med* 14: 688–693

- Qin Y et al., Clonal expansion and somatic hypermutation of V(H) genes of B cells from cerebrospinal fluid in multiple sclerosis. *J Clin Invest.* 1998; 102:1045–1050.
- Oechtering J, Lincke T, Schaedelin S, Décard BF, Maceski A, Orleth A, Meier S, Willemse E, Buchmann A, Khalil M, et al (2022) Intrathecal IgM Synthesis Is Associated with Spinal Cord Manifestation and Neuronal Injury in Early MS . *Ann Neurol*
- Oechtering J, Schaedelin S, Benkert P, Müller S, Achtnichts L, Vehoff J, Disanto G, Findling O, Fischer-Barnicol B, Orleth A, et al (2021) Intrathecal Immunoglobulin M Synthesis is an Independent Biomarker for Higher Disease Activity and Severity in Multiple Sclerosis. *Ann Neurol* 90: 477–489
- Ojala JRM, Pikkarainen T, Elmberger G & Tryggvason K (2013) Progressive reactive lymphoid connective tissue disease and development of autoantibodies in scavenger receptor A5-deficient mice. *Am J Pathol* 182: 1681–1695
- Ozakbas S, Cinar BP, Özcelik P, Baser H & Kosehasanoğullari G (2017) Intrathecal IgM index correlates with a severe disease course in multiple sclerosis: Clinical and MRI results. *Clin Neurol Neurosurg* 160: 27–29
- Perini P, Ranzato F, Calabrese M, Battistin L & Gallo P (2006) Intrathecal IgM production at clinical onset correlates with a more severe disease course in multiple sclerosis. *J Neurol Neurosurg Psychiatry* 77: 953–955
- Petzold A (2013) Intrathecal oligoclonal IgG synthesis in multiple sclerosis. *J Neuroimmunol* 262: 1–10 doi:10.1016/j.jneuroim.2013.06.014
- Pfuhl C, Grittner U, Gieß RM, Scheel M, Behrens JR, Rasche L, Pache FC, Wenzel R, Brandt AU, Bellmann-Strobl J, et al (2019) Intrathecal IgM production is a strong risk factor for early conversion to multiple sclerosis. *Neurology* 93: e1439–e1451
- Platt N, Haworth R, Darley L & Gordon S (2002) The many roles of the class A macrophage scavenger receptor. In *International Review of Cytology* pp 1–40. Academic Press Inc.
- Plüddemann A, Neyen C & Gordon S (2007) Macrophage scavenger receptors and host-derived ligands. *Methods* 43: 207–217
- Pröbstel AK et al., Multiple Sclerosis and Antibodies against KIR4.1. *N Engl J Med.* 2016; 374(15):1496-8.
- Reichert F & Rotshenker S (2003) Complement-receptor-3 and scavenger-receptor-AI/II mediated myelin phagocytosis in microglia and macrophages. *Neurobiol Dis* 12: 65–72
- Sawcer S, Franklin RJM & Ban M (2014) Multiple sclerosis genetics. *Lancet Neurol* 13: 700–709 doi:10.1016/S1474-4422(14)70041-9
- Smith ME (2001) Phagocytic properties of microglia in vitro: Implications for a role in multiple sclerosis and EAE. *Microsc Res Tech* 54: 81–94
- Stangel M, Fredrikson S, Meinl E, Petzold A, Stüve O & Tumani H (2013) The utility of cerebrospinal fluid analysis in patients with multiple sclerosis. *Nat Rev Neurol* 9: 267–276 doi:10.1038/nrneuro.2013.41
- Todorich B, Pasquini JM, Garcia CI, Paez PM & Connor JR (2009) Oligodendrocytes and

myelination: The role of iron. *Glia* 57: 467–478 doi:10.1002/glia.20784

- Villar LM, Casanova B, Ouamara N, Comabella M, Jalili F, Leppert D, De Andrés C, Izquierdo G, Arroyo R, Avşar T, *et al* (2014) Immunoglobulin M oligoclonal bands: Biomarker of targetable inflammation in primary progressive multiple sclerosis. *Ann Neurol* 76: 231–240
- Villar LM, Masjuan J, González-Porqué P, Plaza J, Sádaba MC, Roldán E, Bootello A & Alvarez-Cermeño JC (2002) Intrathecal IgM synthesis predicts the onset of new relapses and a worse disease course in MS. *Neurology* 59: 555–559
- Villar LM, Masjuan J, González-Porqué P, Plaza J, Sádaba MC, Roldán E, Bootello A & Alvarez-Cermeño JC (2003) Intrathecal IgM synthesis is a prognostic factor in multiple sclerosis. *Ann Neurol* 53: 222–226
- Villar LM, Masjuan J, Sádaba MC, Gonzalez-Porqué P, Plaza J, Bootello A & Álvarez-Cermeño JC (2005a) Early differential diagnosis of multiple sclerosis using a new oligoclonal band test. *Arch Neurol* 62: 574–577
- Villar LM, Sádaba MC, Roldán E, Masjuan J, González-Porqué P, Villarrubia N, Espiño M, García-Trujillo JA, Bootello A & Álvarez-Cermeño JC (2005b) Intrathecal synthesis of oligoclonal IgM against myelin lipids predicts an aggressive disease course in MS. *J Clin Invest* 115: 187–194
- Wallin MT, Culpepper WJ, Campbell JD, Nelson LM, Langer-Gould A, Marrie RA, Cutter GR, Kaye WE, Wagner L, Tremlett H, *et al* (2019) The prevalence of MS in the United States: A population-based estimate using health claims data. *Neurology* 92: E1029–E1040
- Yamada Y, Doi T, Hamakubo T & Kodama T (1998) Scavenger receptor family proteins: Roles for atherosclerosis, host defence and disorders of the central nervous system. *Cell Mol Life Sci* 54: 628–640 doi:10.1007/s000180050191
- Yu B, Cheng C, Wu Y, Guo L, Kong D, Zhang Z, Wang Y, Zheng E, Liu Y & He Y (2020) Interactions of ferritin with scavenger receptor class A members. *J Biol Chem* 295: 15727–15741

Table 1

	MS	
	Anti-PNET IgM positive	Anti-PNET IgM negative
Age at sampling (y, median, st error)	47 ± 6	47 ± 2
Gender, f (%)	57%	65%
Phenotype		
CIS/RRMS	7	55
PPMS	0	2
SPMS	1	3
NMOSD	0	2
EDSS at sampling (median, st error)	3 ± 0.59	2.75 ± 0.22
Tested under immune treatment	42%	20%

Table 1. Clinical features of multiple sclerosis patients positive for CSF PNET-binding IgM

Figure Legend

Figure 1

A Comparison of IgM binding on PNET cells between MS patients and controls from two independent cohorts pooled. Each dot represents a single donor. The vertical axis is ratio of GMFI of cells incubated with the sample to cells incubated only with secondary antibody. P value is derived from a two-tailed, Wilcoxon matched pairs signed rank test.

B IgM binding is plotted against CSF IgM quotient. The results shown are from the Graz cohort only. Each dot represents a single donor. Blue dots correspond to MS donors. Yellow dots correspond to non-MS controls.

Figure 2

A Gating strategy for B cell sorting from D2358. Cells are first selected based on forward and side scatter, then CD19 positive, CD3/CD4/CD14/CD56-negative are selected and sorted.

B After sorting, B cells are expanded 1 cell/well in a total volume of 75 uL. After 10 days of culture, 15 uL are tested by flow cytometry to verify the production of antibodies binding to PNET cells. The top row shows the binding on PNET cells of IgM contained in 5 supernatants after B cell expansion. After testing, B cells from positive wells are lysed and the RNA retrieved and cDNA sequenced. The heavy and light chain sequences are used for production of monoclonal antibodies. The lower row shows the binding to PNET cells of 5 monoclonal IgM obtained from the wells shown above. The vertical axis is ratio of GMFI of cells incubated with the sample to cells incubated only with secondary antibody.

C V and J genes usage and amount of hypermutations from all the cloned antibodies.

D Binding of B3 and M16 on PNET cells after reversion of their somatic hypermutations to the germline sequence.

Figure 3

A Flow cytometric determination of antibody-dependent complement deposition on cells. PNET cells were incubated with each antibody in the presence of fresh human serum as source of complement. Activation of the complement cascade was measured by flow cytometric assessment of complement component C3b deposition on the surface of the cells. Results for B3, M16 and serum control are shown. P values were calculated by two-way analysis of variance.

B Binding of CSF derived monoclonal IgM or D2358 CSF on a panel of cell lines.

C Binding of CSF derived monoclonal IgM on PNET cells, treated or not with different combinations of glycosylation enzymes, to remove surface glycans. The vertical axis is ratio of GMFI of cells incubated with the sample to cells incubated only with secondary antibody.

D Binding of CSF derived monoclonal IgM or D2358 to PNET cells, treated or not with Pronase, to cleave surface proteins.

Figure 4

A Binding of CSF derived monoclonal antibodies expressed as IgM, as they were first isolated and cloned, or as artificially class switched IgG1. The vertical axis is ratio of GMFI of cells incubated with the sample to cells incubated only with secondary antibody.

B Binding of MAB4900 anti-SCARA5 or B3 on HEK293 transiently transfected with SCARA5 isoform 1, SCARA5 isoform 3 and a newly cloned SCARA5 which is 176 amino acids long.

Figure 5

A Results from the screening of a cohort of 307 CSF samples from MS patients and controls (either inflammatory or not inflammatory syndromes). Each dot represents one donor. The binding from each disease subgroup on two different SCARA5 isoforms or PNET cells is plotted independently. The vertical axis is ratio of GMFI of cells incubated with the sample to cells incubated only with secondary antibody.

B SCARA5 staining in neurons, foamy macrophages and astrocytes on a chronic active lesion.

Figure 1

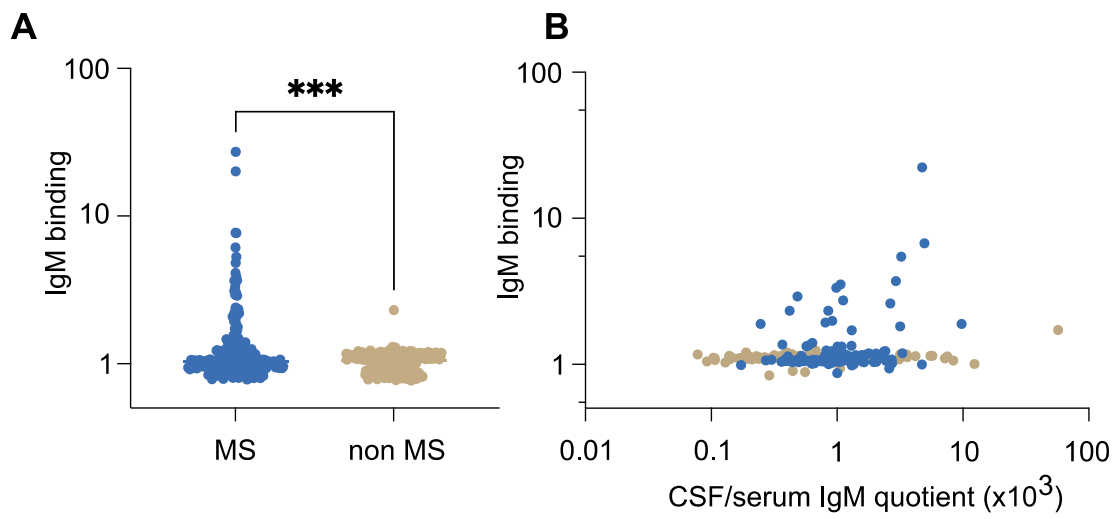
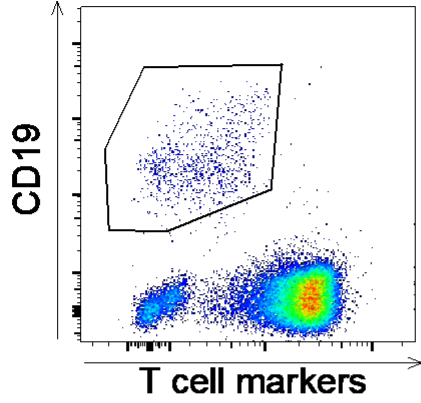
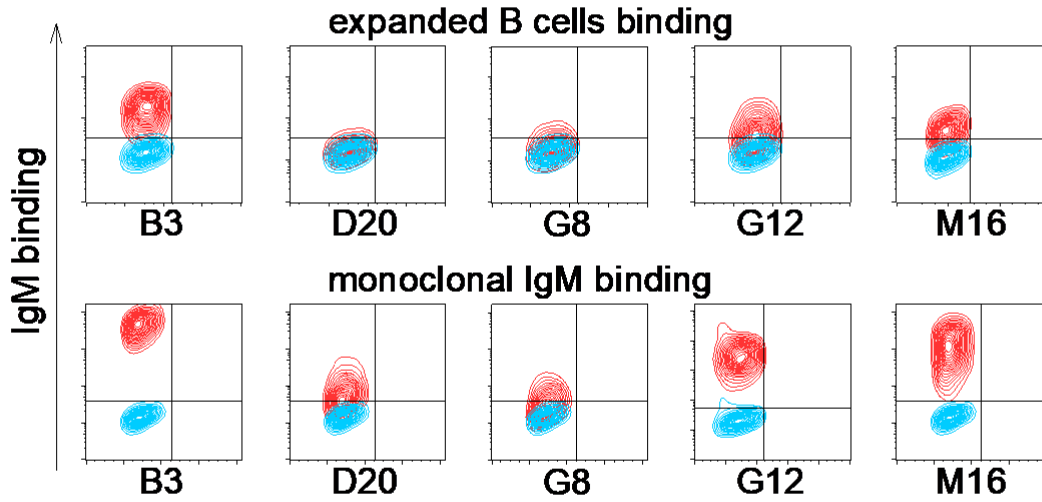


Figure 2

A D2358 B cell sorting



B



C

Antibody	Heavy and light chain	V gene	J gene	Hypermutations
B3	mu	IGHV4-59*01	IGHJ4*02	21
	kappa	IGKV2-28*01	IGKJ2*01	6
D20	mu	IGHV4-34*01	IGHJ6*02	0
	lambda3	IGLV3-19*01	IGLJ3*02	0
G8	mu	IGHV3-11*06	IGHJ4*02	0
	lambda2	IGLV3-25*03	IGLJ2*01	0
G12	mu	IGHV5-51*01	IGHJ4*02	0
	lambda1	IGLV3-1*01	IGLJ1*01	0
M16	mu	IGHV1-3*01	IGHJ5*02	4
	lambda1	IGLV2-23*02	IGLJ1*01	4

D

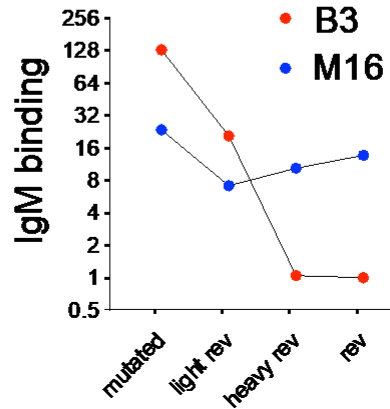


Figure 3

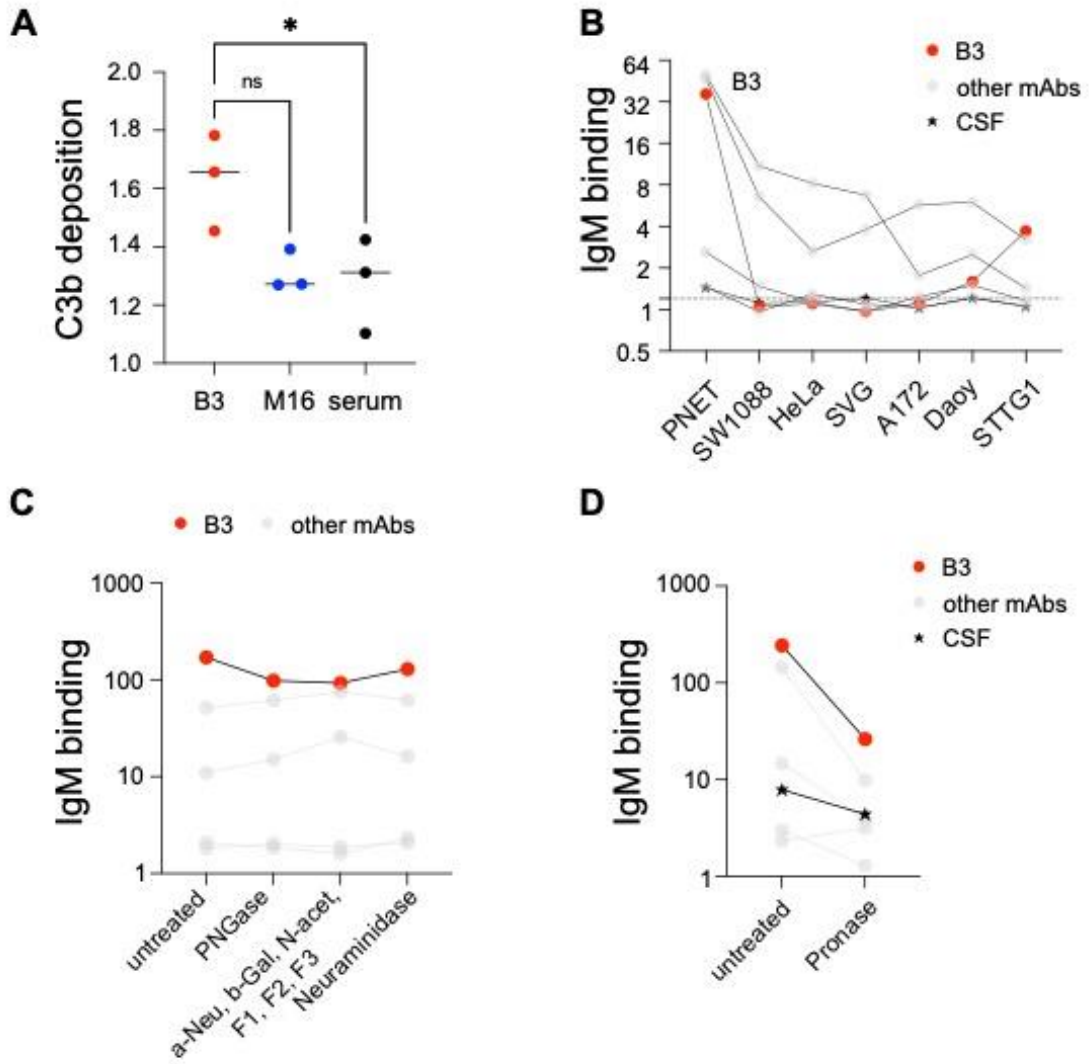


Figure 4

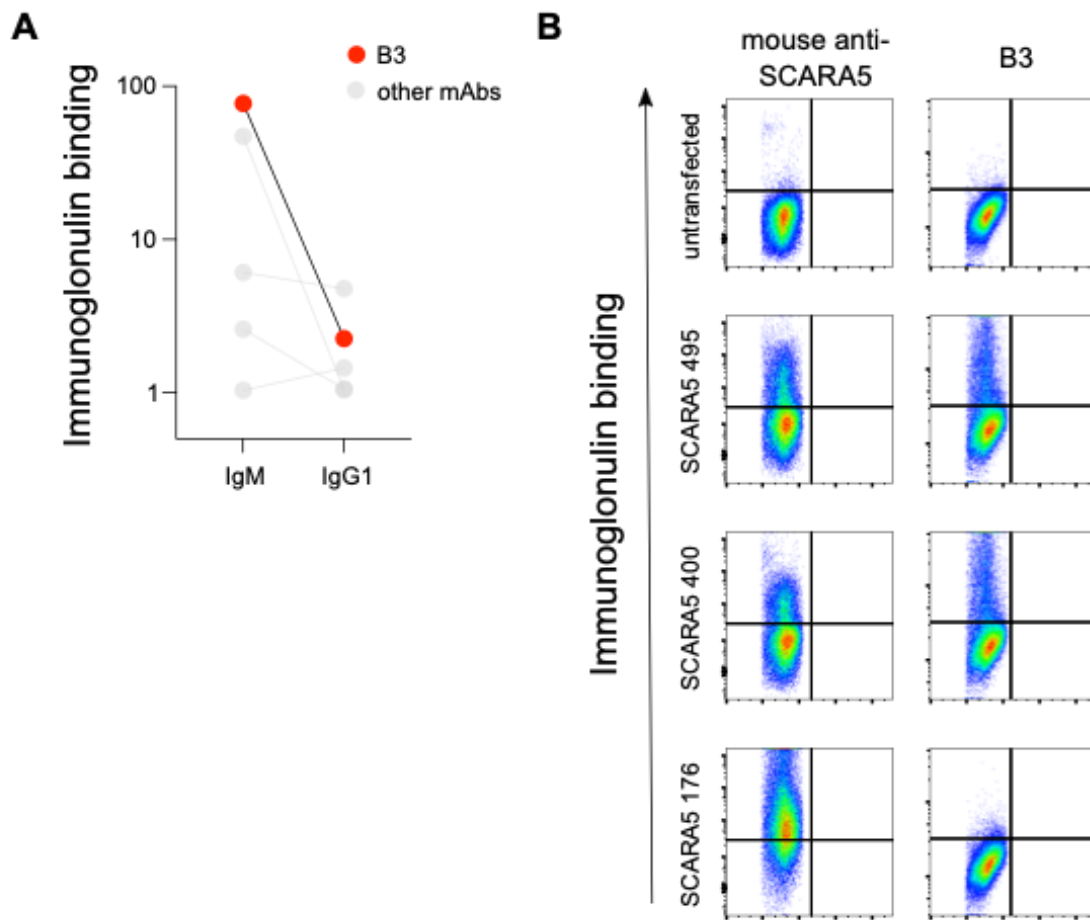
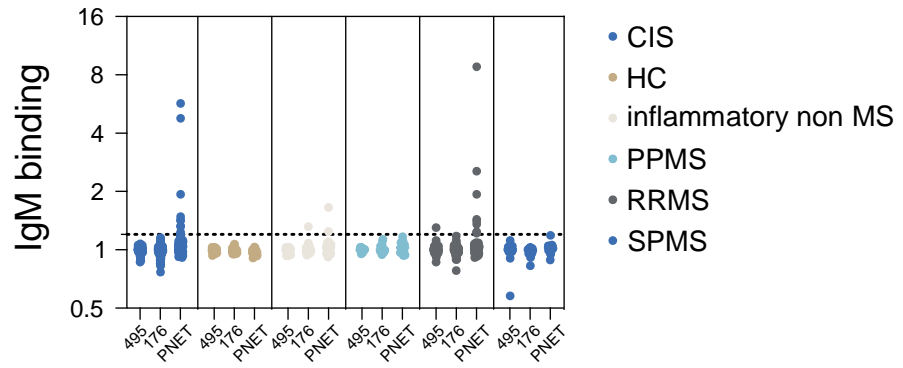
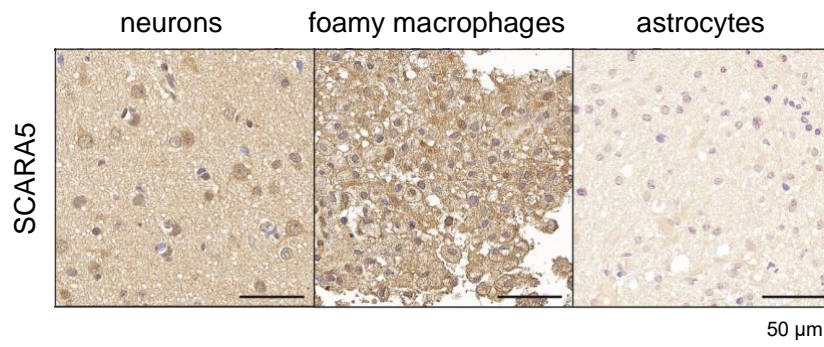


Figure 5

A



B



Natalizumab in cerebrospinal fluid and breastmilk of patients with multiple sclerosis

Ilaria Callegari^{1,2}, Mika Schneider¹, Vera Aebischer¹, Margarete M. Voortman³, Bettina Fischer-Barnicol², Michael Khalil³, Ludwig Kappos², Jens Kuhle², Nicholas Sanderson^{1,2}, Tobias Derfuss^{1,2}

1. Department of Biomedicine, University of Basel and University Hospital Basel
2. MS Center, Neurologic Clinic and Policlinic, Research Center for Clinical Neuroimmunology and Neuroscience Basel (RC2NB), University Hospital Basel, University of Basel, Switzerland
3. Medical University of Graz, Department of Neurology, Graz, Austria

Keywords

Natalizumab, cerebrospinal fluid, milk, natalizumab concentration, multiple sclerosis

Abstract

Background

Natalizumab is a highly effective monoclonal antibody for the treatment of multiple sclerosis (MS) which can diffuse in different anatomical compartments, including cerebrospinal fluid (CSF) and milk.

Objectives & Methods

Starting from incidental detection of natalizumab in the CSF of MS patients, we developed a flow-cytometry based assay and applied it to quantify natalizumab in body fluids, including milk collected from a nursing patient over 125 days.

Results

Our assay was sensitive enough to detect natalizumab in CSF, with a lower detection limit of 2 ng/ml. In breastmilk, the peak concentration was observed during the first two weeks after infusion and the average concentration over the observation time was 173.3 ng/ml, with a trend towards increased average milk concentration over subsequent administrations.

Conclusion

Routine use of such an assay would enable a better understanding of the safety of therapeutic antibody administration during pregnancy and lactation.

Introduction

Natalizumab is a recombinant humanized antibody approved for the treatment of MS that binds to the alpha4beta1-integrin, thus preventing the adhesion and migration of lymphocytes across the blood–brain barrier (BBB). As a monoclonal antibody of the IgG4 class, its molecular weight is thought to limit crossing of the BBB or diffusion into other anatomical compartments, such as breastmilk. However, in diseases characterized by BBB disruption, large pharmacological molecules may diffuse into the CSF in a less predictable way (Lampson, 2011), and depending on the concentration gradient, monoclonal antibodies as well as other therapeutic molecules can passively diffuse into milk (Anderson & Sauberan, 2016). In this study, we initially detected natalizumab in the CSF of treated patients while looking for antibodies binding to a peripheral neuroendocrine tumor cell line PFSK1 that expresses the alpha4beta1-integrin. Starting from this finding, we developed a flow cytometry based assay and used it to determine natalizumab concentration in CSF, serum and breastmilk of patients with MS.

Methods

Sample collection

CSF samples were collected from diagnostic lumbar punctures from 250 patients from two independent cohorts (N=150 for cohort 1, N=100 for cohort 2). All procedures were approved by the Ethical Committee of Northwest Switzerland. Milk samples were collected from a 35-year-old woman, affected by relapsing remitting multiple sclerosis (RRMS), under natalizumab treatment for the past 14 years. Informed consent for publication was provided by the patient. Natalizumab administration was stopped 6 weeks before delivery and resumed 4 weeks post-partum, with an infusion every 6 weeks after conception. Eighteen milk samples were collected before the first post-partum infusion (T0), and on a weekly basis for the following 125 days (average of interval between samples 8 days \pm 1). Matching serum samples were collected after 112, 122 and 143 days from the first infusion (9, 19 and 40 days from the previous infusion). Seventeen other serum samples from untreated donors were tested as controls. Serum, CSF and milk samples were aliquoted and kept at -20 °C until analysis.

Flow cytometry

Before measurement, milk samples were thawed and centrifuged at 2000g for 10 minutes for lipid separation. For the assay, 50,000 PFSK1 cells were distributed into each well of 96-well plates. For the first experiment a serial two-fold dilution of milk was done, from undiluted until 1:512 dilution. A 1:4 dilution of milk was chosen for the following three independent replicates. CSF was tested at 1:4 dilution. Serum was tested using a serial 2-fold titration starting from 1:20. A standard curve was prepared by incubating the same cells with T0 milk, spiked with natalizumab starting from 10 μ g/ml and serially diluted to 0.15 ng/ml. Cells were incubated on ice for 30 minutes, washed twice in PBS and labeled with 1:200 dilution of Alexafluor-488-conjugated anti-human IgG (JIR 109-096-098) or anti-IgG4 (Southern Biotech, 9200-30) for 30 minutes on ice. After 2 washes in PBS, cells were resuspended in 4% paraformaldehyde and acquired using a Beckman Coulter CytoFLEX flow cytometer equipped with a 96-well plate reader.

Statistical analysis

Concentrations were calculated using the quadrantic interpolator from dcr package in R and by noncompartmental pharmacokinetic methods, provided by GraphPad Prism (GraphPad Software, La Jolla, California), subtracting the geometric mean of the fluorescent intensity (GMFI) of cells incubated with a titration of T0 milk to the GMFI of the standard curve. Average milk concentration over a 6-week period was calculated excluding the concentration obtained during the first two weeks after infusion to eliminate the peak effect.

Results

Free natalizumab is detected in CSF, serum and milk of treated patients

While screening a cohort of 150 CSF samples for antibodies binding to a panel of neural derived cell lines, we identified a subset of MS patients (n=3 out of 63 MS patients) with CSF IgG binding to PFSK1 cells. None of the non-inflammatory controls (n= 87) showed IgG reactivity against this cell line (Fig 1A). The test of an independent CSF cohort (n= 100) (Neurologie, Medizinische Universität Graz) and analysis of the clinical features of positive patients, revealed that all PFSK1-binding IgG positive patients (n= 5 from the two cohorts) were under natalizumab treatment (Fig 1B). We confirmed that the identified PFSK1 reactivity was due to the detection of free natalizumab by using an anti-IgG4 secondary antibody and by testing binding of natalizumab on the same cell line. We tested 22 CSF and 20 serum samples in a blind fashion: all 3 patients under natalizumab showed IgG4 binding to PFSK1 in both CSF and serum while none of the untreated patients showed this reactivity (Fig 1C-D). Average CSF natalizumab concentration was 63.6 \pm 32.1 ng/ml (mean \pm SE). CSF

natalizumab content correlated with the time from previous infusion but did not correlate with treatment duration.

Having demonstrated the feasibility of measuring natalizumab concentration with a lower detection limit of 2 ng/ml, we applied the technique to measuring free natalizumab in breastmilk. IgG4 binding from the milk at T0, obtained after 70 days from the last pre-delivery administration, was comparable with the one obtained incubating the cells only with the secondary antibody. Free natalizumab was detectable in all the milk samples after the first drug exposure, with a concentration of 173.3 \pm 52.7 ng/ml (mean \pm SE) overall. Peak natalizumab concentration was reached after one week from each infusion, with a maximum concentration of 878 ng/ml after the first infusion. Parallel serum samples were available at 2 timepoints, after 9 and 19 days from the third infusion, with an average concentration of 4639 ng/ml and a breastmilk to serum ratio of 5.38 % and 1.7 % respectively. When comparing natalizumab concentration over each dose interval, we observed a tendency towards reduction of the peak effect and a progressive increase of the average concentration over the time, although this did not reach statistical significance (Fig 2A-B).

Discussion

During an unbiased screening of CSF samples looking for autoantibodies binding to novel antigenic targets in MS patients, we encountered a subset of MS samples with IgG reactivity against PFSK1 cells which could have been misinterpreted as MS specific antibodies but were actually due to a confounding variable (natalizumab treatment). We decided to apply this result to develop a flow cytometric assay to measure natalizumab in different biological samples, including serum, CSF and milk. Diffusion of natalizumab in CSF and milk has been reported (Table 1) (Baker *et al*, 2015; Proschmann *et al*, 2018; Matro *et al*, 2018; Ciplea *et al*, 2020; Proschmann *et al*, 2021; Sehr *et al*, 2016; Harrer *et al*, 2015). Our newly developed assay for detection of natalizumab is easy to establish, reproducible and sensitive enough to enable measurement in two biological compartments where diffusion of monoclonal antibodies is considered low or negligible (Lampson, 2011). The measured concentrations are comparable to those reported by others (Table 1).

Currently natalizumab administration is contraindicated during pregnancy and lactation, as are most of the disease-modifying treatments approved for MS, due to lack of safety information (Callegari *et al*, 2021). On the other hand, natalizumab discontinuation has been associated with MS reactivation and MS rebound activity (Hellwig *et al*, 2022) that requires close monitoring after withdrawal. While the limited number of samples tested does not allow to make a generalized statement about natalizumab kinetics and safety, the incorporation of our assay into routine patient monitoring would provide further guidance for the management of therapeutic antibody administration during pregnancy and lactation.

References

- Anderson PO & Sauberan JB (2016) Modelling drug passage into human milk. *Clin Pharmacol Ther* 100: 42–52
- Baker TE, Cooper SD, Kessler L & Hale TW (2015) Transfer of natalizumab into breast milk in a mother with multiple sclerosis. *J Hum Lact* 31: 233–236
- Callegari I, Derfuss T & Galli E (2021) Update on treatment in multiple sclerosis. *Press Medicale* 50: 104068
- Ciplea AI, Langer-Gould A, de Vries A, Schaap T, Thiel S, Ringelstein M, Gold R & Hellwig K (2020) Monoclonal antibody treatment during pregnancy and/or lactation in women with MS or neuromyelitis optica spectrum disorder. *Neurol Neuroimmunol neuroinflammation* 7(4):e723
- Harrer A, Pilz G, Wipfler P, Oppermann K, Sellner J, Hitzl W, Haschke-Becher E, Afazel S, Rispens T, van der Kleij D, *et al* (2015) High interindividual variability in the CD4/CD8 T cell ratio and natalizumab concentration levels in the cerebrospinal fluid of patients with multiple sclerosis. *Clin Exp Immunol* 180: 383–392
- Hellwig K, Tokic M, Thiel S, Esters N, Spicher C, Timmesfeld N, Ciplea AI, Gold R & Langer-Gould A (2022) Multiple Sclerosis Disease Activity and Disability Following Discontinuation of Natalizumab for Pregnancy. *JAMA Netw Open* 5: E2144750
- Lampson LA (2011) Monoclonal antibodies in neuro-oncology: Getting past the blood-brain barrier. *MAbs* 3: 153–160
- Matro R, Martin CF, Wolf D, Shah SA & Mahadevan U (2018) Exposure Concentrations of Infants Breastfed by Women Receiving Biologic Therapies for Inflammatory Bowel Diseases and Effects of Breastfeeding on Infections and Development. *Gastroenterology* 155: 696–704
- Proschmann U, Haase R, Inojosa H, Akgün K & Ziemssen T (2021) Drug and Neurofilament Levels in Serum and Breastmilk of Women With Multiple Sclerosis Exposed to Natalizumab During Pregnancy and Lactation. *Front Immunol* 12
- Proschmann U, Thomas K, Thiel S, Hellwig K & Ziemssen T (2018) Natalizumab during pregnancy and lactation. *Mult Scler* 24: 1627–1634
- Sehr T, Proschmann U, Thomas K, Marggraf M, Straube E, Reichmann H, Chan A & Ziemssen T (2016) New insights into the pharmacokinetics and pharmacodynamics of natalizumab treatment for patients with multiple sclerosis, obtained from clinical and in vitro studies. *J Neuroinflammation* 13

Figure Legend

Figure 1

A IgG binding on PFSK1 cells from CSF of MS donors compared to non-inflammatory controls ($p = 0.008$, Mann-Whitney test) using an anti-IgG antibody. Each dot corresponds to the binding of IgG on PFSK1 (ratio of geometric mean of the fluorescence intensity – GMFI – of cells incubated with the sample to cells incubated only with secondary antibody) from each CSF sample.

B IgG binding on PFSK1 cells in natalizumab treated compared to untreated patients; results from two independently tested cohorts are pooled and expressed as the number of standard deviations by which each sample is above or below the mean value of the control samples ($p < 0.0001$, Mann-Whitney test). Each dot corresponds to one sample.

C Natalizumab detection in CSF from treated patients compared to untreated patients ($p < 0.0015$, Mann-Whitney test) using an anti-IgG4 antibody. Each dot corresponds to the binding of IgG4 on PFSK1 (ratio of geometric mean of the fluorescence intensity – GMFI – of cells incubated with the sample to cells incubated only with secondary antibody) from each serum sample.

D Natalizumab detection in serum from treated patients compared to untreated patients ($p < 0.0018$, Mann-Whitney test) using an anti-IgG4 antibody. Each dot corresponds to the binding of IgG4 on PFSK1 (ratio of GMFI of cells incubated with the sample to cells incubated only with secondary antibody) from each serum sample

Figure 2

A Natalizumab concentration in breastmilk and paired serum samples. The horizontal axis shows the number of days from the first infusion. The vertical axis shows natalizumab concentration in ng/ml. Each dot corresponds to the mean of three replicates. Error bars are standard error. Arrows indicate single infusions.

B Comparison of milk average concentration during three subsequent infusion intervals. Natalizumab concentration from each inter-dose timeframe is plotted, excluding the first two-week timepoints, and compared by Mann-Whitney test, showing non-significant progressive accumulation of the drug in milk. Error bars show standard error.

Table 1

Summary of studies reporting measurement of Natalizumab in breastmilk in women with MS or IBD treated during pregnancy and breastfeeding and in CSF of treated MS patients. C_{max} is maximum measured concentration.

Table 2

Demographic features of the two independent CSF cohorts.

Table 1

Publication	Type of study	Material	NTZ Dose	Interval	Analytical method	N of Patients	Cmax	Peak
Baker et al., 2015	Case report	Milk	300 mg	4 w	ELISA at Biogen	1	2.83 µg/ml	50 d
Ciplea et al., 2020	Prospective	Milk	300 mg	4-6 w	ELISA with anti-idiotipe antibody	2	140 ng/ml	2-5 d
Matro et al., 2018	Prospective	Milk	300 mg	4 w	Homogenous mobility shift assay	2	460 ng/ml	24 h
Porschmann et al., 2018	Cohort study	Milk	300 mg	4 w	Flow cytometry	4	412 ng/ml	1-8 d
Porschmann et al., 2021	Prospective	Milk	300 mg	4 w	Flow cytometry	11	306 ng/ml	1-8 d
Sehr et al., 2016	Prospective	CSF	300 mg	4-8 w	Flow cytometry	27	44.8 ng/ml	
Harrer et al., 2015	Prospective	CSF	300 mg	3.9 □ 1.5 w	ELISA	15	111 ng/ml	

Table 2

	Basel Cohort	Graz Cohort
N samples	150	100
CIS	1	1
CDMS	62	32
Non-MS	87	67
Age at sampling (average \pm SD)	49 \pm 16	35 \pm 11
Sex (female %)	63%	60%
Under therapy at LP	15	4
Natalizumab	3	2

Figure 1

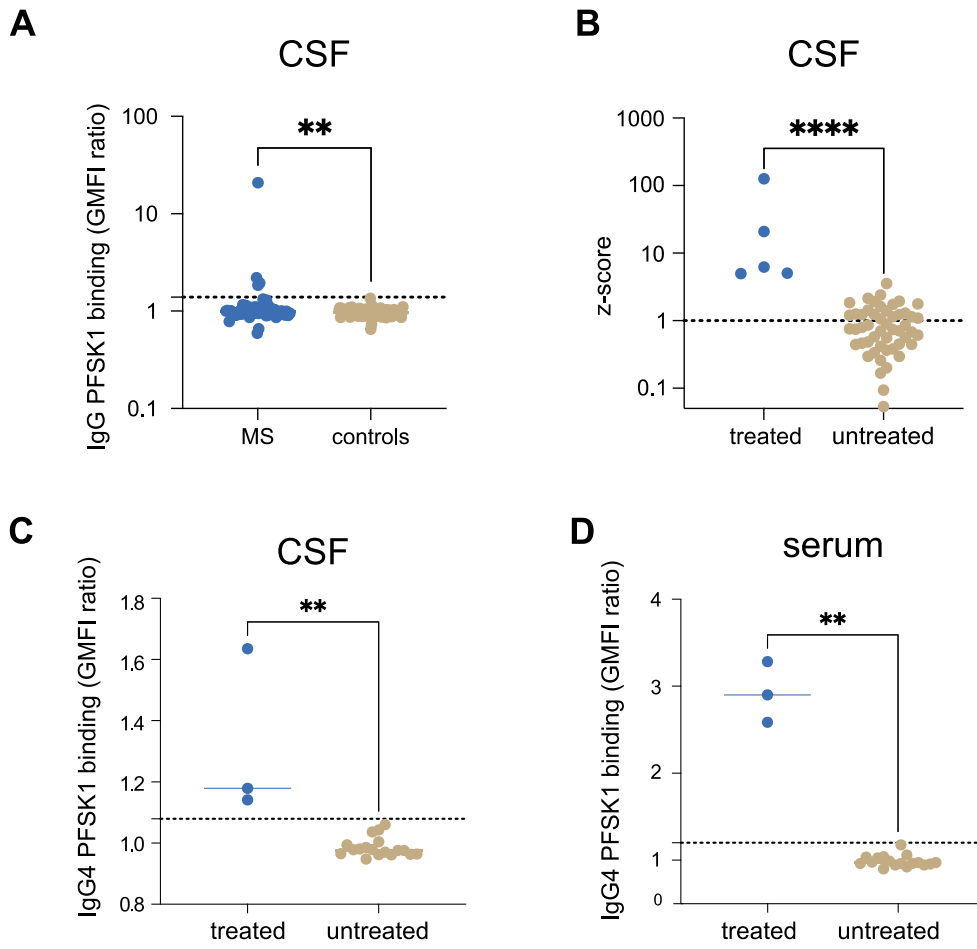
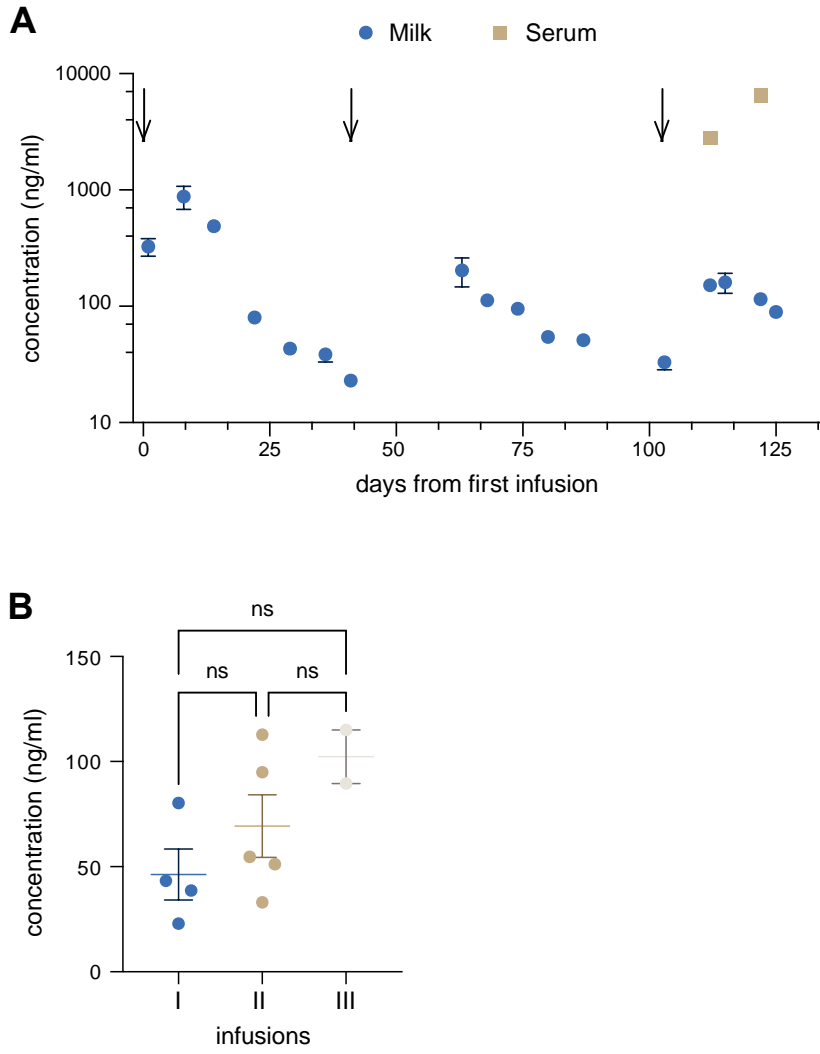


Figure 2



DISCUSSION AND CONCLUSIONS

In this work we first focused on dissecting the class specific properties of antibodies raised against a viral infection, by isolating potentially neutralizing IgM, whose neutralizing ability was dramatically impaired by the artificial class switch to IgG1.

IgM are poorly characterized antibodies, perhaps because of the common confusion between natural unspecific antibodies that are present normally in the serum independently from antigen exposure and the antigen-specific antibodies that rise after acute immunization. In our study, in contrast to total serum IgM, SARS-CoV-2 spike-specific IgM antibodies did not show increased auto-reactivity and SARS-CoV-2 spike-binding IgM antibodies were exquisitely specific as their IgG counterparts. Feldman *et al* (Feldman *et al*, 2021) also reported that spike-specific antibodies cloned from naïve donors exhibited no polyreactivity. One possible reason why we did not observe unspecific binding by the anti-spike IgM antibodies lies in the method used for isolating the B cells: membrane antigen capture requires a higher affinity than is needed simply to bind the antigen (Natkanski *et al*, 2013).

Early studies of recombinantly produced human monoclonal antibodies (Tiller *et al*, 2008) often involved switching of IgM antibodies to IgG for recombinant production and testing, and this approach has been employed by the few workers to study the properties of IgM antibodies against SARS-CoV-2 (Wang *et al*, 2021; Feldman *et al*, 2021). Our results make clear that this exchange is likely to have a dramatic effect on their functional properties. Wang *et al* (Wang *et al*, 2021) successfully isolated a large number of RBD-binding monoclonal antibodies of IgM, IgG, and IgA classes; the IgG and IgA included several highly potent neutralizing antibodies, but the IgM, which were expressed as IgG1 after artificial class switch were fewer and less potent. Thouvenel *et al* (Thouvenel *et al*, 2021) also observed that IgM antibodies against Plasmodium parasites lost their potency if converted to monomeric IgG. An obvious question is what the mechanistic basis for this IgM class- dependent potency might be. The effect could be ascribed to the reduction in avidity (Rodda *et al*, 2021) but also to other factors like enhanced steric blockade or epitope accessibility.

Thus IgM antibodies may have potential in a therapeutic context (Keyt *et al*, 2020). The same technical problems that have retarded their study are also relevant for the commercial development, but if these can be overcome, their potency, their ability to activate complement, and their transport over mucosa by the polymeric immunoglobulin receptor (Turula & Wobus, 2018) could all be exploited for therapeutic applications.

The powerful influence of class on neutralization we observed here was unexpected, and the influence of isotype must be considered when investigating the properties of naturally produced antibodies. Other important functions of antibodies are known to be class- and subclass-dependent. The influence of antibody class on complement activation, for example, is well established (Lu *et al*, 2018). Antibodies of different classes also affect the immune system via class- specific Fc receptors in different ways (Boudreau & Alter, 2019; Zohar *et al*, 2020). Using membrane antigen capture to identify high affinity antigen-specific B cells reveals properties of IgM in acute infection that may previously have been

obscured by abundant polyreactive B cells and antibodies. The next challenge will be to develop assays that visualize the complex, class- and specificity- dependent interactions of antibodies with the rest of the immune system, that are nonetheless simple enough to be used at revealingly high throughput.

Next, we used the optimized methods for monoclonal antibody production to produce monoclonal antibodies targeting an unknown surface protein target and used them for antigen identification.

For the identification of the target of CSF IgM, we initially screened patients CSF samples for antibodies of any class binding to the cell surface of neural or glial derived cell lines. We focused on membrane antigens because we believe that antigen conformation and expression in the context of a cell membrane is relevant for a proper antibody binding and that membrane antigens are continually accessible to the immune system, therefore autoantibodies directed against them are likely to be pathogenic.

Previous reports of specific autoantibodies in multiple sclerosis have often been dismissed as epiphenomena (Ruutiainen *et al*, 1981). One reason for this is the inflammatory nature of multiple sclerosis, which could increase levels of non-specific «natural» antibodies, as is the case in other inflammatory autoimmune conditions (Jasani *et al*, 1999).

Our identification of IgM targeting a PNET cell line, present only in MS donors, supports the possibility that autoantibody-mediated processes are important at least in a subgroup of multiple sclerosis patients. Using monoclonal antibodies cloned from the CSF of a MS patient we identified SCARA5 as a target for B3, whose expression is altered in MS lesions, in line with altered iron extracellular accumulation in chronic active lesion. We could not demonstrate SCARA5 specific IgM response in a large subset of MS patients. Also, we cannot exclude that the identified target is part of a membrane complex against which CSF B cells are reactive. We will perform a series of experiment to better understand the role of SCARA5 IgM in the pathogenesis of MS. To confirm the involvement of SCARA5 in B3 binding, it will be necessary further validate the immunoprecipitation results by western blot, by probing the lysate of transfected cells with B3. Binding pattern on human fetal brain by our recombinant monoclonal antibodies will be evaluated, to assess binding on proteins appearing early in brain development. SCARA5 protein expression in different brain areas will be evaluated as well. The pathogenic role of anti-SCARA5 IgM will be assessed *in vivo*.

Finally, we applied the incidental finding of natalizumab in the CSF of treated multiple sclerosis patients to develop a flow-cytometry based assay enabling to quantify natalizumab concentration in CSF, serum and breastmilk of multiple sclerosis patients.

Data regarding Natalizumab diffusion into milk are not abundant in literature. The assay we developed is highly sensitive, with a lower detection limit of 2 ng/ml, enabling the measurement of natalizumab concentration in both milk and CSF, where its diffusion of monoclonal antibodies is considered low or negligible (Lampson, 2011)(Lampson, 2011). The concentration we detected in the different type of samples is comparable with that already reported in literature. The inter-individual variability in terms

of milk absolute amount and tendency to accumulate observed in different studies could be explained by the different natalizumab concentration in the maternal serum or by the different intervals between administration and milk collection. Other influencing factors include differences milk pH, protein and lipid content.

The detection of Natalizumab in breast milk raises the question of safety. While the benefits of breastfeeding on infant health are well known, there is limited information available on the safety of disease modifying treatments use during lactation. Currently Natalizumab administration is contraindicated during pregnancy and lactation, as most of the approved DMT, due to lack of safety statements (Callegari *et al*, 2021). However, Natalizumab discontinuation has been associated with MS reactivation and MS rebound activity (Hellwig *et al*, 2022) that requires close monitoring after withdrawal. Data on other therapeutic monoclonal antibodies show low breastmilk transfer of rituximab (Bragnes *et al*, 2017; Krysko *et al*, 2020) with median RID 0.08% (range 0.06–0.10%), and normal B-cell counts in infants receiving breastmilk during rituximab or ocrelizumab treatment (Ciplea *et al*, 2020), suggesting that the transfer of these drugs is compatible with breastfeeding and that the amount of monoclonal antibodies that enter the circulation after oral intake with breastmilk is biologically negligible. Nevertheless, the neonatal Fc receptor may allow transport of some IgG molecules into circulation and further studies are needed to better understand the transfer of monoclonal antibodies compound across the infant's gut.

Our case expands the current literature about Natalizumab treatment during lactation and highlights the problem safe DMT administration during postpartum. While the limited number of samples tested does not allow to make a generalized statement, the incorporation of our assay into routinary analysis could provide further guidance for the management of monoclonal antibodies administration during pregnancy and lactation.

REFERENCES

- Aloisi F & Pujol-Borrell R (2006) Lymphoid neogenesis in chronic inflammatory diseases. *Nat Rev Immunol* 6: 205–217 doi:10.1038/nri1786 [PREPRINT]
- Åman P, Ehlin-Henriksson B & Klein G (1984) Epstein-barr virus susceptibility of normal human B lymphocyte populations. *J Exp Med* 159: 208–220
- Archelos JJ, Storch MK & Hartung H-P (2000) The role of B cells and autoantibodies in multiple sclerosis. *Ann Neurol* 47: 694–706
- Banatvala JE & Chrystie IL (1977) BK antibody and virus-specific IgM responses in renal transplant recipients, patients with malignant disease, and healthy people. *Br Med J* 2: 220–223
- Banchereau J (2015) Generation of human B-cell lines dependent on CD40-ligation and interleukin-4. *Front Immunol* 6 doi:10.3389/fimmu.2015.00055 [PREPRINT]
- Barr TA, Shen P, Brown S, Lampropoulou V, Roch T, Lawrie S, Fan B, O'Connor RA, Anderton SM, Bar-Or A, *et al* (2012) B cell depletion therapy ameliorates autoimmune disease through ablation of IL-6-producing B cells. *J Exp Med* 209: 1001–1010
- Batista FD, Iber D & Neuberger MS (2001) B cells acquire antigen from target cells after synapse formation. *Nature* 411: 489–494
- Bohannon C, Powers R, Satyabhama L, Cui A, Tipton C, Michaeli M, Skountzou I, Mittler RS, Kleinstein SH, Mehr R, *et al* (2016) Long-lived antigen-induced IgM plasma cells demonstrate somatic mutations and contribute to long-Term protection. *Nat Commun* 7
- Bonsignori M, Hwang K-K, Chen X, Tsao C-Y, Morris L, Gray E, Marshall DJ, Crump JA, Kapiga SH, Sam NE, *et al* (2011) Analysis of a Clonal Lineage of HIV-1 Envelope V2/V3 Conformational Epitope-Specific Broadly Neutralizing Antibodies and Their Inferred Unmutated Common Ancestors. *J Virol* 85: 9998–10009
- Boudreau CM & Alter G (2019) Extra-neutralizing FcR-mediated antibody functions for a universal influenza vaccine. *Front Immunol* 10 doi:10.3389/fimmu.2019.00440 [PREPRINT]
- Bragnes Y, Boshuizen R, de Vries A, Lexberg Å & Østensen M (2017) Low level of Rituximab in human breast milk in a patient treated during lactation. *Rheumatol (United Kingdom)* 56: 1047–1048 doi:10.1093/rheumatology/kex039 [PREPRINT]
- Braren I, Blank S, Seismann H, Deckers S, Ollert M, Grunwald T & Spillner E (2007) Generation of human monoclonal allergen-specific IgE and IgG antibodies from synthetic antibody libraries. *Clin Chem* 53: 837–844
- Brewer JW, Randall TD, Parkhouse RME & Corley RB (1994) Mechanism and subcellular localization of secretory IgM polymer assembly. *J Biol Chem* 269: 17338–17348
- Von Büdingen HC, Palanichamy A, Lehmann-Horn K, Michel BA & Zamvil SS (2015) Update on the autoimmune pathology of multiple sclerosis: B-cells as disease-drivers and therapeutic targets. *Eur Neurol* 73: 238–246
- Callegari I, Derfuss T & Galli E (2021) Update on treatment in multiple sclerosis. *Press Medicale* 50: 104068 doi:10.1016/j.lpm.2021.104068 [PREPRINT]
- Casali P, Inghirami G, Nakamura M, Davies TF & Notkins AL (1986) Human monoclonals from

antigen-specific selection of B lymphocytes and transformation by EBV. *Science* (80-) 234: 476–479

- Ciplea AI, Langer-Gould A, de Vries A, Schaap T, Thiel S, Ringelstein M, Gold R & Hellwig K (2020) Monoclonal antibody treatment during pregnancy and/or lactation in women with MS or neuromyelitis optica spectrum disorder. *Neurol Neuroimmunol neuroinflammation* 7
- Dalmau J, Tüzün E, Wu HY, Masjuan J, Rossi JE, Voloschin A, Baehring JM, Shimazaki H, Koide R, King D, *et al* (2007) Paraneoplastic anti-N-methyl-D-aspartate receptor encephalitis associated with ovarian teratoma. *Ann Neurol* 61: 25–36
- Dodev TS, Karagiannis P, Gilbert AE, Josephs DH, Bowen H, James LK, Bax HJ, Beavil R, Pang MO, Gould HJ, *et al* (2014) A tool kit for rapid cloning and expression of recombinant antibodies. *Sci Rep* 4
- Eggers EL, Michel BA, Wu H, Wang SZ, Bevan CJ, Abounasr A, Pierson NS, Bischof A, Kazer M, Leitner E, *et al* (2017) Clonal relationships of CSF B cells in treatment-naïve multiple sclerosis patients. *JCI Insight* 2
- Eisen HN (2014) Affinity enhancement of antibodies: how low-affinity antibodies produced early in immune responses are followed by high-affinity antibodies later and in memory B-cell responses. *Cancer Immunol Res* 2: 381–392 doi:10.1158/2326-6066.CIR-14-0029 [PREPRINT]
- Feldman J, Bals J, Altomare CG, Denis KS, Lam EC, Hauser BM, Ronsard L, Sangesland M, Moreno TB, Okonkwo V, *et al* (2021) Naive human B cells engage the receptor binding domain of SARS-CoV-2, variants of concern, and related sarbecoviruses. *Sci Immunol* 6
- Fellah JS, Wiles M V., Charlemagne J & Schwager J (1992) Evolution of vertebrate IgM: complete amino acid sequence of the constant region of *Ambystoma mexicanum* μ chain deduced from cDNA sequence. *Eur J Immunol* 22: 2595–2601
- Fleire SJ, Goldman JP, Carrasco YR, Weber M, Bray D & Batista FD (2006) B cell ligand discrimination through a spreading and contraction response. *Science* (80-) 312: 738–741
- Gilhus NE (2016) Myasthenia Gravis. *N Engl J Med* 375: 2570–2581
- Gold R, Linington C & Lassmann H (2006) Understanding pathogenesis and therapy of multiple sclerosis via animal models: 70 Years of merits and culprits in experimental autoimmune encephalomyelitis research. *Brain* 129: 1953–1971 doi:10.1093/brain/awl075 [PREPRINT]
- Graus F, Titulaer MJ, Balu R, Benseler S, Bien CG, Cellucci T, Cortese I, Dale RC, Gelfand JM, Geschwind M, *et al* (2016) A clinical approach to diagnosis of autoimmune encephalitis. *Lancet Neurol* 15: 391–404 doi:10.1016/S1474-4422(15)00401-9 [PREPRINT]
- Haghikia A, Hohlfeld R, Gold R & Fugger L (2013) Therapies for multiple sclerosis: Translational achievements and outstanding needs. *Trends Mol Med* 19: 309–319 doi:10.1016/j.molmed.2013.03.004 [PREPRINT]
- Harada Y, Muramatsu M, Shibata T, Honjo T & Kuroda K (2003) Unmutated immunoglobulin M can protect mice from death by influenza virus infection. *J Exp Med* 197: 1779–1785
- Hauser SL (2015) The Charcot Lecture | Beating MS: A story of B cells, with twists and turns. *Mult Scler J* 21: 8–21 doi:10.1177/1352458514561911 [PREPRINT]
- Hauser SL, Waubant E, Arnold DL, Vollmer T, Antel J, Fox RJ, Bar-Or A, Panzara M, Sarkar N,

- Agarwal S, *et al* (2008a) B-cell depletion with rituximab in relapsing-remitting multiple sclerosis. *N Engl J Med* 358: 676–688
- Hauser SL, Waubant E, Arnold DL, Vollmer T, Antel J, Fox RJ, Bar-Or A, Panzara M, Sarkar N, Agarwal S, *et al* (2008b) B-Cell Depletion with Rituximab in Relapsing–Remitting Multiple Sclerosis. *N Engl J Med* 358: 676–688
- Hellwig K, Tokic M, Thiel S, Esters N, Spicher C, Timmesfeld N, Ciplea AI, Gold R & Langer-Gould A (2022) Multiple Sclerosis Disease Activity and Disability Following Discontinuation of Natalizumab for Pregnancy. *JAMA Netw Open* 5: E2144750
- Hohlfeld R & Meinl E (2017) Ocrelizumab in multiple sclerosis: markers and mechanisms. *Lancet Neurol* 16: 259–261 doi:10.1016/S1474-4422(17)30048-0 [PREPRINT]
- Howell OW, Reeves CA, Nicholas R, Carassiti D, Radotra B, Gentleman SM, Serafini B, Aloisi F, Roncaroli F, Magliozzi R, *et al* (2011) Meningeal inflammation is widespread and linked to cortical pathology in multiple sclerosis. *Brain* 134: 2755–2771
- Huda S, Whittam D, Bhojak M, Chamberlain J, Noonan C & Jacob A (2019) Neuromyelitis optica spectrum disorders. *Clin Med J R Coll Physicians London* 19: 169–176 doi:10.7861/CLINMEDICINE.19-2-169 [PREPRINT]
- Irani SR, Alexander S, Waters P, Kleopa KA, Pettingill P, Zuliani L, Peles E, Buckley C, Lang B & Vincent A (2010) Antibodies to Kv1 potassium channel-complex proteins leucine-rich, glioma inactivated 1 protein and contactin-associated protein-2 in limbic encephalitis, Morvan’s syndrome and acquired neuromyotonia. *Brain* 133: 2734–2748
- Janda A, Eryilmaz E, Nakouzi A, Cowburn D & Casadevall A (2012) Variable region identical immunoglobulins differing in isotype express different paratopes. *J Biol Chem* 287: 35409–35417
- Jasani B, Ternynck T, Lazarus JH, Phillips DI, Avrameas S & Parkes AB (1999) Natural antibody status in patients with Hashimoto’s thyroiditis. *J Clin Lab Immunol* 51: 9–20
- Johnson KP, Arrigo SC, Nelson BJ & Ginsberg A (1977) Agarose electrophoresis of cerebrospinal fluid in multiple sclerosis: A simplified method for demonstrating cerebrospinal fluid oligoclonal immunoglobulin bands. *Neurology* 27: 273–277
- Keyt BA, Baliga R, Sinclair AM, Carroll SF & Peterson MS (2020) Structure, Function, and Therapeutic Use of IgM Antibodies. *Antibodies (Basel, Switzerland)* 9: 53
- Krumbholz M, Derfuss T, Hohlfeld R & Meinl E (2012) B cells and antibodies in multiple sclerosis pathogenesis and therapy. *Nat Rev Neurol* 8: 613–623 doi:10.1038/nrneurol.2012.203 [PREPRINT]
- Krysko KM, LaHue SC, Anderson A, Rutatangwa A, Rowles W, Schubert RD, Marcus J, Riley CS, Bevan C, Hale TW, *et al* (2020) Minimal breast milk transfer of rituximab, a monoclonal antibody used in neurological conditions. *Neurol Neuroimmunol neuroinflammation* 7
- Kutzelnigg A & Lassmann H (2014) Pathology of multiple sclerosis and related inflammatory demyelinating diseases. In *Handbook of Clinical Neurology* pp 15–58. Elsevier B.V.
- Kwakkenbos MJ, Diehl SA, Yasuda E, Bakker AQ, Van Geelen CMM, Lukens M V., Van Bleek GM, Widjoatmodjo MN, Bogers WMJM, Mei H, *et al* (2010) Generation of stable monoclonal

antibody-producing B cell receptor-positive human memory B cells by genetic programming. *Nat Med* 16: 123–128

Lampson LA (2011) Monoclonal antibodies in neuro-oncology: Getting past the blood-brain barrier. *MAbs* 3: 153–160 doi:10.4161/mabs.3.2.14239 [PREPRINT]

Lehmann-Horn K, Sagan SA, Bernard CCA, Sobel RA & Zamvil SS (2015) B-cell very late antigen-4 deficiency reduces leukocyte recruitment and susceptibility to central nervous system autoimmunity. *Ann Neurol* 77: 902–908

Li R, Rezk A, Miyazaki Y, Hilgenberg E, Touil H, Shen P, Moore CS, Michel L, Althekair F, Rajasekharan S, *et al* (2015) Proinflammatory GM-CSF-producing B cells in multiple sclerosis and B cell depletion therapy. *Sci Transl Med* 7

Lindner JM, Cornacchione V, Sathe A, Be C, Srinivas H, Riquet E, Leber XC, Hein A, Wrobel MB, Scharenberg M, *et al* (2019) Human Memory B Cells Harbor Diverse Cross-Neutralizing Antibodies against BK and JC Polyomaviruses. *Immunity* 50: 668-676.e5

Lisak RP (1998) Intravenous immunoglobulins in multiple sclerosis. *Neurology* 51

Lorscheider J, Buzzard K, Jokubaitis V, Spelman T, Havrdova E, Horakova D, Trojano M, Izquierdo G, Girard M, Duquette P, *et al* (2016) Defining secondary progressive multiple sclerosis. *Brain* 139: 2395–2405

Lu LL, Suscovich TJ, Fortune SM & Alter G (2018) Beyond binding: Antibody effector functions in infectious diseases. *Nat Rev Immunol* 18: 46–61 doi:10.1038/nri.2017.106 [PREPRINT]

Lublin FD & Reingold SC (1996) Defining the clinical course of multiple sclerosis: Results of an international survey. *Neurology* 46: 907–911 doi:10.1212/WNL.46.4.907 [PREPRINT]

Machado-Santos J, Saji E, Tröschler AR, Paunovic M, Liblau R, Gabriely G, Bien CG, Bauer J & Lassmann H (2018) The compartmentalized inflammatory response in the multiple sclerosis brain is composed of tissue-resident CD8⁺ T lymphocytes and B cells. *Brain* 141: 2066–2082

Magalhães R, Stiehl P, Morawietz L, Berek C & Krenn V (2002) Morphological and molecular pathology of the B cell response in synovitis of rheumatoid arthritis. *Virchows Arch* 441: 415–427 doi:10.1007/s00428-002-0702-1 [PREPRINT]

Magliozzi R, Howell O, Vora A, Serafini B, Nicholas R, Puopolo M, Reynolds R & Aloisi F (2007) Meningeal B-cell follicles in secondary progressive multiple sclerosis associate with early onset of disease and severe cortical pathology. *Brain* 130: 1089–1104

Mao S, Gao C, Lo CHL, Wirsching P, Wong CH & Janda KD (1999) Phage-display library selection of high-affinity human single-chain antibodies to tumor-associated carbohydrate antigens sialyl Lewisx and Lewisx. *Proc Natl Acad Sci U S A* 96: 6953–6958

Mehta PD, Frisch S, Thormar H, Tourtellotte WW & Wisniewski HM (1981) Bound antibody in multiple sclerosis brains. *J Neurol Sci* 49: 91–98

Miller DH & Leary SM (2007) Primary-progressive multiple sclerosis. *Lancet Neurol* 6: 903–912 doi:10.1016/S1474-4422(07)70243-0 [PREPRINT]

Natkanski E, Lee W-Y, Mistry B, Casal A, Molloy JE & Tolar P (2013) B cells use mechanical energy to discriminate antigen affinities. *Science* 340: 1587–90

- Di Niro R, Mesin L, Raki M, Zheng N-Y, Lund-Johansen F, Lundin KEA, Charpilienne A, Poncet D, Wilson PC & Sollid LM (2010) Rapid Generation of Rotavirus-Specific Human Monoclonal Antibodies from Small-Intestinal Mucosa. *J Immunol* 185: 5377–5383
- Olsson T, Barcellos LF & Alfredsson L (2016) Interactions between genetic, lifestyle and environmental risk factors for multiple sclerosis. *Nat Rev Neurol* 13: 26–36
doi:10.1038/nrneurol.2016.187 [PREPRINT]
- Plaisant P, Burioni R, Manzin A, Solforosi L, Candela M, Gabrielli A, Fadda G & Clementi M (1997) Human monoclonal recombinant Fabs specific for HCV antigens obtained by repertoire cloning in phage display combinatorial vectors. In *Research in Virology* pp 165–169. Elsevier Masson SAS
- Prüss H (2021) Autoantibodies in neurological disease. *Nat Rev Immunol* 21: 798–813
doi:10.1038/s41577-021-00543-w [PREPRINT]
- Racine R, McLaughlin M, Jones DD, Wittmer ST, MacNamara KC, Woodland DL & Winslow GM (2011) IgM Production by Bone Marrow Plasmablasts Contributes to Long-Term Protection against Intracellular Bacterial Infection. *J Immunol* 186: 1011–1021
- Robbiani DF, Gaebler C, Muecksch F, Lorenzi JCC, Wang Z, Cho A, Agudelo M, Barnes CO, Gazumyan A, Finkin S, *et al* (2020) Convergent antibody responses to SARS-CoV-2 in convalescent individuals. *Nature* 584: 437–442
- Rodda LB, Netland J, Shehata L, Pruner KB, Morawski PA, Thouvenel CD, Takehara KK, Eggenberger J, Hemann EA, Waterman HR, *et al* (2021) Functional SARS-CoV-2-Specific Immune Memory Persists after Mild COVID-19. *Cell* 184: 169-183.e17
- Roxanis I, Micklem K, McConville J, Newsom-Davis J & Willcox N (2002) Thymic myoid cells and germinal center formation in myasthenia gravis; possible roles in pathogenesis. *J Neuroimmunol* 125: 185–197
- Ruutiainen J, Arnadóttir T, Molnár G, Salmi A & Frey H (1981) Myelin basic protein antibodies in the serum and CSF of multiple sclerosis and subacute sclerosing panencephalitis patients. *Acta Neurol Scand* 64: 196–206
- Sawcer S, Franklin RJM & Ban M (2014) Multiple sclerosis genetics. *Lancet Neurol* 13: 700–709
doi:10.1016/S1474-4422(14)70041-9 [PREPRINT]
- Scheid JF, Mouquet H, Feldhahn N, Walker BD, Pereyra F, Cutrell E, Seaman MS, Mascola JR, Wyatt RT, Wardemann H, *et al* (2009) A method for identification of HIV gp140 binding memory B cells in human blood. *J Immunol Methods* 343: 65–67
- Schroeder HW, Imboden JB & Torres RM (2019) Antigen Receptor Genes, Gene Products, and Coreceptors. In *Clinical Immunology* pp 55-77.e1. Elsevier
- Serafini B, Rosicarelli B, Magliozzi R, Stigliano E & Aloisi F (2004) Detection of ectopic B-cell follicles with germinal centers in the meninges of patients with secondary progressive multiple sclerosis. *Brain Pathol* 14: 164–174
- Shen C, Zhang M, Chen Y, Zhang L, Wang G, Chen J, Chen S, Li Z, Wei F, Chen J, *et al* (2019) An IgM antibody targeting the receptor binding site of influenza B blocks viral infection with great breadth and potency. *Theranostics* 9: 210–231

- Skountzou I, Satyabhama L, Stavropoulou A, Ashraf Z, Esser ES, Vassilieva E, Koutsonanos D, Compans R & Jacob J (2014) Influenza virus-specific neutralizing IgM antibodies persist for a lifetime. *Clin Vaccine Immunol* 21: 1481–1489
- Smith K, Garman L, Wrammert J, Zheng NY, Capra JD, Ahmed R & Wilson PC (2009) Rapid generation of fully human monoclonal antibodies specific to a vaccinating antigen. *Nat Protoc* 4: 372–384
- Spadaro M, Winklmeier S, Beltrán E, Macrini C, Höftberger R, Schuh E, Thaler FS, Gerdes LA, Laurent S, Gerhards R, *et al* (2018) Pathogenicity of human antibodies against myelin oligodendrocyte glycoprotein. *Ann Neurol* 84: 315–328
- Stangel M, Fredrikson S, Meinl E, Petzold A, Stüve O & Tumani H (2013) The utility of cerebrospinal fluid analysis in patients with multiple sclerosis. *Nat Rev Neurol* 9: 267–276 doi:10.1038/nrneuro.2013.41 [PREPRINT]
- Storch MK, Piddlesden S, Haltia M, Iivanainen M, Morgan P & Lassmann H (1998) Multiple sclerosis: In situ evidence for antibody- and complement- mediated demyelination. *Ann Neurol* 43: 465–471
- Theofilopoulos AN, Kono DH & Baccala R (2017) The multiple pathways to autoimmunity. *Nat Immunol* 18: 716–724 doi:10.1038/ni.3731 [PREPRINT]
- Thouvenel CD, Fontana MF, Netland J, Krishnamurty AT, Takehara KK, Chen Y, Singh S, Miura K, Keitany GJ, Lynch EM, *et al* (2021) Multimeric antibodies from antigen-specific human IgM+ memory B cells restrict Plasmodium parasites. *J Exp Med* 218
- Throsby M, van den Brink E, Jongeneelen M, Poon LLM, Alard P, Cornelissen L, Bakker A, Cox F, van Deventer E, Guan Y, *et al* (2008) Heterosubtypic neutralizing monoclonal antibodies cross-protective against H5N1 and H1N1 recovered from human IgM+ memory B cells. *PLoS One* 3
- Tiller T, Meffre E, Yurasov S, Tsuiji M, Nussenzweig MC & Wardemann H (2008) Efficient generation of monoclonal antibodies from single human B cells by single cell RT-PCR and expression vector cloning. *J Immunol Methods* 329: 112–124
- Tobita T, Oda M & Azuma T (2004) Segmental flexibility and avidity of IgM in the interaction of polyvalent antigens. *Mol Immunol* 40: 803–811
- Tonegawa S (1983) Somatic generation of antibody diversity
- Torres M & Casadevall A (2008) The immunoglobulin constant region contributes to affinity and specificity. *Trends Immunol* 29: 91–97 doi:10.1016/j.it.2007.11.004 [PREPRINT]
- Traggiai E, Becker S, Subbarao K, Kolesnikova L, Uematsu Y, Gismondo MR, Murphy BR, Rappuoli R & Lanzavecchia A (2004) An efficient method to make human monoclonal antibodies from memory B cells: Potent neutralization of SARS coronavirus. *Nat Med* 10: 871–875
- Turula H & Wobus CE (2018) The role of the polymeric immunoglobulin receptor and secretory immunoglobulins during mucosal infection and immunity. *Viruses* 10 doi:10.3390/v10050237 [PREPRINT]
- Victora GD & Nussenzweig MC (2012) Germinal centers. *Annu Rev Immunol* 30: 429–457 doi:10.1146/annurev-immunol-020711-075032 [PREPRINT]
- Wallin MT, Culpepper WJ, Nichols E, Bhutta ZA, Gebrehiwot TT, Hay SI, Khalil IA, Krohn KJ,

- Liang X, Naghavi M, *et al* (2019) Global, regional, and national burden of multiple sclerosis 1990–2016: a systematic analysis for the Global Burden of Disease Study 2016. *Lancet Neurol* 18: 269–285
- Wang Z, Lorenzi JCC, Muecksch F, Finkin S, Viant C, Gaebler C, Cipolla M, Hoffmann HH, Oliveira TY, Oren DA, *et al* (2021) Enhanced SARS-CoV-2 neutralization by dimeric IgA. *Sci Transl Med* 13
- Weinshenker BG, O’Brien PC, Petterson TM, Noseworthy JH, Lucchinetti CF, Dodick DW, Pineda AA, Stevens LN & Rodriguez M (1999) A randomized trial of plasma exchange in acute central nervous system inflammatory demyelinating disease. *Ann Neurol* 46: 878–886
- Williams AF & Barclay AN (1988) The immunoglobulin superfamily - Domains for cell surface recognition. *Annu Rev Immunol* 6: 381–405 doi:10.1146/annurev.iy.06.040188.002121 [PREPRINT]
- Zimmermann M, Rose N, Lindner JM, Kim H, Gonçalves AR, Callegari I, Syedbasha M, Kaufmann L, Egli A, Lindberg RLP, *et al* (2019) Antigen extraction and B cell activation enable identification of rare membrane antigen specific human B cells. *Front Immunol* 10
- Zohar T, Loos C, Fischinger S, Atyeo C, Wang C, Slein MD, Burke J, Yu J, Feldman J, Hauser BM, *et al* (2020) Compromised Humoral Functional Evolution Tracks with SARS-CoV-2 Mortality. *Cell* 183: 1508-1519.e1

